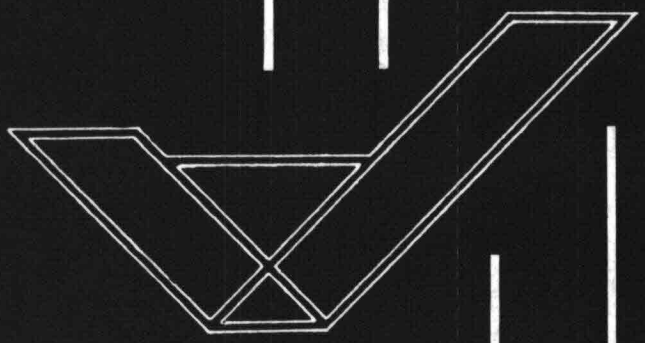

Steady turbulent flow in curved rectangular channels

H.J. de Vriend

Internal report no. 5-79

Laboratory of Fluid Mechanics

Department of Civil Engineering

Delft University of Technology

Steady turbulent flow in curved rectangular channels

H.J. de Vriend

Internal report no. 5-79
Laboratory of Fluid Mechanics
Department of Civil Engineering
Delft University of Technology
Delft, The Netherlands

CONTENTS

Appendix D: Stream function equation for the secondary flow

Appendix E: Computation of the vertical distribution of the secondary flow

Appendix F: Computation of the depth-averaged stream function of the secondary flow

LIST OF FIGURES

LIST OF SYMBOLS

a	normalized turbulence viscosity
$a' = a/k_m\bar{u}$	vertical distribution function of the turbulence viscosity
$a'' = a/U_\tau$	
A_t	dynamic turbulence viscosity
$\bar{A}_0$	overall mean value of $A_t + \eta$ in the equivalent uniform rectilinear shear flow
B	channel width
c	inverse secondary flow intensity factor
C	Chezy's factor
c_μ	constant of proportionality in the k-ε-model
d	depth of flow
dp	pressure correction
De_0	effective Dean number
E	roughness parameter for smooth walls
E^*	roughness parameter in terms of Chezy's factor
f	vertical distribution function of the main flow
F	primitive function of f
$\hat{f}$	estimate of f
f_1, f_2, f_3	constituents of f
g	acceleration due to gravity
g	vertical distribution function of the stream function of the secondary flow
$\hat{g}$	maximum of g
g_1, g_2, g_3	constituents of g
i_0	normalized longitudinal pressure gradient in the equivalent uniform rectilinear shear flow
k	bottom shear stress factor
k	Nikuradse sand roughness
k_l, k_r	sidewall shear stress factors for the main flow
k_{ls}, k_{rs}	sidewall shear stress factors for the secondary flow
k_m	bottom shear stress factor for the main flow
$\tilde{k}_m$	estimate of k_m
k_s	bottom shear stress factor for the secondary flow
k_t	turbulence kinetic energy

l_m	normalized mixing length
n	transverse coordinate in the stream-oriented system
p	pressure
p	normalized total pressure p + ρgz
P	scalefactor for the total pressure
$\bar{p}$	cross-sectional mean value of p
$\tilde{p}$	estimate of p
Q	total discharge
r	radial coordinate normalized by R_0
R	radial coordinate in the cylindrical system
R_c	radius of curvature of the channel axis
R_{c_k}	R_c in the k-th channel section
Re_o	effective Reynolds number
r_n	normalized local radius of curvature of the normal lines in the stream-oriented coordinate system
r_s	normalized local radius of curvature of the streamlines in the stream-oriented coordinate system
R_0	characteristic radius of curvature for the channel that is considered
s	normalized longitudinal coordinate
s	streamwise coordinate in the stream-oriented system
S	longitudinal coordinate
u	normalized axial (tangential) velocity component
$\bar{u}$	depth-averaged value of u
$\bar{\bar{u}}$	cross-sectional mean value of u
$\tilde{\bar{u}}$	estimate of $\bar{u}$
$\bar{u}_j$	value of $\bar{u}$ in cross-section j
u_m	main flow part of the normalized longitudinal velocity component
$\tilde{u}_m$	streamwise main velocity component (normalized)
U_{res}	resultant velocity parallel to the wall considered
$\bar{u}_{res}$, $\bar{u}_t$	total depth-averaged main velocity (normalized)
u_s	secondary flow part of the normalized longitudinal velocity component
$\bar{u}_1$, $\bar{u}_2$, $\bar{u}_3$	constituents of $\bar{u}$
u_τ	normalized bottom friction velocity

U_τ	resultant friction velocity for the wall considered
$u_{\tau l}$, $u_{\tau r}$	longitudinal component of the sidewall friction velocity
$U_{\tau l}$, $U_{\tau r}$	resultant sidewall friction velocity
$u_{\tau w}$	sidewall friction velocity in the equivalent fully developed straight channel flow
v	normalized transverse (radial) coordinate
V	overall mean velocity
v_m	main flow part of the normalized transverse velocity component
$\tilde{v}_m$	transverse main velocity component in the stream-oriented system (normalized)
v_R	radial velocity component
v_s	secondary flow part of the normalized transverse velocity component
$\tilde{v}_s$	transverse secondary velocity component in the stream-oriented system (normalized)
v_z	vertical velocity component
v_0	velocity in uniform rectilinear shear flow
v_τ	transverse component of U_τ/ε at the bottom
$v_{\tau s}$	transverse component of the normalized bottom friction velocity due to the secondary flow
v_ϕ	tangential velocity component
v'_ϕ, v'_z	turbulent fluctuations of v_ϕ and v_z
v_*	bottom friction velocity in uniform rectilinear shear flow
w	normalized vertical velocity component
w_m	main flow part of the normalized vertical velocity component
w_s	secondary flow part of the normalized vertical velocity component
$w_{\tau l}$, $w_{\tau r}$	vertical component of the normalized sidewall friction velocity
y	transverse coordinate
$\tilde{y}$	wall distance
$y^+ = \frac{U_\tau \tilde{y}}{\nu}$	dimensionless wall distance
z	vertical coordinate

α	underrelaxation factor
β_k	weight factor for the pressure correction
γ	constant in the expression for the effective Reynolds number
δ	normalized thickness of the bottom-layer
δ_1, δ_r	normalized thickness of the sidewall-layers
δ_0	normalized bottom distance for the lowest points of the computational grid
δ_l	normalized wall distance for the nodal points of the computational grid nearest to the sidewalls
$\Delta\xi$	size of the sidewall-nearest mesh of the computional grid
ε	depth to radius of curvature ratio
ε_t	rate of turbulence energy dissipation
ζ	normalized vertical coordinate
ζ^*	value of ζ in the point where the logarithmic velocity distribution becomes equal to zero
$\hat{\zeta}$	normalized vertical coordinate of the point where $\hat{g}$ occurs
ζ_l	normalized vertical coordinate of the lowest-but-one nodal points of the computational grid
η	dynamic viscosity of the fluid
κ	Von Karman's constant
ν	kinematic viscosity of the fluid
ξ	transverse coordinate normalized by d
ξ_1, ξ_2	normalized transverse coordinate of the nodal points nearest-but-one to the left and the right wall, respectively
ρ	mass density of the fluid
$\tau_{b_{res}}$	resultant normalized bottom shear stress
$\tau_{b\xi}$	transverse component of the normalized bottom shear stress
$\tau_{b\xi_m}$	part of $\tau_{b\xi}$ due to the main flow
$\tau_{b\phi}$	longitudinal component of the normalized bottom shear stress
$\tau_{b\phi_m}$	part of $\tau_{b\phi}$ due to the main flow
$\tau_{l\phi}$, $\tau_{r\phi}$	longitudinal component of the normalized sidewall shear stress
$\tau_{l\zeta}$, $\tau_{r\zeta}$	vertical component of the normalized sidewall shear stress
τ_{res}	resultant normalized wall shear stress
τ_{sz}	shear stress in uniform rectilinear shear flow
ϕ	angular coordinate in the cylindrical system
Φ	stream function of the normalized depth-averaged flow
$\psi = \psi'/Re_0$	

ψ'	stream function of the normalized secondary flow
$\bar{\psi}_1$, $\bar{\psi}_2$, $\bar{\psi}_3$	constituents of $\bar{\psi}$
$\bar{\omega}$	vorticity of the normalized depth-averaged flow
ω_s	vorticity of the normalized secondary flow

$$\nabla^2 = \frac{1}{R^2}\frac{\partial^2}{\partial\phi^2} + \frac{\partial^2}{\partial R^2} + \frac{1}{R}\frac{\partial}{\partial R} + \frac{\partial^2}{\partial z^2}$$

$$\nabla_1^2 = \frac{\partial^2}{\partial\xi^2} + \frac{1}{r}\frac{\partial}{\partial\xi} + \frac{\partial^2}{\partial\zeta^2}$$

Summary

After the study of fully developed and developing steady laminar flow in curved channels of shallow rectangular wet cross-section (see earlier reports in this series), steady turbulent flow in such channels is investigated as a next step towards a mathematical model of the flow in shallow river bends.

A mathematical model is developed for this type of flow, using a turbulence model with a prescribed distribution of the turbulence viscosity and starting from the same similarity hypothesis as in the equivalent laminar flow models. The influence of various characteristics of the turbulence model and the admissability of the most important assumptions underlying the mathematical system that is solved are tested for the flow in a rather sharply curved flume with rather strong effects of curvature. The performance of the model is tested by comparing its results with experimental data from various laboratory flumes.

The turbulence model appears to be of great importance to the secondary flow and the related quantities. The similarity hypothesis yields satisfactory results for the main flow, but it needs to be refined for the calculation of the magnitude and the direction of the bed shear stress.

The model appears to be applicable to curved channels of not very sharp curvature (i.e. flows with a small or intermediate equivalent Dean number), although the secondary flow intensity tends to be underestimated.

1. Introduction

1.1. General

The flow and the bed topography in curved alluvial river channels play a prominent part in several aspects of river engineering, such as navigability, bank protection and dispersion of pollutants. Hitherto, engineering problems concerning river bends are mostly investigated using physical scale models, even though the complex character of the flow may give rise to scale effects that make the model data hard to interpret in prototype terms. The increasing facilities of electronic computers, however, make it more and more attractive to develop mathematical models. They would facilitate the understanding of the physical phenomena and could be used together with or even instead of physical models.
As it is impossible to reliably predict the bed topography withouth knowing the flow field, an adequate model of the flow in a curved channel with an uneven bed must be developed first. Assuming disturbances of the flow to travel at a much higher celerity than disturbances of the bed, as is the case in most of the navigable alluvial rivers, the bed can be considered as being fixed when computing the flow. In addition, the flow can be assumed to be steady, which is allowable under many practical conditions.
The development of a mathematical model of steady flow in river bends with a fixed uneven bed is one of the research projects of the Laboratory of Fluid Mechanics of the Delft University of Technology, as a part of the river bend project of the joint hydraulic research programme T.O.W.*).

1.2. The present investigations

After studying fully developed and developing laminar flow in curved channels of shallow rectangular cross-section (DE VRIEND, 1978a and 1978b), the development of a mathematical model of steady turbulent flow in such channels is the next step on the way to a mathematical model of the flow in shallow river bends.

---

*) (Toegepast Onderzoek Waterstaat), in which Rijkswaterstaat, the Delft Hydraulics Laboratory and the Delft University of Technology participate.

Passing from laminar to turbulent flow implies an essential complication of the problem. Steady laminar flow is properly described by the time-independent version of the Navier-Stokes equations. The turbulence-averaged motion in steady turbulent flow, however, must be described by the Reynolds equations, in which the Reynolds stresses account for the turbulence. These equations can only be solved if additional assumptions are made for the Reynolds stresses (the turbulence model). Establishing a turbulence model that is appropriate to the type of flow considered here is one of the purposes of the present project.

Another purpose of this step is to further develop the computational procedure needed to solve the mathematical system, which is essentially complicated by the introduction of turbulence, or rather: of the turbulence model.

Furthermore, the development of a model of turbulent flow in curved rectangular channels is attractive because it provides the possibility of testing the model, and so the turbulence model and the computational procedure, against laboratory experiments, many of which were carried out in rectangular flumes.

2. Mathematical formulation of the problem

2.1. Channel configuration and coordinate system

The present part of the investigations on flow in river bends is to deal with a computational technique for turbulent flow in curved shallow channels. From this point of view a free surface and more or less arbitrary channel patterns and bed configurations can be expected to be only complicating factors that will not essentially influence the computational method. Therefore considerations are limited to channels of uniform rectangular wet cross-section with a channel axis consisting of circular arcs with radii of curvature R_{c_k} *). Accordingly, the coordinate system to be used in the mathematical formulation of the present problem consists of a set of cylindrical coordinate systems, each of which has a vertical axis that goes through the centre of the circle forming the channel axis of the relevant section (see figure 1). For the sake of simplicity, the explanation of the model and the underlying assumptions will be limited to one channel section with a circular axis of radius R_c, using a cylindrical coordinate system (R,ϕ,z) with the z-axis vertically upward and $z=0$ at the surface (figure 2). If necessary, a transformation to curvilinear, stream-oriented coordinates will be carried out.

2.2. Differential equations

The mathematical model is based on a set of differential equations representing the conservation of mass and turbulence-averaged momentum in stationary turbulent flow of an incompressible fluid. Anticipating on what is stated in chapter 3 on the modeling of the Reynolds-stresses, a scalar turbulence viscosity is assumed to be applicable. If A_t denotes this turbulence viscosity, η the dynamic molecular viscosity of the fluid, ρ its mass density, g the acceleration due to gravity, p the pressure and v_R, v_ϕ and v_z the velocity-components in R-, ϕ- and z-direction, respectively, the differential equations read

$$\frac{1}{R}\frac{\partial v_\phi}{\partial \phi} + \frac{\partial v_R}{\partial R} + \frac{v_R}{R} + \frac{\partial v_z}{\partial z} = 0 \qquad (2.1)$$

*) R_{c_k} may be chosen infinitely large, so that the relevant k-th channel section is straight.

$$\frac{v_\phi}{R}\frac{\partial v_\phi}{\partial \phi} + v_R\frac{\partial v_\phi}{\partial R} + v_z\frac{\partial v_\phi}{\partial z} + \frac{v_R v_\phi}{R} = -\frac{1}{\rho}\frac{1}{R}\frac{\partial p}{\partial \phi} + \frac{A_t+\eta}{\rho}\left(\nabla^2 v_\phi - \frac{v_\phi}{R^2} + \frac{2}{R^2}\frac{\partial v_R}{\partial \phi}\right) +$$

$$+ \frac{1}{\rho}\left\{\frac{2}{R}\frac{\partial A_t}{\partial \phi}\left(\frac{1}{R}\frac{\partial v_\phi}{\partial \phi} + \frac{v_R}{R}\right) + \frac{\partial A_t}{\partial R}\left(\frac{1}{R}\frac{\partial v_R}{\partial \phi} + \frac{\partial v_\phi}{\partial R} - \frac{v_\phi}{R}\right) + \frac{\partial A_t}{\partial z}\left(\frac{\partial v_\phi}{\partial z} + \frac{1}{R}\frac{\partial v_z}{\partial \phi}\right)\right\} \qquad (2.2)$$

$$\frac{v_\phi}{R}\frac{\partial v_R}{\partial \phi} + v_R\frac{\partial v_R}{\partial R} + v_z\frac{\partial v_R}{\partial z} - \frac{v_\phi^2}{R} = -\frac{1}{\rho}\frac{\partial p}{\partial R} + \frac{A_t+\eta}{\rho}\left(\nabla^2 v_R - \frac{v_R}{R^2} - \frac{2}{R^2}\frac{\partial v_\phi}{\partial \phi}\right) +$$

$$+ \frac{1}{\rho}\left\{\frac{1}{R}\frac{\partial A_t}{\partial \phi}\left(\frac{1}{R}\frac{\partial v_R}{\partial \phi} + \frac{\partial v_\phi}{\partial R} - \frac{v_\phi}{R}\right) + 2\frac{\partial A_t}{\partial R}\frac{\partial v_R}{\partial R} + \frac{\partial A_t}{\partial z}\left(\frac{\partial v_R}{\partial z} + \frac{\partial v_z}{\partial R}\right)\right\} \qquad (2.3)$$

$$\frac{v_\phi}{R}\frac{\partial v_z}{\partial \phi} + v_R\frac{\partial v_z}{\partial R} + v_z\frac{\partial v_z}{\partial z} = -\frac{1}{\rho}\frac{\partial p}{\partial z} - g + \frac{A_t+\eta}{\rho}\nabla^2 v_z +$$

$$+ \frac{1}{\rho}\left\{\frac{1}{R}\frac{\partial A_t}{\partial \phi}\left(\frac{\partial v_\phi}{\partial z} + \frac{1}{R}\frac{\partial v_z}{\partial \phi}\right) + \frac{\partial A_t}{\partial R}\left(\frac{\partial v_z}{\partial R} + \frac{\partial v_R}{\partial z}\right) + 2\frac{\partial A_t}{\partial z}\frac{\partial v_z}{\partial z}\right\} \qquad (2.4)$$

in which $\nabla^2 = \frac{1}{R^2}\frac{\partial^2}{\partial \phi^2} + \frac{\partial^2}{\partial R^2} + \frac{1}{R}\frac{\partial}{\partial R} + \frac{\partial^2}{\partial z^2}$

2.3. Boundary conditions

The boundary conditions at the surface arising from the impermeability of this surface and the vanishing of the shear stresses along it read

$$v_z\Big|_{z=0} = 0 \qquad (2.5)$$

and

$$\left\{(A_t+\eta)\frac{\partial v_\phi}{\partial z}\right\}\Big|_{z=0} = 0; \quad \left\{(A_t+\eta)\frac{\partial v_R}{\partial z}\right\}\Big|_{z=0} = 0 \qquad (2.6)$$

, respectively. As the surface is kept fixed, it must be considered as a frictionless rigid plate exerting normal stresses on the fluid. Consequently, the dynamic free surface condition p=0 is not applicable here.

The boundary conditions at the fixed boundaries stem from the impermeability of these boundaries and the no-slip conditions.

$$v_R = 0;\ v_\phi = 0;\quad v_z = 0 \quad \text{for} \quad z = -d \text{ and for } R = R_c \pm \frac{B}{2} \tag{2.7}$$

in which B denotes the channel width. It should be noted that, depending on the turbulence model adopted, the above conditions at the fixed boundaries will necessitate a special treatment of the flow in the vicinity of these boundaries (see chapter 3)).

In addition to these "lateral" boundary conditions, inflow and outflow conditions must be given. Most of these conditions will be formulated in a later stage. Only the discharge Q is mentioned here, since it plays a part in the integral conditions of continuity (cf. equation 2.1).

$$\int_{R_c-B/2}^{R_c+B/2} dR \int_{-d}^{0} v_\phi \, dz = Q \tag{2.8}$$

and it will be used in the normalization of the system.

2.4. Normalization

The normalization carried out in order to make all variables dimensionless and to estimate the order of magnitude of the various terms in the differential equations is almost the same as in case of laminar flow (DE VRIEND, 1978a and b).
In summary:

$$v_\phi = Vu;\ v_R = \frac{d}{R_c} V v;\ v_z = \frac{d}{R_c} V w \quad \text{with } V = Q/Bd \tag{2.9}$$

$$y = R - R_c = d\xi, \quad \text{so } \frac{\partial}{\partial R} = \frac{1}{d}\frac{\partial}{\partial \xi};\quad z = d\zeta, \quad \text{so } \frac{\partial}{\partial z} = \frac{1}{d}\frac{\partial}{\partial \zeta} \tag{2.10}$$

$$\frac{1}{R} = \frac{1}{R_0}\frac{1}{r};\ S = R(\phi - \phi_0) = R_0 s, \text{ so } \frac{1}{R}\frac{\partial}{\partial \phi} = \frac{1}{R_0}\frac{\partial}{\partial s} = \frac{1}{R_0}\frac{1}{r}\frac{\partial}{\partial \phi} \tag{2.11}$$

in which S denotes the longitudinal coordinate and R_0 is a characteristic radius of curvature of the channel to be considered.
The only difference from the laminar flow case lies in the normalization of the turbulence viscosity and the total pressure. The turbulence viscosity is normalized by

$$A_t + \eta = \bar{A}_0 a \tag{2.12}$$

, in which $\bar{A}_0$ denotes the overall mean value of $A_t + \eta$ in the equivalent fully developed flow in an infinitely wide straight channel. Supposing the total pressure to be normalized by

$$p + \rho g z = P p \tag{2.13}$$

, the longitudinal momentum equation for fully developed flow in an infinitely wide shallow channel reads

$$0 = - \frac{P}{\rho R_0} \frac{\partial p}{\partial s} + \frac{\bar{A}_0 V}{\rho d^2} \left(a \frac{\partial^2 u}{\partial \zeta^2} + \frac{\partial a}{\partial \zeta} \frac{\partial u}{\partial \zeta} \right) \tag{2.14}$$

The pressure gradient term and the diffusion terms in this equation must be of the same importance. As the model to be developed should include the flow case described by (2.14), the scalefactors of the pressure gradient term and the vertical diffusion terms are chosen equal. Hence

$$P = \bar{A}_0 V \frac{R_0}{d^2} = \rho V^2 \frac{1}{Re_0} \frac{R_0}{d} \tag{2.15}$$

in which $Re_0 = \rho V d / \bar{A}_0$ can be considered as a Reynolds number based on the mean turbulence viscosity.

Defining $\varepsilon = d/R_0$, the normalized system of differential equations and boundary conditions becomes

$$\frac{1}{r} \frac{\partial u}{\partial \phi} + \frac{\partial v}{\partial \xi} + \frac{\varepsilon}{r} v + \frac{\partial w}{\partial \zeta} = 0 \tag{2.16}$$

$$\varepsilon Re_0 \left(\frac{u}{r} \frac{\partial u}{\partial \phi} + v \frac{\partial u}{\partial \xi} + w \frac{\partial u}{\partial \zeta} + \frac{\varepsilon}{r} uv \right) = - \frac{1}{r} \frac{\partial p}{\partial \phi} + a \left\{ \frac{\partial^2 u}{\partial \zeta^2} + \frac{\partial^2 u}{\partial \xi^2} + \frac{\varepsilon^2}{r^2} \frac{2}{\partial \phi^2} u + \right.$$

$$\left. + \frac{\varepsilon}{r} \frac{\partial u}{\partial \xi} - \frac{\varepsilon^2}{r^2} u + \frac{\varepsilon^3}{r^2} 2 \frac{\partial v}{\partial \phi} \right\} + 2 \frac{\varepsilon^2}{r} \frac{\partial a}{\partial \phi} \left(\frac{1}{r} \frac{\partial u}{\partial \phi} + \varepsilon \frac{v}{r} \right) + \frac{\partial a}{\partial \xi} \left(\frac{\partial u}{\partial \xi} - \frac{\varepsilon}{r} u + \frac{\varepsilon^2}{r} \frac{\partial v}{\partial \phi} \right) +$$

$$+ \frac{\partial a}{\partial \zeta} \left(\frac{\partial u}{\partial \zeta} + \frac{\varepsilon^2}{r} \frac{\partial w}{\partial \phi} \right) \tag{2.17}$$

$$\varepsilon^3 Re_0 \left(\frac{u}{r}\frac{\partial v}{\partial \phi} + v\frac{\partial v}{\partial \xi} + w\frac{\partial v}{\partial \zeta}\right) - \varepsilon^2 Re_0 \frac{u^2}{r} = -\frac{\partial p}{\partial \xi} + \varepsilon^2 a\left\{\frac{\partial^2 v}{\partial \zeta^2} + \frac{\partial^2 v}{\partial \xi^2} + \frac{\varepsilon^2}{r^2}\frac{\partial^2 v}{\partial \phi^2} + \right.$$

$$\left. + \frac{\varepsilon}{r}\frac{\partial v}{\partial \xi} - \frac{\varepsilon^2}{r^2} v - \frac{\varepsilon}{r^2} 2\frac{\partial u}{\partial \phi}\right\} + \frac{\varepsilon^2}{r}\frac{\partial a}{\partial \phi}\left(\frac{\partial u}{\partial \xi} - \frac{\varepsilon}{r} u + \frac{\varepsilon^2}{r}\frac{\partial v}{\partial \phi}\right) + 2\varepsilon^2 \frac{\partial a}{\partial \xi}\frac{\partial v}{\partial \xi} +$$

$$+ \varepsilon^2 \frac{\partial a}{\partial \zeta}\left(\frac{\partial v}{\partial \zeta} + \frac{\partial w}{\partial \xi}\right) \qquad (2.18)$$

$$\varepsilon^3 Re_0 \left(\frac{u}{r}\frac{\partial w}{\partial \phi} + v\frac{\partial w}{\partial \xi} + w\frac{\partial w}{\partial \xi}\right) = -\frac{\partial p}{\partial \zeta} + \varepsilon^2 a\left\{\frac{\partial^2 w}{\partial \zeta^2} + \frac{\partial^2 w}{\partial \xi^2} + \frac{\varepsilon^2}{r^2}\frac{\partial^2 w}{\partial \phi^2} + \frac{\varepsilon}{r}\frac{\partial w}{\partial \xi}\right\} +$$

$$+ \frac{\varepsilon^2}{r}\frac{\partial a}{\partial \phi}\left(\frac{\partial u}{\partial \zeta} + \frac{\varepsilon^2}{r}\frac{\partial w}{\partial \phi}\right) + \varepsilon^2 \frac{\partial a}{\partial \xi}\left(\frac{\partial v}{\partial \zeta} + \frac{\partial w}{\partial \xi}\right) + 2\varepsilon^2 \frac{\partial a}{\partial \zeta}\frac{\partial w}{\partial \zeta} \qquad (2.19)$$

$$\int_{-B/2d}^{B/2d} d\xi \int_{-1}^{0} u\, d\zeta = \frac{B}{d} \qquad (2.20)$$

$$w = 0;\ a\frac{\partial u}{\partial \zeta} = 0;\ a\frac{\partial v}{\partial \zeta} = 0 \quad \text{at} \quad \zeta = 0 \qquad (2.21)$$

$$u = 0;\ v = 0;\ w = 0 \quad \text{at } \zeta = -1 \quad \text{and at } \xi = \pm \frac{B}{2d} \qquad (2.22)$$

3. Turbulence model

In case of turbulent flow, two types of diffusion terms occur in the turbulence-averaged momentum equations, viz. the molecular diffusion terms, which are the same as in case of laminar flow, and the turbulent diffusion terms arising from the net exchange of momentum due to turbulence (Reynolds stress terms).
On the analogy of the viscous stresses, the components of the Reynolds stress tensor can be assumed proportional to the relevant components of the rate-of-strain tensor of the turbulence-averaged flow. For instance

$$- \rho \overline{v'_\phi v'_z} = A_t \left(\frac{\partial v_\phi}{\partial z} + \frac{1}{R} \frac{\partial v_z}{\partial \phi}\right) \tag{3.1}$$

in which v'_ϕ and v'_z denote the turbulent fluctuations of v_ϕ and v_z, respectively. The coefficient of proportionality A_t, called eddy viscosity or turbulence viscosity, is assumed to be a scalar quantity that depends on the turbulence-averaged flow. Although many objections can be made against this eddy viscosity concept, it appears to yield a satisfactory description of the mean flow properties in many cases of turbulent flow (HINZE, 1975).
As A_t depends on the mean flow, which in turn depends on A_t, the mathematical system is not closed until either a direct relationship between A_t and the mean flow properties has been established or additional differential equations have been formulated from which such a relationship can be derived (transport equations, describing the production, transport and dissipation of turbulence properties; see, for instance, LAUNDER, AND SPALDING (1972)). As a direct relationship between A_t and the mean flow properties is mathematically simpler, such a relationship will be adopted here. Only if this concept proves to fail, more advanced turbulence models will be used.
To obtain an impression how A_t could be related to the mean flow, fully developed turbulent flow in an infinitely wide straight channel is considered. The streamwise momentum equation for that flow case reads

$$0 = - \frac{\partial p}{\partial s} + a \frac{\partial^2 u}{\partial \zeta^2} + \frac{\partial a}{\partial \zeta} \frac{\partial u}{\partial \zeta} \tag{3.2}$$

If the molecular part of the viscosity is neglected and a is related to the mean flow by the mixing length hypothesis.

$$a = -\kappa^2 \zeta (1+\zeta)^2 \left|\frac{\partial u}{\partial \zeta}\right| Re_0 \tag{3.3}$$

, κ denoting Von Kármán's constant, then the vertical distribution of u is a logarithmic function. Since this distribution cannot satisfy the no-slip condition at the fixed bottom $\zeta = -1$ (cf. Equation 2.22), the velocity is prescribed to vanish at a level $\zeta = \zeta^*$ slightly above the bed, so that

$$u = \frac{Re_0^{-1/2}}{\kappa} \left(-\frac{\partial p}{\partial s}\right)^{1/2} \ln\left(\frac{1+\zeta}{1+\zeta^*}\right) \tag{3.4}$$

If Chézy's coefficient C is adopted as an indication of the bed resistance, ζ^* is given by (DE VRIEND, 1976)

$$\zeta^* = -1 + \exp\left(-1 - \frac{\kappa C}{\sqrt{g}}\right) \tag{3.5}$$

and the velocity distribution can be expressed as

$$u = \bar{u} \left\{1 + \frac{\sqrt{g}}{\kappa C} + \frac{\sqrt{g}}{\kappa C} \ln (1+\zeta)\right\} \tag{3.6}$$

, in which $\bar{u}$ denotes the depth-averaged value of u ($\bar{u} = 1$ by definition in the present case). Substitution of this result into (3.3) yields

$$a = -\frac{\kappa\sqrt{g}}{C} \zeta(1+\zeta) Re_0 \tag{3.7}$$

So the distribution of a along the vertical is a parabola vanishing at the bottom and at the surface and having its maximum at half depth. The scalefactor $\bar{A}_0$ of the turbulence viscosity was defined such, that in the present flow case $\bar{a} = 1$. Hence

$$Re_0 = \frac{6}{\kappa}\frac{C}{\sqrt{g}} \quad \text{and} \quad a = -6\zeta(1+\zeta) \tag{3.8}$$

(cf. ENGELUND (1974) and RASTOGI AND RODI (1978), applying a turbulence viscosity with a depth-averaged value corresponding with $Re_0 = 13 \frac{C}{\sqrt{g}}$).
In case of a straight channel of finite width, but without secondary flow, the streamwise momentum equation for fully developed flow becomes

$$0 = - \frac{\partial p}{\partial s} + a \frac{\partial^2 u}{\partial \zeta^2} + \frac{\partial a}{\partial \zeta} \frac{\partial u}{\partial \zeta} + a \frac{\partial^2 u}{\partial \xi^2} + \frac{\partial a}{\partial \xi} \frac{\partial u}{\partial \xi} \tag{3.9}$$

and the equivalent of the mixing length hypothesis (3.3) reads

$$a = l_m^2 \{ (\frac{\partial u}{\partial \zeta})^2 + (\frac{\partial u}{\partial \xi})^2 \}^{1/2} \tag{3.10}$$

in which l_m denotes the mixing length. For a given distribution of l_m, equation (3.9) and (3.10) can be solved to yield the transverse distribution of u. The choice of l_m, however, introduces important uncertainties, so that the computational effort needed to solve the rather complicated system (3.9)-(3.10) may be unjustified. In that case, either more complicated turbulence models have to be applied (see, for instance, RASTOGI AND RODI (1978) and LESCHZINER (1978)) or more crude, but simpler models may just as well be used. As in the present curved flow computations the modelling of turbulence is not expected to be of primary importance (RODI, 1978), it will be attempted to use models that are simpler than (3.10).
The channels to be considered are shallow, so the vertical exchange of momentum due to turbulence will be predominant in the greater part of the cross-section. Only at relatively small distances (order of magnitude d) from the sidewalls the influence of the horizontal exchange will be perceptible. Although, especially in curved channel flow, it may be necessary to describe the flow in the sidewall regions accurately in order to have a good prediction of the flow in the rest of the cross-section (DE VRIEND, 1978a), this accurate prediction in the sidewall regions in itself is not a purpose of the investigations. Therefore it will be attempted to apply a turbulence model similar to the one for infinitely wide streams (see equations 3.8) to shallow channels of finite width, as well.

The vertical distribution of the turbulence viscosity is taken the same as in the fully developed flow case treated in the foregoing, i.e.

$$a \sim 6\zeta(1+\zeta) \tag{3.11}$$

It should be noted, however, that this is a rather arbitrary choice. As an alternative, the vertical distribution of a could be derived from a turbulence model that is different from the mixing length model underlying (3.11). A model that was applied with success in fully three-dimensional computations of curved channel flow (PRATAP, 1975; PRATAP AND SPALDING, 1975; LESCHZINER, 1978) is the so-called 'k-ε-model' (LAUNDER AND SPALDING, 1972; RASTOGI AND RODI, 1978; RODI, 1978). This "higher order" turbulence model is based on the solution of the turbulent kinetic energy k and its rate of dissipation ε from two transport equations and the determination of the eddy viscosity from an algebraic relationship with k and ε.

If the free surface is assumed to be a plane of symmetry, as was done by all the aforementioned authors dealing with three-dimensional curved flow computations, the eddy viscosity distribution found from the k-ε-model appears to differ considerably from the parabolic distribution (3.11), especially in the upper half of the vertical (see figure 3). Nonetheless, the differences between the corresponding velocity distributions are rather small, which suggests the distribution of ε in the upper half of the vertical to be not very important.

Regarding this conclusion, the parabolic distribution (3.11) is adopted, mainly because of its simple form. In a later stage, however, the influence of replacing this distribution by the one found from the k-ε-model will be investigated.

In the shallow flows considered here, turbulence is mainly generated at the bottom. Therefore it is rather obvious to assume a relationship between the turbulence viscosity and the bed shear stress: A_t is taken proportional to the bed friction velocity. In case of fully developed, infinitely wide streams, the normalized friction velocity u_τ equals $\sqrt{g}/C$, so that it seems logical to describe the normalized turbulence viscosity in channels of finite width by

$$a = -6\frac{C}{\sqrt{g}}\, u_\tau \zeta(1+\zeta) \tag{3.12}$$

Although the quantity $C u_\tau / \sqrt{g}$ is not always equal to unity in the flows to be considered, it will be of the order O(1), so that the turbulence viscosity is adequately normalized in this way.
The eddy viscosity distribution (3.12) implies that α goes to zero at the bottom, where $1+\zeta$ goes to zero, and at the sidewalls, where the bottom friction velocity u_τ vanishes. This gives rise to difficulties when attempting to impose the no-slip conditions there (cf. the problems near the bottom in case of uniform flow as discussed earlier in this chapter). LAUNDER AND SPALDING (1974) suggest the use of a "wall function technique" in order to avoid these difficulties: the distribution of the velocity near a fixed boundary is given as a function of the distance to that boundary. For smooth walls the following "universal law of the wall" (RASTOGI AND RODI, 1978) is widely used:

$$U_{res} = \frac{U_\tau}{\kappa} \ln(Ey^+) \tag{3.13}$$

, in which: U_{res} = resultant velocity parallel to the wall,
U_τ = resultant friction velocity for the wall,
E = roughness parameter ($\simeq 9$ for smooth walls),
$y^+ = U_\tau \tilde{y}/\nu$ = dimensionless wall distance,
$\tilde{y}$ = wall distance,
ν = kinematic viscosity of the fluid.

As in alluvial rivers the bottom uses to be rough, however, a rough wall equivalent of (3.13) or a generalized form holding good for smooth and for rough walls is needed. Therefore the following generalized wall function is adopted:

$$U_{res} = \frac{U_\tau}{\kappa} \{\frac{\kappa C}{\sqrt{g}} + 1 + \ln \frac{\tilde{y}}{d}\} \tag{3.14}$$

(cf. the logarithmic velocity distribution (3.6)). Rewriting this expression into the form of (3.13) yields

$$U_{res} = \frac{U_\tau}{\kappa} \ln(E^* \frac{\tilde{y}}{d}) \quad \text{with} \quad E^* = \exp(1 + \frac{\kappa C}{\sqrt{g}}) \tag{3.15}$$

In case of a smooth wall Chezy's factor can be approximated by

$$\frac{C}{\sqrt{g}} \simeq 2.5 \ln(3.7 \frac{U_\tau d}{\nu}) \tag{3.16}$$

, so that

$$E^* \simeq 10 \frac{U_\tau d}{\nu} \tag{3.17}$$

, which is almost in accordance with the aforementioned value of 9 for E.
The rough wall approximation of Chezy's factor given by CHOW (1959) reads

$$\frac{C}{\sqrt{g}} \simeq 2.5 \ln(12.2 \frac{d}{k}) \tag{3.18}$$

, in which k denotes the Nikuradse sand roughness. Then

$$E^* \simeq 33 \frac{d}{k} \tag{3.19}$$

so that (3.15) can be elaborated to

$$U_{res} = \frac{U_\tau}{\kappa} \ln(33 \frac{\tilde{y}}{k}) \tag{3.20}$$

The dependence on the dimensionless wall distance $\tilde{y}/k$ is in accordance with the theory of turbulent boundary layers along rough flat plates (HINZE, 1975).

In order to have an indication of the performance of this turbulence model, it is applied to fully developed flow in a straight shallow channel. Assuming the logarithmic distribution (3.6) to hold good for the velocity in any vertical, equations (3.9) and (3.12) can be elaborated to

$$0 = - \frac{\partial p}{\partial s} - 6 \frac{C}{\sqrt{g}} \zeta(1+\zeta) \{1 + \frac{\sqrt{g}}{\kappa C} + \frac{\sqrt{g}}{\kappa C} \ln(1+\zeta)\} \frac{\partial}{\partial \xi} (u_\tau \frac{\partial \bar{u}}{\partial \xi}) - \frac{6}{\kappa} u_\tau \bar{u} \tag{3.21}$$

As the velocity has the same vertical distribution in all verticals, the bed friction velocity will be proportional to $\bar{u}$. For the logarithmic velocity distribution adopted, the constant of proportionality equals $\frac{\sqrt{g}}{C}$.
Averaging equation (3.21) over the depth of flow then yields

$$0 = -\frac{\partial \bar{p}}{\partial s} + \left(1+\frac{1}{6}\frac{\sqrt{g}}{\kappa C}\right)\frac{\partial}{\partial \xi}\left(\bar{u}\frac{\partial \bar{u}}{\partial \xi}\right) - 6\frac{\sqrt{g}}{\kappa C}\bar{u}^2 \qquad (3.22)$$

The distribution of $\bar{u}$ near the sidewalls is given by

$$\bar{u}\Big|_{\xi \leq B/2d+\delta} = \frac{\left|\bar{u}_{\tau w}\right|}{\kappa}\left\{\frac{\kappa C}{\sqrt{g}} + 1 + \ln(\xi + B/2d)\right\}$$

$$\bar{u}\Big|_{\xi \leq B/2d-\delta} = \frac{\left|\bar{u}_{\tau w}\right|}{\kappa}\left\{\frac{\kappa C}{\sqrt{g}} + 1 + \ln(B/2d - \xi)\right\} \qquad (3.23)$$

, in which $\bar{u}_{\tau w}$ is the depth-averaged sidewall friction velocity.
The system (3.22) - (3.23) contains two unknown constants, viz. $\frac{\partial \bar{p}}{\partial s}$, which can be determined from the integral conditions of continuity, and $\left|\bar{u}_{\tau w}\right|$, which must be estimated or determined from an additional condition near the sidewalls. Such an additional condition can be obtained, for instance, by assuming the regions where the depth-averaged velocity is described by (3.23) to overlap with the region where equation (3.22) must be solved. In that case (3.23) can be imposed not only in the points of the computational grid nearest to the sidewalls, but also in the points one step further inwards. Schematically

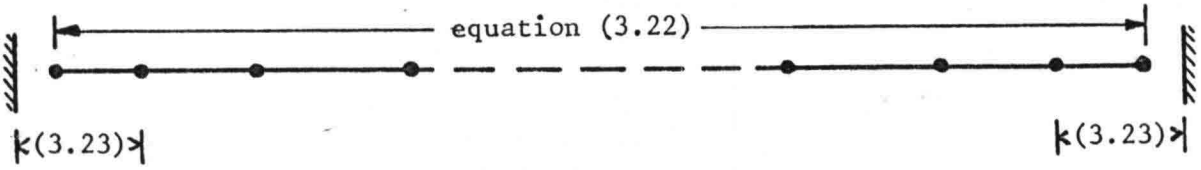

In figure 4 the results of this depth-averaged computation, the details of which are given in Appendix A, are compared with experimental data for a narrow, smooth-walled pipe (TRACY, 1965; height/width = 6.4; C $\simeq$ 60 $m^{\frac{1}{2}}/s$)

and with experimental data as well as computational results*) for a shallow rough-walled open channel (RODI, 1978; depth/width ≈ 1/30; $C \approx 20\ m^{\frac{1}{2}}/s$). The differences between the measured and the predicted depth-averaged velocities occur within a distance d from the sidewalls, but even there these differences, which are likely to arise mainly from the secondary flow due to the transverse anisotropy of turbulence in this non-circular conduit (GESSNER AND JONES, 1965; TRACY, 1965; GERARD, 1978), never exceed 15% of the overall mean velocity. In addition, only very small differences are found between the present results and those obtained by the depth-averaged k-ε-model.
Regarding this positive result, a generalized version of the turbulence model used here will be applied in the curved flow computations.
The turbulence viscosity in this generalized model is described by

$$a = -6 \frac{C}{\sqrt{g}} U_\tau \zeta(1+\zeta) \tag{3.24}$$

, in which U_τ denotes the resultant bed friction velocity. The velocity distribution near the bottom is assumed to be given by

$$u_{res}\Big|_{\zeta \leq -1+\delta} = \frac{U_\tau}{\kappa} \{\frac{\kappa C}{\sqrt{g}} + 1 + \ln(1+\zeta)\} \tag{3.25}$$

, u_{res} denoting the resultant velocity parallel to the bottom. If the bottom is horizontal, this condition can be split up into

$$u\Big|_{\zeta \leq -1+\delta} = \frac{u_\tau}{\kappa} \{\frac{\kappa C}{\sqrt{g}} + 1 + \ln(1+\zeta)\} \tag{3.26}$$

$$v\Big|_{\zeta \leq -1+\delta} = \frac{v_\tau}{\kappa} \{\frac{\kappa C}{\sqrt{g}} + 1 + \ln(1+\zeta)\} \tag{3.27}$$

, where u_τ and εv_τ are the longitudinal and the transverse component of U_τ, respectively. These components are determined from additional conditions obtained by assuming an overlap of the region where (3.25)

---

*) From a mathematical model based on a depth-averaged version of the k-ε-model (RASTOGI AND RODI, 1978; RODI, 1978).

holds good and the region where u and v must be solved from the system of differential equations (see also Appendix B).
The velocity distributions near the sidewalls are generalized to

$$u\Big|_{\xi \leq -B/2d+\delta_l} = \frac{u_{\tau l}}{\kappa}\left\{\frac{\kappa C}{g} + 1 + \ln\left(\frac{B}{2d} + \xi\right)\right\} \tag{3.28}$$

$$w\Big|_{\xi \leq -B/2d+\delta_l} = \frac{w_{\tau l}}{\kappa}\left\{\frac{\kappa C}{\sqrt{g}} + 1 + \ln\left(\frac{B}{2d} + \xi\right)\right\} \tag{3.29}$$

$$u\Big|_{\xi \geq B/2d-\delta_r} = -\frac{u_{\tau r}}{\kappa}\left\{\frac{\kappa C}{\sqrt{g}} + 1 + \ln\left(\frac{B}{2d} - \xi\right)\right\} \tag{3.30}$$

$$w\Big|_{\xi \geq B/2d-\delta_r} = -\frac{w_{\tau r}}{\kappa}\left\{\frac{\kappa C}{\sqrt{g}} + 1 + \ln\left(\frac{B}{2d} - \xi\right)\right\} \tag{3.31}$$

, where $u_{\tau l}$ and $\varepsilon w_{\tau l}$ are the longitudinal and the vertical component of the friction velocity at the left wall and $u_{\tau r}$ and $\varepsilon w_{\tau r}$ are the components at the right wall.
Averaging (3.28) and (3.29) over the depth of flow yields the following generalization of (3.23):

$$\bar{u}\Big|_{\xi \leq -B/2d+\delta_l} = \frac{\bar{u}_{\tau l}}{\kappa}\left\{\frac{\kappa C}{\sqrt{g}} + 1 + \ln\left(\frac{B}{2d} + \xi\right)\right\} \tag{3.32}$$

$$\bar{u}\Big|_{\xi \geq B/2d-\delta_r} = -\frac{\bar{u}_{\tau r}}{\kappa}\left\{\frac{\kappa C}{\sqrt{g}} + 1 + \ln\left(\frac{B}{2d} - \xi\right)\right\} \tag{3.33}$$

The wall friction velocities $\bar{u}_{\tau l}$ and $\bar{u}_{\tau r}$ are determined from additional conditions obtained in the same way as in the case of straight channel flow discussed before.
The wall function approximations used for the velocities parallel to the fixed boundaries of the flow have implications for the velocities normal to these boundaries, as well. The equation of continuity in the bottom layer,

for instance, can be elaborated using (3.26) and (3.27) to yield an expression for the vertical derivative of w, which can be integrated to

$$w\Big|_{\zeta \leq -1+\delta} = -\frac{1}{\kappa}\left(\frac{\partial v_\tau}{\partial \xi} + \frac{\varepsilon}{r} v_\tau + \frac{1}{r}\frac{\partial u_\tau}{\partial \phi}\right)(1+\zeta)\left\{\frac{\kappa C}{\sqrt{g}} + \ln(1+\zeta)\right\} \tag{3.34}$$

Similarly, the radial velocity in the sidewall layers is given by

$$v\Big|_{\xi \leq -B/2d+\delta_l} \simeq -\frac{1}{\kappa}\left(\frac{1}{r}\frac{\partial u_{\tau l}}{\partial \phi} + \frac{\partial w_{\tau l}}{\partial \zeta}\right)\left(\frac{B}{2d}+\xi\right)\left\{\frac{\kappa C}{\sqrt{g}} + \ln\left(\frac{B}{2d}+\xi\right)\right\} \tag{3.35}$$

$$v\Big|_{\xi \geq B/2d-\delta_r} \simeq -\frac{1}{\kappa}\left(\frac{1}{r}\frac{\partial u_{\tau r}}{\partial \phi} + \frac{\partial w_{\tau r}}{\partial \zeta}\right)\left(\frac{B}{2d}-\xi\right)\left\{\frac{\kappa C}{\sqrt{g}} + \ln\left(\frac{B}{2d}-\xi\right)\right\} \tag{3.36}$$

The shear stresses at the fixed boundaries of the flow are related to the wall friction velocities through the definition

$$u_{\tau_{res}} = \left|\tau_{res}\right|^{\frac{1}{2}} \operatorname{sign}(\tau_{res}) \tag{3.37}$$

On the other hand the shear stress components are related to the corresponding components of the rate of strain through the eddy viscosity. The bottom shear stress components, for instance, follow from

$$\tau_{b\phi} = \lim_{\zeta \downarrow -1} \frac{a}{Re_0}\frac{\partial u}{\partial \zeta} \quad ; \qquad \tau_{b\xi} = \lim_{\zeta \downarrow -1} \frac{a}{Re_0}\frac{\partial v}{\partial \zeta} \tag{3.38}$$

These expressions can be elaborated using (3.24), (3.26) and (3.27), to yield

$$\tau_{b\phi} = U_\tau u_\tau; \quad \tau_{b\xi} = U_\tau v_\tau \quad \text{and hence} \quad \tau_{b_{res}} = U_\tau^2 \ (U_\tau > 0) \tag{3.39}$$

, which is in accordance with (3.37).
The shear stresses at the left wall can be determined in a similar way. Assuming a in the wall region to increase linearly with the distance to the wall.

$$a\Big|_{\xi \leq -B/2d+\delta_1} = \kappa U_{\tau 1} \left(\frac{B}{2d} + \xi\right) Re_0 \qquad (U_{\tau 1} > 0) \tag{3.40}$$

, in which $U_{\tau 1}$ is the resultant wall friction velocity, these shear stresses are given by

$$\tau_{1\phi} = \lim_{\xi \downarrow -B/2d} \frac{a}{Re_0} \frac{\partial u}{\partial \xi} = U_{\tau 1} u_{\tau 1}; \quad \tau_{1\zeta} = \lim_{\xi \downarrow -B/2d} \frac{a}{Re_0} \frac{\partial w}{\partial \xi} = U_{\tau 1} w_{\tau 1} \tag{3.41}$$

Similarly, the shear stresses at the right wall are

$$\tau_{r\phi} = |U_{\tau r}| u_{\tau r} \quad \text{and} \quad \tau_{r\zeta} = |U_{\tau r}| w_{\tau r} \qquad (U_{\tau r} < 0) \tag{3.42}$$

Both (3.41) and (3.42) are consistent with (3.37).

4. Simplification

The normalized system (2.16) through (2.22) will be simplified using the experience gained in the development of the laminar flow model (DE VRIEND, 1978b). The simplifying assumptions that have proved to be applicable in case of laminar flow are supposed to hold for turbulent flow, as well. As in the laminar flow case, the applicability of these assumptions will be verified in a later stage.

4.1. Main and secondary flow; equation of continuity

To allow for the simplifications to be carried out, a main and a secondary flow are distinguished. The main flow is defined such, that its horizontal component is the component of the velocity in the direction of the streamlines of the depth-averaged flow, to be called "streamwise direction" hereafter (see figure 5). The secondary flow is defined in planes normal to this streamwise direction.
According to this definition, the vertical distribution of the main flow may vary in the streamwise direction. Consequently, the main flow may have a non-zero vertical component. In accordance with the laminar flow case, where it was shown to be negligible, this vertical component of the main velocity is neglected. Then the following separation between the main and the secondary flow can be made

$$u = u_m + \varepsilon^2 u_s; \quad v = v_m + v_s; \quad w = w_s \tag{4.1}$$

so that

$$\frac{1}{r}\frac{\partial u_m}{\partial \phi} + \frac{\partial v_m}{\partial \xi} + \frac{\varepsilon}{r} v_m = 0 \tag{4.2}$$

$$\frac{\varepsilon^2}{r}\frac{\partial u_s}{\partial \phi} + \frac{\partial v_s}{\partial \xi} + \frac{\varepsilon}{r} v_s + \frac{\partial w_s}{\partial \zeta} = 0 \tag{4.3}$$

Thus the equations of continuity for the main and the secondary flow are separated.

As terms being an order $0(\varepsilon^2)$ smaller than the leading terms of the same type in the same equation will be neglected in the present model, the first term of equation (4.3) can be omitted to yield

$$\frac{\partial v_s}{\partial \xi} + \frac{\varepsilon}{r} v_s + \frac{\partial w_s}{\partial \zeta} = 0 \tag{4.4}$$

4.2. Simplification of the momentum equations

Substituting definition (4.1) into the normalized momentum equations (2.17) through (2.19) and neglecting terms being an order $0(\varepsilon^2)$ smaller than the leading terms of the same type in the same equation, these momentum equations are reduced to

$$\varepsilon Re_0 \left(\frac{u_m}{r}\frac{\partial u_m}{\partial \phi} + v_m \frac{\partial u_m}{\partial \xi} + \frac{\varepsilon}{r} v_m u_m + v_s \frac{\partial u_m}{\partial \xi} + w_s \frac{\partial u_m}{\partial \zeta} + \frac{\varepsilon}{r} v_s u_m\right) =$$

$$- \frac{1}{r}\frac{\partial p}{\partial \phi} + a\nabla_1^2 u_m + \frac{\partial a}{\partial \xi}\left(\frac{\partial u_m}{\partial \xi} - \frac{\varepsilon}{r} u_m\right) + \frac{\partial a}{\partial \zeta}\frac{\partial u_m}{\partial \zeta} \tag{4.5}$$

$$\varepsilon^3 Re_0 \left(\frac{u_m}{r}\frac{\partial v_m}{\partial \phi} + v_m \frac{\partial v_m}{\partial \xi} + v_s \frac{\partial v_m}{\partial \xi} + w_s \frac{\partial v_m}{\partial \zeta} + \frac{u_m}{r}\frac{\partial v_s}{\partial \phi} + v_m \frac{\partial v_s}{\partial \xi} + v_s \frac{\partial v_s}{\partial \xi} + w_s \frac{\partial v_s}{\partial \zeta}\right) +$$

$$- \varepsilon^2 Re_0 \frac{u_m^2}{r} = - \frac{\partial p}{\partial \xi} + \varepsilon^2 a\left(\nabla_1^2 v_m + \nabla_1^2 v_s - 2\frac{\varepsilon}{r^2}\frac{\partial u_m}{\partial \phi}\right) + \frac{\varepsilon^2}{r}\frac{\partial a}{\partial \phi}\left(\frac{\partial u_m}{\partial \xi} - \frac{\varepsilon}{r} u_m\right) +$$

$$+ 2\varepsilon^2 \frac{\partial a}{\partial \xi}\left(\frac{\partial v_m}{\partial \xi} + \frac{\partial v_s}{\partial \xi}\right) + \varepsilon^2 \frac{\partial a}{\partial \zeta}\left(\frac{\partial v_m}{\partial \zeta} + \frac{\partial v_s}{\partial \zeta} + \frac{\partial w_s}{\partial \xi}\right) \tag{4.6}$$

$$\varepsilon^3 Re_0 \left(\frac{u_m}{r}\frac{\partial w_s}{\partial \phi} + v_m \frac{\partial w_s}{\partial \xi} + v_s \frac{\partial w_s}{\partial \xi} + w_s \frac{\partial w_s}{\partial \zeta}\right) = - \frac{\partial p}{\partial \zeta} + \varepsilon^2 a\nabla_1^2 w_s + \frac{\varepsilon^2}{r}\frac{\partial a}{\partial \phi}\frac{\partial u_m}{\partial \zeta} +$$

$$+ \varepsilon^2 \frac{\partial a}{\partial \xi}\left(\frac{\partial v_m}{\partial \zeta} + \frac{\partial v_s}{\partial \zeta} + \frac{\partial w_s}{\partial \xi}\right) + 2\varepsilon^2 \frac{\partial a}{\partial \zeta}\frac{\partial w_s}{\partial \zeta} \tag{4.7}$$

in which $\nabla_1^2 = \frac{\partial^2}{\partial\zeta^2} + \frac{\partial^2}{\partial\xi^2} + \frac{\varepsilon}{r}\frac{\partial}{\partial\xi}$

According to the conclusions drawn from the investigations of fully developed and developing laminar flow, the transverse inertia of the secondary flow, i.e. the terms with

$$v_s \frac{\partial v_s}{\partial\xi}, \quad w_s \frac{\partial v_s}{\partial\zeta}, \quad v_s \frac{\partial w_s}{\partial\xi}, \quad w_s \frac{\partial w_s}{\partial\zeta}$$

in equations (4.6) and (4.7) can be neglected (DE VRIEND, 1978a), but the streamwise inertia, i.e. the terms with

$$\frac{u_m}{r}\frac{\partial v_s}{\partial\phi}, \quad v_m \frac{\partial v_s}{\partial\xi}, \quad \frac{u_m}{r}\frac{\partial w_s}{\partial\phi}, \quad v_m \frac{\partial w_s}{\partial\xi}$$

must be retained (DE VRIEND, 1978b). Hence the transverse momentum equations can be simplified to

$$\varepsilon^3 Re_0 \left(\frac{u_m}{r}\frac{\partial v_m}{\partial\phi} + v_m \frac{\partial v_m}{\partial\xi} + v_s \frac{\partial v_m}{\partial\xi} + w_s \frac{\partial v_m}{\partial\zeta} + \frac{u_m}{r}\frac{\partial v_s}{\partial\phi} + v_m \frac{\partial v_s}{\partial\xi}\right) +$$

$$- \varepsilon^2 Re_0 \frac{u_m^2}{r} = -\frac{\partial p}{\partial\xi} + \varepsilon^2 a\left(\nabla_1^2 v_m + \nabla_1^2 v_s - 2\frac{\varepsilon}{r^2}\frac{\partial u_m}{\partial\phi}\right) + \frac{\varepsilon^2}{r}\frac{\partial a}{\partial\phi}\left(\frac{\partial u_m}{\partial\xi} - \frac{\varepsilon}{r}u_m\right) +$$

$$+ 2\varepsilon^2 \frac{\partial a}{\partial\xi}\left(\frac{\partial v_m}{\partial\xi} + \frac{\partial v_s}{\partial\xi}\right) + \varepsilon^2 \frac{\partial a}{\partial\zeta}\left(\frac{\partial v_m}{\partial\zeta} + \frac{\partial v_s}{\partial\zeta} + \frac{\partial w_s}{\partial\xi}\right) \qquad (4.8)$$

$$\varepsilon^3 Re_0 \left(\frac{u_m}{r}\frac{\partial w_s}{\partial\phi} + v_m \frac{\partial w_s}{\partial\xi}\right) = -\frac{\partial p}{\partial\zeta} + \varepsilon^2 a\nabla_1^2 w_s + \frac{\varepsilon^2}{r}\frac{\partial a}{\partial\phi}\frac{\partial u_m}{\partial\zeta} +$$

$$+ \varepsilon^2 \frac{\partial a}{\partial\xi}\left(\frac{\partial v_m}{\partial\zeta} + \frac{\partial v_s}{\partial\zeta} + \frac{\partial w_s}{\partial\xi}\right) + 2\varepsilon^2 \frac{\partial a}{\partial\zeta}\frac{\partial w_s}{\partial\zeta} \qquad (4.9)$$

4.3. Transformation to streamwise coordinates

In order to gain more insight into the system of differential equations, a transformation to the stream-oriented curvilinear coordinate system (n, s, ζ) is carried out. Herein s denotes the distance, normalized by R_c, along the streamlines of the depth-averaged flow and n denotes the distance, normalized by d, along the normal lines of the depth-averaged flow*).

If $\tilde{u}_m$ and $\tilde{v}_m + \tilde{v}_s$ are the horizontal velocity components in s- and n-direction, respectively, $\tilde{v}_m$ is identically equal to zero by definition. Then the transformation of the equations of continuity (4.2) and (4.4) and the momentum equations (4.5), (4.8) and (4.9) leads to

$$\frac{\partial \tilde{u}_m}{\partial s} - \frac{\tilde{u}_m}{r_n} = 0 \tag{4.10}$$

$$\frac{\partial \tilde{v}_s}{\partial n} - \frac{\varepsilon}{r_s}\tilde{v}_s + \frac{\partial w_s}{\partial \zeta} = 0 \tag{4.11}$$

$$\varepsilon Re_0 \left(\tilde{u}_m \frac{\partial \tilde{u}_m}{\partial s} + \tilde{v}_s \frac{\partial \tilde{u}_m}{\partial n} - \frac{\varepsilon}{r_s}\tilde{v}_s \tilde{u}_m + w_s \frac{\partial \tilde{u}_m}{\partial \zeta}\right) = -\frac{\partial p}{\partial s} + a\nabla_2^2 \tilde{u}_m +$$

$$+ \frac{\partial a}{\partial n}\left(\frac{\partial \tilde{u}_m}{\partial n} + \varepsilon \frac{\tilde{u}_m}{r_s}\right) + \frac{\partial a}{\partial \zeta}\frac{\partial \tilde{u}_m}{\partial \zeta} \tag{4.12}$$

$$\varepsilon^3 Re_0 \tilde{u}_m \frac{\partial \tilde{v}_s}{\partial s} + \varepsilon^2 Re_0 \frac{\tilde{u}_m^2}{r_s} = -\frac{\partial p}{\partial n} + \varepsilon^2 a\left(\nabla_2^2 \tilde{v}_s + \frac{\partial \tilde{\omega}_m}{\partial s}\right) +$$

$$+ 2\varepsilon^2 \frac{\partial a}{\partial n}\left(\frac{\partial \tilde{v}_s}{\partial n} - \frac{\tilde{u}_m}{r_n}\right) + \varepsilon^2 \frac{\partial a}{\partial \zeta}\left(\frac{\partial \tilde{v}_s}{\partial \zeta} + \frac{\partial w_s}{\partial n}\right) + \varepsilon^2 \frac{\partial a}{\partial s}\left(-\tilde{\omega}_m + 2\frac{\varepsilon}{R_s}\tilde{u}_m\right) \tag{4.13}$$

$$\varepsilon^3 Re_0 \tilde{u}_m \frac{\partial w_s}{\partial s} = -\frac{\partial p}{\partial \zeta} + \varepsilon^2 a\nabla_2^2 w_s + \varepsilon^2 \frac{\partial a}{\partial n}\left(\frac{\partial \tilde{v}_s}{\partial \zeta} + \frac{\partial w_s}{\partial n}\right) + 2\varepsilon^2 \frac{\partial a}{\partial \zeta}\frac{\partial w_s}{\partial \zeta} + \varepsilon^2 \frac{\partial a}{\partial s}\frac{\partial u_m}{\partial \zeta} \tag{4.14}$$

*) s increases in the main flow direction, n from the left bank on (see also figure 5).

in which $\nabla_2^2 = \frac{\partial^2}{\partial \zeta^2} + \frac{\partial^2}{\partial n^2} - \frac{\varepsilon}{r_s}\frac{\partial}{\partial n}$ and $\tilde{\omega}_m = -\frac{\partial \tilde{u}_m}{\partial n} + \frac{\varepsilon}{r_s}\tilde{u}_m$

and where $1/r_s$ and $1/r_n$ denote the curvature, normalized by $1/R_c$, of the streamlines and the normal lines, respectively*).
These transformed equations are very similar to those for laminar flow (DE VRIEND, 1978b), as was to be expected. The only difference lies in some additional terms due to the variation of the eddy viscosity.
The transformation hardly affects most of the equations; only the "radial" momentum equation is simplified considerably. It becomes evident from the transformed equation (4.13), in combination with (4.14), that the sources of secondary flow are the main flow curvature and, to a much lower extent, the streamwise variation of the main flow vorticity.

4.4. Similarity approximation

A similarity approximation for the main and the secondary flow has proved to be most effective in computations of laminar flow in curved shallow channels (DE VRIEND, 1978a and 1978b). As measurements in turbulent flow suggest such a similarity approximation to be applicable to turbulent flow, as well (DE VRIEND AND KOCH, 1977 and 1978), the main velocity is approximated by

$$u_m = \bar{u}_m f(\zeta) \quad \text{and} \quad v_m = \bar{v}_m f(\zeta) \tag{4.15}$$

Regarding the equation of continuity (4.4), the secondary flow must have a

*) The curvature of a horizontal coordinate line is taken positive when the outward normal of this line is directed opposite to the positive direction of the other horiozontal coordinate line. In other words: the curvature of a normal line is positive when the streamlines converge and the streamline curvature is positive when the normal lines converge.

scalar stream function ψ', which can be defined by *)

$$v_s = -\frac{1}{r}\frac{\partial\psi'}{\partial\zeta} \quad \text{and} \quad w_s = \frac{1}{r}\frac{\partial\psi'}{\partial\xi} \tag{4.16}$$

As the scalefactor of the main source term of the secondary flow (viz. the centrifugal term in equation (4.13)) is proportional to Re_0, it is obvious to define a stream function $\psi = \psi'/Re_0$ instead of ψ', so that

$$v_s = -\frac{Re_0}{r}\frac{\partial\psi}{\partial\zeta} \quad \text{and} \quad w_s = \frac{Re_0}{r}\frac{\partial\psi}{\partial\xi} \tag{4.17}$$

Accordingly, the similarity approximation for the secondary flow reads

$$\psi = \bar{\psi}\, g(\zeta); \quad v_s = -\frac{Re_0}{r}\bar{\psi}\frac{\partial g}{\partial\zeta}; \quad w_s = \frac{Re_0}{r}\frac{\partial\bar{\psi}}{\partial\xi}\, g(\zeta) \tag{4.18}$$

Substitution of (4.15) and (4.18) into the ϕ-wise momentum equation (4.5) yields

$$\begin{aligned}
&\varepsilon Re_0 f^2 \left(\frac{\bar{u}}{r}\frac{\partial\bar{u}}{\partial\phi} + \bar{v}\frac{\partial\bar{u}}{\partial\xi} + \frac{\varepsilon}{r}\overline{\overline{uv}}\right) + \varepsilon Re_0^2 \left\{- f\frac{\partial g}{\partial\zeta}\frac{\bar{\psi}}{r}\left(\frac{\partial\bar{u}}{\partial\xi} + \frac{\varepsilon}{r}\bar{u}\right) + \right. \\
&\left. + g\frac{\partial f}{\partial\zeta}\frac{\bar{u}}{r}\frac{\partial\bar{\psi}}{\partial\xi}\right\} = -\frac{1}{r}\frac{\partial p}{\partial\phi} + \bar{u}\, U_\tau \left(a''\frac{\partial^2 f}{\partial\zeta^2} + \frac{\partial a''}{\partial\zeta}\frac{\partial f}{\partial\zeta}\right) + \\
&+ a'' f \left\{U_\tau \left(\frac{\partial^2\bar{u}}{\partial\xi^2} + \frac{\varepsilon}{r}\frac{\partial\bar{u}}{\partial\xi}\right) + \frac{\partial U_\tau}{\partial\xi}\left(\frac{\partial\bar{u}}{\partial\xi} - \frac{\varepsilon}{r}\bar{u}\right)\right\}
\end{aligned} \tag{4.19}$$

*) There are other possibilities, but this is the only one in which lines of constant ψ' represent streamlines of the secondary flow (see also DE VRIEND, 1978a and b).

, in which $a'' = a/U_\tau = -6\,C\,g^{-\frac{1}{2}}\,\zeta(1+\zeta)$.

This equation shows that, as in the case of laminar flow, the importance of the secondary flow advection terms in the main flow equations is indicated by the factor εRe_0^2, i.e. by the square of the Dean number $De_0 = Re_0\sqrt{\varepsilon}$.

5. Solution procedure

The mathematical system to be solved in order to compute steady turbulent flow in a curved channel of shallow rectangular cross-section consists of the two equations of continuity (4.2) and (4.4) and the momentum equations (4.5), (4.8) and (4.9), combined with a given distribution of the eddy viscosity (3.24), the integral condition of continuity (2.20), the boundary conditions (2.21) and (2.22) and a number of inflow and outflow conditions to be discussed later. This fairly complex system of non-linear differential equations requires an iterative solution procedure, the most important elements of which will be discussed in the present chapter. An overall review of the procedure is given in section 5.6.

5.1. Vertical distribution of the main velocity

In view of the experience with similar computations for laminar flow (DE VRIEND, 1978b), the similarity approximation for the main flow (4.15) is adopted for the main flow computation. After this computation has been completed, the vertical distribution of the main flow and the bed shear stress will be corrected for the influence of streamwise accelerations varying over the cross-section.
Adopting the similarity approximations (4.15) and (4.18) for the main and the secondary flow and neglecting terms being an order $O(\varepsilon^2)$ smaller than the leading terms of the same type, the ϕ-wise momentum equation (4.19) can be rewritten into an equation for f:

$$\bar{u}\, u_\tau\, a''\, \frac{\partial^2 f}{\partial \zeta^2} + \{\bar{u}\, u_\tau\, \frac{\partial a''}{\partial \zeta} - \varepsilon Re_0^2\, \frac{\bar{u}}{r}\, \frac{\partial \bar{\psi}}{\partial \xi}\, g\}\, \frac{\partial f}{\partial \zeta} - \varepsilon Re_0\, (\frac{\bar{u}}{r}\, \frac{\partial \bar{u}}{\partial \phi} + \bar{v}\, \frac{\partial \bar{u}}{\partial \xi} + \frac{\varepsilon}{r}\, \overline{\bar{u}\bar{v}})f^2$$

$$+ \left[\varepsilon Re_0^2\, \frac{\bar{\psi}}{r}\, (\frac{\partial \bar{u}}{\partial \xi} + \frac{\varepsilon}{r}\, \bar{u})\, \frac{\partial g}{\partial \zeta} + \{u_\tau (\frac{\partial^2 \bar{u}}{\partial \xi^2} + \frac{\varepsilon}{r}\, \frac{\partial \bar{u}}{\partial \xi}) + \frac{\partial u_\tau}{\partial \xi}\, (\frac{\partial \bar{u}}{\partial \xi} - \frac{\varepsilon}{r}\, \bar{u})\}a''\right] f$$

$$= \frac{1}{r}\, \frac{\partial p}{\partial \phi} \qquad (5.1)$$

The main flow inertia term in this equation can be linearized by setting

$$f^2 \simeq \hat{f} f \tag{5.2}$$

, in which $\hat{f}$ is a known estimate of f (for example: the distribution found in the foregoing iteration step). Then equation (5.1) can be considered as an ordinary second-order linear differential equation for f as a function of ζ that can be solved of $\bar{u}$, u_τ, $\bar{v}$, $\bar{\psi}$ $\hat{f}$, g and the tangential pressure gradient are known.
The relevant boundary conditions, to be derived from (2.21) and (3.26)-(3.27), are

$$\alpha'' \frac{\partial f}{\partial \zeta} = 0 \quad \text{at} \quad \zeta = 0 \tag{5.3}$$

$$f = k_m\left(1 + \frac{\sqrt{g}}{\kappa C} + \frac{\sqrt{g}}{\kappa C} \ln \delta_0\right) \quad \text{at} \quad \zeta = -1+\delta_0 \tag{5.4}$$

, in which δ_0 is a small normalized distance to the bottom, within the range of validity of the wall function approximations (3.26) and (3.27). The constant k_m is related to the ratio of the friction velocity and the depth-averaged velocity through

$$k_m = \frac{C}{\sqrt{g}} \frac{u_\tau}{\bar{u}} = \frac{C}{\sqrt{g}} \frac{v_\tau}{\bar{v}} \tag{5.5}$$

This constant is determined from the additional condition (see chapter 3)

$$f = k_m \left\{1 + \frac{\sqrt{g}}{\kappa C} + \frac{\sqrt{g}}{\kappa C} \ln(1 + \zeta_1)\right\} \quad \text{at} \quad \zeta = \zeta_1 \tag{5.6}$$

, ζ_1 denoting the vertical coordinate of the grid point that lies nearest but one to the bottom.

Making use of the proportionality between u_τ and $\bar{u}$ (see equation 5.5), equation (5.1) can be reformulated as

$$\tilde{k}_m \bar{u}^2 a' \frac{\partial^2 f}{\partial \zeta^2} + \{\tilde{k}_m \bar{u}^2 \frac{\partial a'}{\partial \zeta} - \varepsilon Re_0^2 \frac{\bar{u}}{r} \frac{\partial \bar{\psi}}{\partial \xi} g\} \frac{\partial f}{\partial \zeta} - \varepsilon Re_0 (\frac{\bar{u}}{r} \frac{\partial \bar{u}}{\partial \phi} + \bar{v} \frac{\partial \bar{u}}{\partial \xi} + \frac{\varepsilon}{r} \overline{\overline{uv}}) f +$$

$$+ \{\varepsilon Re_0^2 \frac{\bar{\psi}}{r} (\frac{\partial \bar{u}}{\partial \xi} + \frac{\varepsilon}{r} \bar{u}) \frac{\partial g}{\partial \zeta} + \tilde{k}_m (\bar{u} \frac{\partial^2 \bar{u}}{\partial \xi^2} + \frac{\partial \bar{u}}{\partial \xi} \frac{\partial \bar{u}}{\partial \xi}) a'\} f = \frac{1}{r} \frac{\partial p}{\partial \phi} \qquad (5.7)$$

, where $a' = -6\zeta\ (1+\zeta)$ and $\tilde{k}_m$ is a known estimate of k_m. The details of the solution procedure for f and k_m are given in Appendix B. Once the constant k_m is known, the components of the bed shear stress due to the main flow follow from

$$\tau_{b\phi_m} = \frac{g}{C^2} k_m^2 \bar{u}^2 \qquad \text{and} \qquad \tau_{b\xi_m} = \frac{g}{C^2} k_m^2 \overline{\overline{uv}} \qquad (5.8)$$

These relations between the bed shear stress and the depth-averaged velocity are needed in the depth-averaged momentum equations for the main flow to be derived in the next section.

5.2. Depth-averaged main velocity field: mathematical system

The tangential and radial momentum equations (4.5) and (4.8) can be averaged over the depth of flow, making use of the similarity approximations (4.15) and (4.18) and assuming the pressure to be hydrostatic, in accordance with the results of the investigations of fully developed curved laminar flow (DE VRIEND, 1978a). This yields

$$\varepsilon Re_0 \overline{f^2} (\frac{\bar{u}}{r} \frac{\partial \bar{u}}{\partial \phi} + \bar{v} \frac{\partial \bar{u}}{\partial \xi} + \frac{\varepsilon}{r} \overline{\overline{uv}}) + \varepsilon Re_0^2 \{-f \overline{\frac{\partial g}{\partial \zeta}} \frac{\bar{\psi}}{r} (\frac{\partial \bar{u}}{\partial \xi} + \frac{\varepsilon}{r} \bar{u}) + \overline{g \frac{\partial f}{\partial \zeta}} \frac{\bar{u}}{r} \frac{\partial \bar{\psi}}{\partial \xi}\} =$$

$$- \frac{1}{r} \frac{\partial p}{\partial \phi} - k_m \bar{u}^2 (a' \frac{\partial f}{\partial \zeta})\Big|_{\zeta=-1} + k_m \overline{a' f} (\bar{u} \frac{\partial^2 \bar{u}}{\partial \xi^2} + \frac{\partial \bar{u}}{\partial \xi} \frac{\partial \bar{u}}{\partial \xi}) \qquad (5.9)$$

and

$$\varepsilon^3 Re_0 \overline{f^2} \left(\frac{\bar{u}}{r}\frac{\partial \bar{v}}{\partial \phi} + \bar{v}\frac{\partial \bar{v}}{\partial \xi}\right) - \varepsilon Re_0 \overline{f^2}\frac{\bar{u}^2}{r} + \varepsilon^3 Re_0^2 \left(-f\overline{\frac{\partial g}{\partial \zeta}}\frac{\bar{\psi}}{r}\frac{\partial \bar{v}}{\partial \xi} + \overline{g\frac{\partial f}{\partial \zeta}}\frac{\bar{v}}{r}\frac{\partial \bar{\psi}}{\partial \xi}\right) =$$

$$-\frac{\partial p}{\partial \xi} - \varepsilon^2 k_m \overline{uv}\left(a'\frac{\partial f}{\partial \zeta}\right)\Big|_{\zeta=-1} + \varepsilon^2 k_m \overline{a'f}\left\{\bar{u}\frac{\partial^2 \bar{v}}{\partial \xi^2} + \frac{\partial \bar{u}}{\partial \xi}\frac{\partial \bar{v}}{\partial \xi} + 5\frac{\varepsilon}{r}\bar{u}\frac{\partial \bar{v}}{\partial \xi} + \right.$$

$$\left. - \frac{\varepsilon}{r}\bar{v}\frac{\partial \bar{u}}{\partial \xi}\right\} + \text{other terms} \qquad (5.10)$$

, in which the "other terms" are of the order $0(\varepsilon^2, \varepsilon^3 Re_0^2)$ and concern the secondary flow. They are neglected in the main flow computation. It should be noted that for the present parabolic distribution of the eddy viscosity the factor $\left(a'\frac{\partial f}{\partial \zeta}\right)\Big|_{\zeta=-1}$ in these equations follows from

$$\left(a'\frac{\partial f}{\partial \zeta}\right)\Big|_{\zeta=-1} = 6\, k_m \frac{\sqrt{g}}{\kappa C} \simeq \frac{6}{\kappa}\left(\frac{\tau_b}{\bar{u}^2}\right)^{\frac{1}{2}} \qquad (5.11)$$

Together with the depth-averaged equation of continuity

$$\frac{1}{r}\frac{\partial \bar{u}}{\partial \phi} + \frac{\partial \bar{v}}{\partial \xi} + \frac{\varepsilon}{r}\bar{v} = 0 \qquad (5.12)$$

equations (5.9) and (5.10) form a system of three partial differential equations, from which the unknown quantities $\bar{u}$, $\bar{v}$ and p can be solved if an appropriate set of boundary conditions is given.
The boundary conditions imposed on the velocity components near the side-walls are based on the wall function approximations discussed in chapter 3. Hence

$$\bar{u} = \frac{\bar{u}_{\tau l}}{\kappa}\left(\frac{\kappa C}{\sqrt{g}} + 1 + \ln \delta_l\right) \qquad \text{at} \qquad \xi = -\frac{B}{2d} + \delta_l \qquad (5.13)$$

$$\bar{u} = -\frac{\bar{u}_{\tau r}}{\kappa}\left(\frac{\kappa C}{\sqrt{g}} + 1 + \ln \delta_l\right) \qquad \text{at} \qquad \xi = \frac{B}{2d} - \delta_l \qquad (5.14)$$

, where δ_1 is a small normalized wall distance within the domain of validity of the wall functions (3.32) and (3.33). The additional conditions used to determine the wall friction velocities $\bar{u}_{\tau 1}$ and $\bar{u}_{\tau r}$ read

$$\bar{u} = \frac{\bar{u}_{\tau 1}}{\kappa} \{\frac{\kappa C}{\sqrt{g}} + 1 + \ln (\frac{B}{2d} + \xi_1)\} \qquad \text{at } \xi = \xi_1 \tag{5.15}$$

$$\bar{u} = - \frac{\bar{u}_{\tau r}}{\kappa} \{\frac{\kappa C}{\sqrt{g}} + 1 + \ln (\frac{B}{2d} - \xi_2)\} \quad \text{at } \xi = \xi_2 \tag{5.16}$$

, in which ξ_1 and ξ_2 are the transverse coordinates of the nodal points nearest but one to the sidewalls. The sidewall conditions for $\bar{v}$ can be derived from (3.35) and (3.36), taking account of the simplifications introduced in section 4.1. This leads to

$$\bar{v} = - \frac{1}{r} \frac{\partial \bar{u}_{\tau 1}}{\partial \phi} \frac{\delta_1}{\kappa} (\frac{\kappa C}{\sqrt{g}} + \ln \delta_1) \qquad \text{at} \qquad \xi = - \frac{B}{2d} + \delta_1 \tag{5.17}$$

$$\bar{v} = - \frac{1}{r} \frac{\partial \bar{u}_{\tau r}}{\partial \phi} \frac{\delta_1}{\kappa} (\frac{\kappa C}{\sqrt{g}} + \ln \delta_1) \qquad \text{at} \qquad \xi = \frac{B}{2d} - \delta_1 \tag{5.18}$$

At the inflow boundary the longitudinal velocity distribution must be given. Although any distribution satisfying the boundary conditions at the sidewalls could be used, this velocity distribution is derived here from the equivalent fully developed straight channel flow, i.e. the channel section considered is assumed to be preceded by an infinitely long straight channel of the same cross-sectional configuration. The depth-averaged velocity distribution in this fully developed straight channel flow can be computed as described in Appendix A.

Depending on the method of solution, inflow or outflow conditions for $\bar{v}$ and boundary conditions for p will be formulated.

5.3. Depth-averaged main velocity field: method of solution

Various computational methods can be applied to solve the depth-averaged flow problem described in section 5.2. One of the methods, similar to the one used in the model of developing curved laminar flow (DE VRIEND, 1978b), is based on the stream function/vorticity concept. This means that the two velocity components $\bar{u}$ and $\bar{v}$ are not computed directly, but are replaced by the stream function Φ, defined by

$$\bar{u} = \frac{\partial \Phi}{\partial \xi} \qquad \text{and} \qquad \bar{v} = -\frac{1}{r}\frac{\partial \Phi}{\partial \phi} \tag{5.19}$$

and the vorticity $\bar{\omega}$, defined by

$$\bar{\omega} = \frac{\varepsilon^2}{r}\frac{\partial \bar{v}}{\partial \phi} - \frac{\partial \bar{u}}{\partial \xi} - \frac{\varepsilon}{r}\bar{u} \tag{5.20}$$

These two quantities are solved from the relationships between Φ and $\bar{\omega}$ to be derived from (5.19) and (5.20)

$$\frac{\partial^2 \Phi}{\partial \xi^2} + \frac{\varepsilon}{r}\frac{\partial \Phi}{\partial \xi} + \frac{\varepsilon^2}{r^2}\frac{\partial^2 \Phi}{\partial \phi^2} = -\bar{\omega} \tag{5.21}$$

and the vorticity transport equation to be derived from the momentum equations (5.9) and (5.10) by eliminating the pressure.
When attempting to apply this method to the present turbulent flow case, the problem of convergence, which was already encountered in the laminar flow model, turns out to be acute here: even if, in accordance with Appendix A, the quantity $\bar{u}_{res}\bar{\omega}$ is solved instead of $\bar{\omega}$, convergence is very poor and the computations are quite expensive or even fail. This deterioration of convergence with respect to the laminar flow model is likely to be caused by the extra degree of freedom in the sidewall boundary conditions: the

velocities at the sidewalls are not strictly prescribed, as in case of laminar flow, but depend on the solution in the relevant cross-section.

A family of computational methods that were applied with success to a great variety of flows in two and three dimensions is based on the solution of the velocity components from the momentum equations with guessed pressure gradients and the correction of the pressure field in such a way that the equation of continuity is satisfied everywhere (PATANKAR AND SPALDING, 1972; PATANKAR, 1975; PRATAP AND SPALDING, 1976; see also RODI a.o., 1978). All computational methods applied so far in three-dimensional models of turbulent flow in curved channels (PRATAP, 1975; PRATAP AND SPALDING, 1975 ; LESCHZINER, 1978) belong to this family, which can be divided into three groups, dealing with

. "parabolic" flows, in which only downstream influencing occurs, i.e. the velocity components and the pressure are only influenced by what happens further upstream (PATANKAR AND SPALDING, 1972),
. "partially-parabolic" flows, in which upstream influencing occurs only through the pressure (PRATAP AND SPALDING, 1976), and
. "elliptic" flows, in which upstream influencing occurs both through longitudinal diffusion and through the pressure (GOSMAN AND PUN, 1973; PATANKAR, 1975).

The character of the partial differential equations, and hence the solution procedure to be applied, is essentially different for these three groups: parabolic flows allow for a much simpler and more economical procedure than partially-parabolic flows, which in turn are easier to be computed than elliptic flows.

In the present case of curved channel flow, the parabolic flow approximation applies to gentle bends only (McGUIRK, 1978), as in sharper bends the pressure will give rise to considerable upstream influencing, especially near the transitions between channel sections of different curvature. If, for instance a straight channel section is followed by a bend, the transverse pressure gradient will start to develop before the bend entrance, as became evident from measurements of the free surface elevation there (ROZOVSKII, 1961; DE VRIEND, 1976) and also from potential flow approximations (BÖSS, 1938). So in sharper bends at least the partially parabolic or, if

flow separation occurs, even the elliptic procedure has to be applied. As flow separation is not included in the present model, the longitudinal diffusion terms in the momentum equations being neglected, the elliptic solution procedure can be left out of consideration. In general, the partially-parabolic method will be used, but in addition it will be investigated to what extent the more ecomonical parabolic procedure is applicable.

The computational procedures actually used in the present model are quite similar to the ones in the original publications (see PATANKAR AND SPALDING (1972) for the parabolic procedure and PRATAP AND SPALDING (1976) for the partially-parabolic one; see also RODI a.o. (1978) for a review of all methods belonging to this family). Therefore only the main outlines and some computational details that differ from the original ones will be treated here.

An important feature of the procedures is the use of a staggered computational grid with $\bar{u}$, $\bar{v}$ and p defined in different points (see figure 6). The finite difference representations of the momentum equations and the equation of continuity are obtained by a formal integration over an elementary area, indicated in figure 6 as $\bar{u}$, $\bar{v}$-, and p-elements, respectively. The coefficients in the non-linear terms of the momentum equations are evaluated using the velocities immediately upstream of the cross-section considered and the transverse velocity gradients remaining after integration of the diffusion terms are approximated using a second order finite difference scheme.

In contrast with the original procedures, the depth-averaged longitudinal component of the friction velocity is not estimated here, but is is made part of the solution of the longitudinal momentum equation (5.9) by adopting the additional conditions (5.15) and (5.16). Appendix C describes how the solution of the system (5.9), (5.13) through (5.16) proceeds. Once the sidewalls friction velocities $\bar{u}_{\tau l}$ and $\bar{u}_{\tau r}$ are known, the boundary conditions (5.17) and (5.18) can be evaluated and $\bar{v}$ can be solved from the transverse momentum equation (5.10).

In general, the velocities calculated from the momentum equations will not exactly satisfy the equations of continuity (5.12). Therefore the pressure field (and hence the velocities) are corrected in such a way, that the conservation of mass is guaranteed. This pressure correction

consists of two parts, one correcting the longitudinal gradient of the cross-sectional mean value of the pressure in order to satisfy the integral condition of continuity

$$\int_{-B/2d}^{B/2d} \bar{u} d\xi = \frac{B}{d} \tag{5.22}$$

, the other one guaranteeing the conservation of mass in each cell on the computational grid.
In each cross-section the longitudinal gradient of the mean pressure, and accordingly $\bar{u}$, are corrected immediately after solving the longitudinal momentum equation. If necessary, the steps of solving the momentum equation and correcting the pressure gradient and $\bar{u}$ are repeated several times before proceeding to the solution of $\bar{v}$.
The local pressure correction is the only point at which the parabolic and the partially-parabolic procedure essentially differ. A most important feature of the parabolic procedure is the "uncoupling" of the longitudinal and the transverse pressure gradients by setting

$$\frac{\partial p}{\partial \phi} \simeq \frac{\partial \bar{p}}{\partial \phi} \tag{5.23}$$

, in which $\bar{p}$ denotes the cross-sectional mean value of p. This makes it possible to calculate $\bar{u}$ and the correction of the mean pressure gradient independently of $\bar{v}$ and the local pressure correction, which serves only for correcting the transverse pressure distribution and $\bar{v}$.
In the partially-parabolic procedure, however, the pressure gradients are not uncoupled: there is only one pressure field determining the longitudinal and the transver pressure gradients. After calculating $\bar{u}$, $\partial\bar{p}/\partial\phi$ and $\bar{v}$ in a certain cross-section, the local conservation of mass is satisfied by correcting the pressure. Now this correction influences not only the transverse gradients of the pressure, but also the longitudinal ones immediately upstream and downstream of the pressure-points considered. Accordingly, not only $\bar{v}$ must be corrected, but also $\bar{u}$ in the $\bar{u}$-points immediately upstream and downstream (see figure 6).

This $\bar{u}$-correction introduces the upstream influence through the pressure, which is characteristic for partially-parabolic flows. As this influence extends over only half a cell, the flow field has to be swept through a number of times until the velocity- and pressure-corrections have become sufficiently small. It is this iterative character that makes the partially-parabolic method less economical than the parabolic one.

The parabolic and partially-parabolic solution procedures described in the foregoing are incorporated in the present model through the following algorithm:

1. Compute the velocity-distribution $\bar{u}_0$ and the longitudinal pressure gradient i_0 for fully developed flow in the equivalent straight channel.
2. Estimate the cross-sectional mean values of the pressure by integrating

$$\frac{\partial \bar{p}}{\partial s} = - i_0 \tag{5.24}$$

along the channel axis.

3. Start marching downstream from cross-section to cross-section; in the j-th cross-section (connecting the points where $\bar{u}_j$ is defined):
4. Estimate the longitudinal and transverse velocity-components by

$$\bar{u}_j = \bar{u}_{j-1}; \quad \bar{v}_j = \bar{v}_{j-1} \quad (\bar{v}_0 = 0) \tag{5.25}$$

5. Estimate the transverse distribution of the pressure p_{j+1} by integrating the truncated version of the transverse momentum equation

$$\left(\frac{\partial p}{\partial s}\right)_{j+1} = - \varepsilon^2 Re_0 \left(\overline{f^2}\, \frac{\bar{u}^2}{r}\right)_j \tag{5.26}$$

, requiring the cross-sectional mean value of p_{j+1} to be equal to the estimated one*).

*) In the partially-parabolic procedure the estimation by (5.26) is carried out in the first sweep only.

6. Solve $\bar{u}_j$ and $\bar{p}_{j+1}$ from the longitudinal momentum equation (5.9) with the boundary conditions (5.13) and (5.14), the additional conditions (5.15) and (5.16) and the integral condition of continuity (5.22). In the original procedures $\bar{u}_j$ is solved from the longitudinal momentum equation and subsequently it is corrected together with the mean pressure gradient in order to satisfy the integral condition of continuity; here the "correct" solutions of $\bar{u}_j$ and $\bar{p}_{j+1}$ are obtained at once (see Appendix C). In order to account for non-linear effects this step can be repeated several times.
7. Solve $\bar{v}_j$ from the transverse momentum equation (5.10) with the boundary conditions (5.17) and (5.18).
8. Ensure continuity in each cell between the cross-sections j and j-1 by correcting either $p_j - \bar{p}_j$ and $\bar{v}_j$ (parabolic case) or p_j, $\bar{v}_j$, $\bar{u}_j$ and $\bar{u}_{j-1}$ (partially-parabolic case).

9. After the entire flow domain has been swept through, the computation is terminated (parabolic case) or the marching procedure 3. through 8. is repeated until a termination criterion is satisfied (partially-parabolic case).

Following a suggestion made by PRATAP (1975), the pressure-corrections in the partially-parabolic procedure are underrelaxed by setting

$$p = \tilde{p} + \alpha \, dp \qquad (5.27$$

, in which $\tilde{p}$ denotes the pressure before correction, dp is the calculated pressure correction and α is a constant between 0 and 1 (here: = 0.5).
If the partially-parabolic procedure described in the foregoing is applied without modifications, the influence of downstream events travels upstream at the rate of only one longitudinal step per sweep through the flow domain. In order to accelerate this process, PRATAP (1975) suggests to apply a weighted part of the pressure correction calculated in any cross-section to the pressures further upstream. So:

$$(p_{j-k})_{new} = (p_{j-k})_{old} + \beta_k \, dp_j \qquad \text{for } 0 < k < j \qquad (5.28$$

, in which β_k decreases as the distance between the cross-sections j and j-k becomes larger. For further details of this additional pressure correction reference is made to the original publication.

5.4. Secondary flow: stream function equation

In view of the experience with a similar model of laminar flow in curved channels (DE VRIEND, 1978b), the computation of the secondary flow will not be simplified when it is part of the main flow calculation procedure. So in any phase of the calculations the secondary flow is determined from the transverse momentum equations (4.8) and (4.9) and the equation of continuity (4.4).
Instead of solving the secondary velocity components themselves, however, the stream function of the secondary flow, ψ (see definition 4.17), is solved from an equation to be derived from (4.8) and (4.9) by eliminating the pressure*).
If only the most important terms are retained, this stream function equation reads (see Appendix D)

$$a\{\frac{\partial^4\psi}{\partial\xi^4} + 2\frac{\partial^4\psi}{\partial\xi^2\partial\zeta^2} + \frac{\partial^4\psi}{\partial\zeta^4}\} + 2\frac{\partial a}{\partial\xi}(\frac{\partial^3\psi}{\partial\xi^3} + \frac{\partial^3\psi}{\partial\xi\partial\zeta^2}) + 2\frac{\partial a}{\partial\zeta}(\frac{\partial^3\psi}{\partial\xi^2\partial\zeta} + \frac{\partial^3\psi}{\partial\zeta^3}) +$$

$$+ 4\frac{\partial^2 a}{\partial\xi\partial\zeta}\frac{\partial^2\psi}{\partial\xi\partial\zeta} + (\frac{\partial^2 a}{\partial\xi^2} - \frac{\partial^2 a}{\partial\zeta^2})(\frac{\partial^2\psi}{\partial\xi^2} - \frac{\partial^2\psi}{\partial\zeta^2}) - \varepsilon Re_0 f\,(\frac{\bar{u}}{r}\frac{\partial}{\partial\phi} + \bar{v}\frac{\partial}{\partial\xi})(\frac{\partial^2\psi}{\partial\xi^2} + \frac{\partial^2\psi}{\partial\zeta^2}) +$$

$$- \varepsilon Re_0\left[f\{\frac{\partial\bar{u}}{\partial\xi}\frac{1}{r}\frac{\partial^2\psi}{\partial\xi\partial\phi} + \frac{\partial\bar{v}}{\partial\xi}(\frac{\partial^2\psi}{\partial\xi^2} + \frac{\partial^2\psi}{\partial\zeta^2})\} + \frac{\partial f}{\partial\zeta}\{\frac{\bar{u}}{r}\frac{\partial^2\psi}{\partial\zeta\partial\phi} + \frac{\partial\bar{v}}{\partial\xi}\frac{\partial\psi}{\partial\zeta}\} - \frac{\partial^2 f}{\partial\zeta^2}\bar{v}\frac{\partial\psi}{\partial\xi}\right] =$$

$$- \frac{\partial(f^2)}{\partial\zeta}\frac{r\bar{u}^2}{r_s} \qquad (5.29$$

If the main velocity field is known, this is a linear fourth order differential equation for ψ that can be solved if the distribution of ψ

*) In contrast with the main flow computation (see sections 5.1 and 5.2), the pressure is not assumed to be hydrostatic here.

at the inflow boundary is given and two boundary conditions are imposed at the bottom, at the surface and at each sidewall. The inflow condition that is consistent with the assumption of fully developed straight channel flow at the inflow boundary simply reads

$$\psi_{inflow} = 0 \tag{5.30}$$

The boundary conditions at the lateral boundaries follow from the conditions to be imposed on the secondary velocity components. The conditions at the surface then become

$$\psi = 0 \quad \text{and} \quad \alpha' \frac{\partial^2 \psi}{\partial \zeta^2} = 0 \quad \text{at} \quad \zeta = 0 \tag{5.31}$$

The conditions at the fixed boundaries are replaced by the wall function approximations treated in chapter 3. If $v_{\tau s}$ denotes the component of the bed friction velocity due to the secondary flow, the bed friction velocities can be expressed as

$$v_\tau = k_m \frac{\sqrt{g}}{C} \bar{v} + v_{\tau s} \quad \text{and} \quad u_\tau = k_m \frac{\sqrt{g}}{C} \bar{u} \tag{5.32}$$

Then the wall function approximations (3.27) and (3.34) can be elaborated using the equation of continuity (5.12), to yield

$$v_s = \frac{v_{\tau s}}{\kappa} \{\frac{\kappa C}{g} + 1 + \ln (1+\zeta)\} \qquad \text{for } \zeta \leq -1+\delta \tag{5.33}$$

$$w = -\frac{1}{\kappa} (\frac{\partial v_{\tau s}}{\partial \xi} + \frac{\varepsilon}{r} v_{\tau s}) (1+\zeta) \{\frac{\kappa C}{\sqrt{g}} + \ln (1+\zeta)\} \quad \text{for } \zeta \leq -1+\delta \tag{5.34}$$

The boundary conditions and the additional condition for ψ to be derived from these wall functions are

$$\left.\begin{aligned} \psi &= -r\frac{v_{\tau s}}{\kappa Re_0}\delta_0\left(\frac{\kappa C}{\sqrt{g}} + \ln\delta_0\right) \\ \frac{\partial\psi}{\partial\zeta} &= -r\frac{v_{\tau s}}{\kappa Re_0}\left(\frac{\kappa C}{\sqrt{g}} + 1 + \ln\delta_0\right) \end{aligned}\right\} \quad \text{at } \zeta = -1+\delta_0 \tag{5.35}$$

$$\psi = -r\frac{v_{\tau s}}{\kappa Re_0}(1+\zeta_1)\left\{\frac{\kappa C}{\sqrt{g}} + \ln(1+\zeta_1)\right\} \qquad \text{at } \zeta = \zeta_1 \tag{5.36}$$

The conditions at the sidewalls must be derived from the wall function approximations (3.29), (3.31), (3.35) and (3.36). The functions (3.35) and (3.36) for v can be split up into two parts, one for v_m (see also condition 5.17) and one for v_s. Near the left wall these functions are

$$v_m = -\frac{1}{\kappa r}\frac{\partial u_{\tau 1}}{\partial\phi}\left(\frac{B}{2d} + \xi\right)\left\{\frac{\kappa C}{\sqrt{g}} + 1 + \ln\left(\frac{B}{2d}+\xi\right)\right\} \quad \text{for } \xi \leq -\frac{B}{2d}+\delta_1 \tag{5.37}$$

$$v_s = -\frac{1}{\kappa}\frac{\partial w_{\tau 1}}{\partial\zeta}\left(\frac{B}{2d} + \xi\right)\left\{\frac{\kappa C}{\sqrt{g}} + 1 + \ln\left(\frac{B}{2d}+\xi\right)\right\} \quad \text{for } \xi \leq -\frac{B}{2d}+\delta_1 \tag{5.38}$$

, so that the conditions for ψ near the left wall become

$$\left.\begin{aligned} \psi &= r\frac{w_{\tau 1}}{\kappa Re_0}\delta_1\left(\frac{\kappa C}{\sqrt{g}} + \ln\delta_1\right) \\ \frac{\partial\psi}{\partial\xi} &= r\frac{w_{\tau 1}}{\kappa Re_0}\left(\frac{\kappa C}{\sqrt{g}} + 1 + \ln\delta_1\right) \end{aligned}\right\} \text{at } \xi = -\frac{B}{2d}+\delta_1 \tag{5.39}$$

$$\psi = r\frac{w_{\tau 1}}{\kappa Re_0}\left(\frac{B}{2d} + \xi_1\right)\left\{\frac{\kappa C}{\sqrt{g}} + \ln\left(\frac{B}{2d} + \xi_1\right)\right\} \qquad \text{at } \xi = \xi_1 \tag{5.40}$$

Similarly, the conditions near the right wall are

$$\left.\begin{aligned} \psi &= -\,r\,\frac{w_{\tau r}}{\kappa Re_0}\,1\,\left(\frac{\kappa C}{\sqrt{g}} + \ln\delta_1\right) \\ \frac{\partial\psi}{\partial\xi} &= -\,r\,\frac{w_{\tau r}}{\kappa Re_0}\left(\frac{\kappa C}{\sqrt{g}} + 1 + \ln\delta_1\right) \end{aligned}\right\} \quad \text{at} \quad \xi = \frac{B}{2d} - \delta_1 \tag{5.41}$$

$$\psi = -r\,\frac{w_{\tau r}}{\kappa Re_0}\left(\frac{B}{2d} - \xi_2\right)\left\{\frac{\kappa C}{\sqrt{g}} + \ln\left(\frac{B}{2d} - \xi_2\right)\right\} \qquad \text{at} \quad \xi = \xi_2 \tag{5.42}$$

In principle the stream function of the secondary flow can be solved from equation (5.29) with inflow condition (5.30), boundary conditions (5.31), (5.35), (5.39) and (5.41) and additional conditions (5.36), (5.49) and (5.42). In the actual model, however, this system is split up into a part for the vertical distribution of ψ and a part of $\bar{\psi}$. How this is done will be shown in the next sections.

5.5. Secondary flow: vertical distribution of the stream function

Making use of the similarity hypothesis (4.18), the stream function equation (5.29) can be split up into an equation for the vertical distribution function g and an equation for the depth-averaged stream function $\bar{\psi}$. These two equations are solved alternately, using the most recent values of $\bar{\psi}$ when solving for g and the most recent values of g when solving for $\bar{\psi}$.

The equation for g is solved in one vertical of each cross-section, viz. in the channel axis. Hence some additional simplifications of the stream function equation (5.29) are possible when deriving the equation for g. As the radial derivatives in the channel axis are at least an order $O(\varepsilon)$ smaller than the vertical ones, all radial derivatives in equation (5.29) can be neglected.

In addition, the streamwise inertia terms are neglected, supposing these terms to be of minor influence, as they appeared to be in laminar flow

(DE VRIEND, 1978b). This hypothesis is confirmed by experimental data (DE VRIEND AND KOCH, 1977 and 1978), showing the streamwise variation of g to be very small.
Taking account of these simplifications, equation (5.29) reduces to

$$a \frac{\partial^4 \psi}{\partial \zeta^4} + 2 \frac{\partial a}{\partial \zeta} \frac{\partial^3 \psi}{\partial \zeta^3} + \frac{\partial^2 a}{\partial \zeta^2} \frac{\partial^2 \psi}{\partial \zeta^2} = - \frac{\partial (f^2)}{\partial \zeta} \frac{\bar{ru}^{-2}}{r_s} \tag{5.43}$$

Substituting the similarity hypothesis (4.18) and the expression for a into this equation leads to

$$k_m \bar{u} \bar{\psi} \frac{\partial^2}{\partial \zeta^2} (a' \frac{\partial^2 g}{\partial \zeta^2}) = - \frac{\partial (f^2)}{\partial \zeta} \frac{\bar{ru}^{-2}}{r_s} \tag{5.44}$$

The boundary conditions at the bottom and at the surface are

$$\left.\begin{aligned} g &= - \frac{rv_{\tau s}}{\kappa \bar{\psi} Re_0} \delta_0 \left(\frac{\kappa C}{\sqrt{g}} + \ln \delta_0\right) \\ \frac{\partial g}{\partial \zeta} &= - \frac{rv_{\tau s}}{\kappa \bar{\psi} Re_0} \left(\frac{\kappa C}{\sqrt{g}} + 1 + \ln \delta_0\right) \end{aligned}\right\} \text{at } \zeta = -1 + \delta_0 \tag{5.45}$$

$$g = 0 \quad \text{and} \quad a' \frac{\partial^2 g}{\partial \zeta^2} = 0 \qquad \text{at } \zeta = 0 \tag{5.46}$$

and the additional condition for the determination of $v_{\tau s}$ is

$$g = - \frac{rv_{\tau s}}{\kappa \bar{\psi} Re_0} (1 + \zeta_1) \left\{\frac{\kappa C}{\sqrt{g}} + 1 + \ln (1 + \zeta_1)\right\} \qquad \text{at } \zeta = \zeta_1 \tag{5.47}$$

The system (5.44) through (5.47) is solved using a method based on repeated vertical integration (see Appendix E).

5.6. Secondary flow: depth-averaged stream function

Substituting the similarity hypothesis (4.18) and $\alpha = k_m \bar{u} \alpha'$ into the stream function equation of the secondary flow and averaging the result over the depth of flow yields, after some elaboration (see Appendix D)

$$\overline{\alpha' g}\,(\bar{u}\frac{\partial^4\bar{\psi}}{\partial\xi^4} + 2\frac{\partial\bar{u}}{\partial\xi}\frac{\partial^3\bar{\psi}}{\partial\xi^3} + \frac{\partial^2\bar{u}}{\partial\xi^3}\frac{\partial^2\bar{\psi}}{\partial\xi^2} + 12(\bar{u}\frac{\partial^2\bar{\psi}}{\partial\xi^2} + 2\frac{\partial\bar{u}}{\partial\xi}\frac{\partial\bar{\psi}}{\partial\xi} + \frac{\partial^2\bar{u}}{\partial\xi^2}\bar{\psi}) +$$

$$+ c_f^2\big|_{\zeta=0}\,\bar{u}\,\bar{\psi} - \varepsilon Re_0\,\{\overline{fg}\,(\frac{\bar{u}}{r}\frac{\partial^3\bar{\psi}}{\partial\phi\partial\xi^2} + \bar{v}\frac{\partial^3\bar{\psi}}{\partial\xi^3} + \frac{\partial\bar{u}}{\partial\xi}\frac{1}{r}\frac{\partial^2\bar{\psi}}{\partial\phi\partial\xi} + \frac{\partial\bar{v}}{\partial\xi}\frac{\partial^2\bar{\psi}}{\partial\xi^2}) +$$

$$+ f\,\frac{\partial g}{\partial\zeta}\Big|_{\zeta=0}\,(\frac{\bar{u}}{r}\frac{\partial\bar{\psi}}{\partial\phi} + \bar{v}\frac{\partial\bar{\psi}}{\partial\xi} + \frac{\partial\bar{v}}{\partial\xi}\bar{\psi})\} = -\frac{r\bar{u}^2}{k_m r_s}\,f^2\big|_{\zeta=0} \qquad (5.48)$$

The boundary conditions needed for the solution of $\bar{\psi}$ from this equation are obtained by averaging conditions (5.30), (5.39) and (5.41) over the depth of flow.

$$\bar{\psi}_{inflow} = 0 \qquad (5.49)$$

$$\left.\begin{aligned}\bar{\psi} &= r\frac{\bar{w}_{\tau 1}}{\kappa Re_0}\,\delta_1\,(\frac{\kappa C}{\sqrt{g}} + \ln\delta_1)\\ \frac{\partial\bar{\psi}}{\partial\xi} &= r\frac{\bar{w}_{\tau 1}}{\kappa Re_0}\,(\frac{\kappa C}{\sqrt{g}} + 1 + \ln\delta_1)\end{aligned}\right\}\ \text{at } \xi = -\frac{B}{2d} + \delta_1 \qquad (5.50)$$

$$\left.\begin{aligned}\bar{\psi} &= -r\frac{\bar{w}_{\tau r}}{\kappa Re_0}\,\delta_1\,(\frac{\kappa C}{\sqrt{g}} + \ln\delta_1)\\ \frac{\partial\bar{\psi}}{\partial\xi} &= -r\frac{\bar{w}_{\tau r}}{\kappa Re_0}\,(\frac{\kappa C}{\sqrt{g}} + 1 + \ln\delta_1)\end{aligned}\right\}\ \text{at } \xi = \frac{B}{2d} - \delta_1 \qquad (5.51)$$

The depth-averaged friction velocities $\bar{w}_{\tau 1}$ and $\bar{w}_{\tau r}$ are determined from the additional conditions

$$\bar{\psi} = r\frac{\bar{w}_{\tau 1}}{\kappa Re_0}\,(\frac{B}{2d} + \xi_1)\,\{\frac{\kappa C}{\sqrt{g}} + 1 + \ln(\frac{B}{2d} + \xi_1)\} \qquad \text{at } \xi = \xi_1 \qquad (5.52)$$

$$\bar{\psi} = -r\frac{\bar{w}_{\tau r}}{\kappa Re_0}\left(\frac{B}{2d} - \xi_2\right)\left\{\frac{\kappa C}{\sqrt{g}} + 1 + \ln\left(\frac{B}{2d} - \xi_2\right)\right\} \qquad \text{at } \xi = \xi_2 \qquad (5.53)$$

A description of the solution procedure applied to the system (5.48) through (5.53) is given in Appendix F.

5.7. Iterative solution procedure

Making use of the elements described in the foregoing sections of this chapter, the following iterative solution procedure can be drawn up (cf. DE VRIEND, 1978b):

1a. Estimate the vertical distribution functions f and g, for instance by taking the logarithmic distribution

$$f = 1 + \frac{\sqrt{g}}{\kappa C} + \frac{\sqrt{g}}{\kappa C}\ln(1+\zeta) \qquad (5.54)$$

and solving g from equation (5.44) with conditions (5.45) through (5.47), as described in Appendix E, or by evaluating the corresponding analytical solution (see also DE VRIEND, 1976 and 1977)

$$g = \frac{8}{2 - 5\frac{\sqrt{g}}{\kappa C} + 4\frac{g}{\kappa^2 C^2}}\left\{-2\zeta F_1 - \frac{\sqrt{g}}{\kappa C}\zeta F_2 + 2\left(1 - \frac{g}{\kappa^2 C^2}\right)(1+\zeta)\ln(1+\zeta)\right.$$

$$\left. + \frac{\sqrt{g}}{\kappa C}(1+\zeta)\ln^2(1+\zeta)\right\} \qquad (5.55)$$

with $F_1 = \int_{-1+\zeta^*}^{\zeta} \frac{\ln(1+\zeta)}{\zeta}\,d\zeta \qquad \left(\zeta^* = e^{-1-\frac{\kappa C}{\sqrt{g}}}\right)$

and $F_2 = \int_{-1+\zeta^*}^{\zeta} \frac{\ln^2(1+\zeta)}{\zeta}\,d\zeta$

1b. Estimate the depth-averaged stream function of the secondary flow, by setting $\bar{\psi} \equiv 0$, for instance.

2. Determine the depth-averaged main velocity field using one of the procedures (parabolic or partially-parabolic) described in section 5.2.

3. Calculate the curvatures of the streamlines and the normal lines of this depth-averaged flow field using the expressions given in Appendix D.

4. Solve for the depth-averaged stream function of the secondary flow $\bar{\psi}$ as described in Appendix F.

5. Determine the vertical distribution function f of the main velocity in the channel axis, making use of the procedure described in Appendix B.

6. Determine the vertical distribution function g of the stream function of the secondary flow in the channel axis (see Appendix E).

7. Repeat the procedure from 2. on, until a termination criterion is satisfied, for instance

$$\max \{|\bar{u}^{(n)} - \bar{u}^{(n-1)}|\} < \gamma_{cr} \quad \text{with} \quad \gamma_{cr} << 1 \tag{5.56}$$

, in which $\bar{u}^{(n)}$ denotes $\bar{u}$ in the n-th iteration step.

8. If necessary, carry out an additional computation of f in all verticals in order to account for the influence of the streamwise accelerations of the main flow (see DE VRIEND, 1978b).

9. Determine the magnitude and the direction of the resultant shear stresses at the fixed boundaries (see chapter 3).

6. Verification of the model

Before carrying out the overall verification of the mathematical model by comparing its results with measured data, the influence of the most important assumptions will be investigated. The assumptions to be considered in this respect are:

- the ones underlying the turbulence model (see chapter 3),
- the neglect of the vertical component of the main flow (see section 4.1),
- the similarity hypothesis for the main flow (see section 4.4), discarding the influence of streamwise accelerations,
- the need of incorporating the streamwise inertia of the secondary flow.

This part of the verification will be carried out making use of the computational results for the LFM-flume (see section 6.5), which has a rather long, sharp bend giving rise to strong effects of curvature, thus providing a rather severe test of the model.

6.1. The turbulence model

Although most interesting in this complex flow case, the verification of the basic hypotheses of the turbulence model, viz. the Boussinesq hypothesis (3.1) and the mixing length hypothesis (3.3), is left out of consideration here*). Only the influence of the overall mean value of the turbulence viscosity and its vertical and horizontal distribution will be treated.

6.1.1. Influence of the overall mean value of the turbulence viscosity

As was stated in chapter 3, the parabolic distribution of the turbulence viscosity (3.7) corresponds with an effective Reynolds number

$$Re_0 = \frac{6}{\kappa} \frac{C}{\sqrt{g}} \tag{6.1}$$

In case of fully developed flow in an infinitely wide straight channel, the overall mean value of the turbulence viscosity is given by

$$\bar{A}_0 \simeq 0.067 \rho v_* d \tag{6.2}$$

*) See for instance, BRADSHAW (1973) and HUNT AND JOUBERT (1979).

, where $v_* = V\, g^{\frac{1}{2}}/C$ is the friction velocity at the bottom. In the literature somewhat different values of the constant of proportionality in (6.2) are suggested: ENGELUND (1964) gives a value of 0.077 and RASTOGI AND RODI (1978) use 0.0765 in a depth-averaged version of the k-ε-model. These two values, however, are based on experimental data on uniform flow in closed channels, so they will only hold good in open channels if the influence of the water surface is negligible. A comparison of turbulence characteristics measured in uniform open channel flow (NAKAGAWA, NEZU AND UEDA, 1975) with those for a closed channel (LAUFER, 1951) shows that the water surface influences turbulence, indeed (see also RODI, 1978)*).

Until recently, the turbulence viscosity used to be determined experimentally from the turbulence-averaged velocity and shear stress distributions in uniform flow, applying the definition

$$A_t = \frac{\tau_{sz}}{\frac{\partial v_o}{\partial z}} \tag{6.3}$$

In uniform open channel flow τ_{sz} varies linearly from its maximum at the bottom to zero at the surface. Adopting Chezy's law, this yields

$$A_t = -\rho \frac{g}{C^2} \frac{\bar{v}_o^2}{d} \frac{z}{\frac{\partial v_o}{\partial z}} \tag{6.4}$$

The vertical distribution of v_o is rather insensitive to the distribution of A_t, except close to the bottom (see section 6.1.2). Inversely, the distribution of A_t in the upper part of the vertical is quite sensitive to the distribution of the velocity there. As A_t decreases strongly near the bottom, the depth-averaged value of A_t is mainly determined by the distribution in the higher parts of the vertical. Regarding, in addition, the sensitivity of $\frac{\partial v_o}{\partial z}$ to errors in v_o, this kind of experiments may be expected to yield a wide variety of $\bar{A}_t$.

---

*) This could explain the velocity reduction near the water surface often observed in open channel flow, even if the channel is straight and shallow (see, for instance, the experiments in the DHL-flume described in section 6.5.2).

ROZOVSKII (1961) gives a review of the empirical values of $\bar{A}_t$ obtained in this way. Grouped according to the approximation of the measured velocity distribution:

- the Boussinesq-Bazin parabola, with A_t constant in a vertical and a finite slip-velocity at the bottom (see also ENGELUND, 1964), which yields values of the constant in (6.2) between 0.065 and 0.071 (cf. ENGELUND: 0.077),
- the elliptic distribution (KARAUSHEV, 1946), yielding values of the constant that are dependent on C:

$$\frac{\bar{A}_t}{\rho v_* d} = (1.9 + 0.7 \frac{C}{\sqrt{g}})^{-1} \qquad \text{for} \qquad 3 < \frac{C}{\sqrt{g}} < 21$$

  , so that for $C = 60\ m^{\frac{1}{2}}/s$ a value of 0.065 is found,
- the logarithmic distribution, yielding $\kappa/6$, as was shown in the foregoing; for $\kappa = 0.4$, the constant has the value 0.067, but if higher values of κ are used (RASTOGI AND RODI (1978) use 0.42, RODI (1978) suggests 0.435, ROZOVSKII (1961) suggests values as large as 0.5), the constant increases in proportion,
- the power law distribution; the 1/7th-power law, for instance, yields a value of $1.15 \frac{\sqrt{g}}{C}$ for the constant, i.e. 0.060 for $C = 60\ m^{\frac{1}{2}}/s$.

Another class of experiments from which A_t can be determined concerns the dispersion of suspended matter in uniform straight channel flow. This indirect determination of A_t is based on the so-called Reynolds-analogy, stating that in turbulent flow the transport of momentum and the transport of mass are analoguous (see HINZE, 1975). During the experiments reported by JOBSON AND SAYRE (1970) dye was injected at the free surface of fully developed straight channel flow. From the rate of vertical spreading of this dye the transfer coefficient was derived. The observed values of this coefficient differ only a few per cent from those predicted by equation (6.2). Similar experiments were carried out with suspensions of fine-grained sand (VANONI, 1946; JOBSON AND SAYRE, 1970; COLEMAN, 1970), but then the dispersion process was complicated by the different densities of the fluid and the suspended particles. Hence the values of $\bar{A}_t$ obtained from these experiments are not quite reliable.

Recent advances in measuring technique (hot film, laser-doppler anemometry) allow for the turbulent velocity fluctuations to be measured. Hence A_t can be determined from turbulence quantities, using, for instance, the basic relationship of the k-ε-model

$$A_t = \frac{k_t^2}{\varepsilon_t} c_\mu \tag{6.5}$$

in which k_t denotes the local turbulence kinetic energy, ε_t the rate of energy dissipation and c_μ a known constant of proportionality (LAUNDER AND SPALDING, 1972; RODI, 1978).
Equation (6.5) was applied to the measured distributions of k_t and ε_t in uniform open channel flow presented by NAKAGAWA, NEZU AND UEDA (1975). The resulting values of A_t are so widely spread, however, that it is impossible to fit a reliable distribution curve through the measured data. (see figure 7). The mean value of A_t is about 0.067, but regarding the large spread in the data, this figure is not reliable either.
This shows that determining A_t from turbulence data requires extremely high measuring accuracies, as well. Besides, it is evident that more experimental work has to be done at this point.
It can be concluded from the foregoing that a great deal of uncertainty exists about the value of the constant of proportionality in (6.2), even in uniform rectilinear shear flow. Moreover, the turbulence in curved channel flow will be influenced by the extra strain rates due to streamline curvature and the skewed velocity field (BRADSHAW, 1976).
Therefore it is worthwhile to investigate the sensitivity of the mathematical model to the mean turbulence viscosity. This is done by setting the effective Reynolds number at

$$Re_0 = \frac{\gamma}{\kappa} \frac{C}{\sqrt{g}} \tag{6.6}$$

with γ varying between 4 and 6, i.e. the constant in (6.2) varying between 0.10 and 0.067.
Accordingly, the parabolic distribution of the turbulence viscosity is modified in such a way, that the mixing length distribution near the bottom is the same in any case:

$$a' = -\zeta(1+\zeta)\{12(1+\zeta) - \gamma(1+2\zeta)\} \qquad (6.7)$$

For $\gamma = 6$ this reduces to the parabola (3.8). For smaller γ the distribution remains almost parabolic, but the maximum shifts somewhat upwards and increases slightly (figure 8a).

The influence of γ on the vertical distributions of the main and the secondary flow, shown in figure 8b, is rather small, and so is the influence on the main bed shear stress factor k_m^2 (figure 8c). The secondary bed shear factor $k_m k_s$, however, increases considerably with decreasing γ (figure 8d) and the fully developed secondary flow intensity $\Phi Re_0/\bar{u}$ as well as the secondary flow advection factor $\overline{uv}_s/\bar{u}^2$ *), shown in figures 8e and 8f, decrease fairly strongly with decreasing γ.
The conclusion drawn from these results is that quantities related to the main flow are influenced only slightly by γ, but quantities related to the secondary flow are much more sensitive to this factor.

6.1.2. Influence of the vertical distribution of the turbulence viscosity

In uniform straight channel flow the parabolic distribution of the turbulence viscosity used in the model leads to a purely logarithmic velocity distribution, as was shwon in chapter 3. If turbulence is described by the k-ε-model, the vertical distribution of the turbulence viscosity closely agrees with the parabola near the bottom, but differs considerably from it in the upper half of the vertical (see figure 3). The resulting velocity distribution, however, hardly differs from the logarithmic one, not even in the upper half of the vertical. Hence it can be concluded that the distribution of the turbulence viscosity there is rather unimportant in a model of uniform flow.
Inversely, this distribution will be quite sensitive to the velocity distribution, so that it is rather difficult to determine it from velocity measurements (see section 6.1.1). Therefore some of the experiments reported in the literature seem to provide evidence in favour of the parabolic distribution (VANONI, 1946; JOBSON AND SAYRE, 1970), whereas others seem to corroborate the more uniform

*) Both quantities evaluated in the channel axis, for fully developed flow in a curved shallow channel, so that $\hat{\Psi}\, Re_0/\bar{u} = Re_0\, \hat{g}/k_m c$ and $-\overline{uv}_s/\bar{u}^2 = -Re_0\, f\, \frac{\partial g}{\partial \zeta}/k_m c$

distribution, so that it is rather difficult to determine it from velocity measurements (see section 6.1.1). Therefore some of the experiments reported in the literature seem to provide evidence in favour of the parabolic distribution (VANONI, 1946; JOBSON AND SAYRE, 1970), whereas others seem to corroborate the more uniform distribution according to the k-ε-model (COLEMAN, 1970). On the basis of physical arguments, however, it can be shown that the water surface can not be exactly a plane of symmetry, as assumed in the k-ε-model used here: some reduction of the turbulence viscosity is likely to occur near the surface (cf. RODI, 1978; see also NAKAGAWA, NEZU AND UEDA, 1975 and, as far as reliable, the elaboration of their data represented in figure 7).

Just as in uniform straight channel flow, the main velocity distribution in mildly curved flow will be hardly influenced by the distribution of the turbulence viscosity in the upper half of the vertical. The effect of a' on the secondary flow and hence on the main velocity distribution in sharply curved flow, however, needs further investigation.
To that end three different vertical distributions of the turbulence viscosity are considered, each of them with the same slope at the bottom and with $\gamma = 5$ (see section 6.1.1):

1) the modified parabolic distribution (6.4)

$$a' = -\zeta(1+\zeta)(7+2\zeta) \tag{6.8}$$

2) an approximation of the k-ε-distribution (see also figure 3)

$$a' = \frac{1}{9}(1+\zeta)(8\zeta^2 - 35\zeta + 2) \quad \text{for} \quad \zeta \leq -0.5$$

$$a' = \frac{43}{36} \quad \text{for} \quad \zeta \geq -0.5 \tag{6.9}$$

3) a uniform distribution in the upper part of the vertical with a linearly decreasing part near the bottom

$$a' = 5(1+\zeta) \quad \text{for} \quad \zeta \leq -0.775$$

$$a' = 1.127 \quad \text{for} \quad \zeta \geq -0.775 \tag{6.10}$$

The vertical distribution functions f, g and $\frac{\partial g}{\partial \zeta}$ and the most important constants in the depth-averaged system, calculated on the basis of each

of the distributions (6.8), (6.9) and (6.10), are represented in figures 9 and 10.

Figures 9a through 9d show the vertical distributions of the velocity components to be influenced only slightly by the distribution of a'. The coefficients in the depth-averaged main flow equations (5.9) and (5.10) and the secondary bed shear stress coefficient $k_m k_s$ are hardly influenced, either (see figures 10a through 10d and 10g). The coefficients in the depth-averaged stream function equation (5.48), however, are influenced to a considerably higher extent (as is shown by figures 10e and 10f and also by the secondary flow intensity far from the sidewalls represented in figure 10h), and so is the secondary flow advection factor $\overline{uv}_s/\bar{u}^2$ given in figure 10i. Nonetheless, the only quantity in which the differences are larger than about 15% is $\overline{ga'}_{\zeta\zeta}$ (figure 10f), which figures in a group of higher order terms in equation (5.48), and even there the difference between the distributions (6.9) and (6.10) is small.

In order to assess the influence of the large difference between the values of $\overline{ga'}_{\zeta\zeta}$ for the distributions (6.8) and (6.9), the complete model was applied to the LFM-flume (see section 6.5.1) with either distribution of a'. A comparison of the results, shown in figure 11, makes clear that the depth-averaged main velocity distribution is hardly influenced and that the influence on the depth-averaged stream function of the secondary flow never exceeds 10%.

Hence it is concluded that the vertical distribution of the turbulence viscosity away from the bottom hardly influences the main flow, whereas its influence on the secondary flow is rather small. The secondary flow and its advective effect on the main flow tend to increase if the turbulence viscosity is taken uniform in the upper part of the vertical.

6.1.3. Influence of the horizontal distribution of the turbulence viscosity

The turbulence viscosity in the present model is related more or less arbitrarily to the local bottom friction velocity (see chapter 3). Far from the sidewalls, where this friction velocity will vary only gradually and the exchange of momentum due to turbulence is predominantly vertical, this

approach will be almost correct. Near the sidewalls, however, steep velocity gradients and hence important momentum transfer due to turbulence will occur both in horizontal and in vertical direction. Consequently, it must be doubted whether in these regions the turbulence viscosity can be based on the bottom friction velocity only.
In order to investigate the influence of setting the turbulence viscosity proportional to the bottom friction velocity, the results obtained when using this turbulence model were compared with those obtained when using a uniform turbulence viscosity, with wall layers in which a increases linearly from zero on:

$$\begin{aligned} a &= 5\,(\tfrac{B}{2d} + \xi)\,a' && \text{for } \xi \leq -\tfrac{B}{2d} + 0.2 \\ a &= a' && \text{for } -\tfrac{B}{2d} + 0.2 \leq \xi \leq \tfrac{B}{2d} - 0.2 \\ a &= 5\,(\tfrac{B}{2d} - \xi)\,a' && \text{for } \xi \geq \tfrac{B}{2d} - 0.2 \end{aligned} \qquad (6.11)$$

The results of fully developed straight channel flow computations based on this distribution of a, combined with any of the distributions of a' given before, agree better with the measured data (TRACY, 1965) than those obtained from the original mathematical model (see figure 4a).
If the combination of (6.10) and (6.11) as a turbulence model in curved flow computations, however, important local errors are introduced near the sidewalls, even in as gentle a bend as the one in the DHL-flume ($d/B = 0.042$, $\varepsilon = 0.005$, $Re_0 = 239$; see also section 6.5.2). A comparison between the the mean velocities in this flume calculated by the original model and those found when using (6.10) and (6.11) is given in figure 12.
This leads to the conclusion that, especially near the sidewalls, the horizontal distribution of the turbulence viscosity needs special attention if local errors have to be avoided. If the sidewalls regions are of no interest, however, the accurate modelling of turbulence there is rather unimportant, either.

6.2. The neglect of the vertical component of the main flow

As was stated in section 4.1, the equation of continuity (4.2) for the main

flow does not account for the vertical component of the main flow. If this component is included, the equation reads

$$\frac{1}{r}\frac{\partial u_m}{\partial \phi} + \frac{\partial v_m}{\partial \xi} + \frac{\varepsilon}{r} v_m + \frac{\partial w_m}{\partial \zeta} = 0 \qquad (6.12)$$

Making use of the depth-averaged version of this equation (5.2), this yields

$$\frac{\partial w_m}{\partial \zeta} = -\frac{\bar{u}}{r}\frac{\partial}{\partial \phi}\left(\frac{u_m}{\bar{u}}\right) - \bar{v}\frac{\partial}{\partial \xi}\left(\frac{v_m}{\bar{v}}\right) - \frac{\varepsilon}{r}\,\bar{v}\left(\frac{v_m}{\bar{v}}\right) \qquad (6.13)$$

Adopting the similarity hypothesis for the main flow

$$u_m = \bar{u}\, f(\zeta;\xi,\phi) \quad \text{and} \quad v_m = \bar{v}\, f(\zeta;\xi,\phi) \qquad (6.14)$$

with f depending only weakly on ξ and ϕ , equation (6.13) can be elaborated to

$$w_m = -\frac{\bar{u}}{r}\frac{\partial F}{\partial \phi} - \bar{v}\frac{\partial F}{\partial \xi} - \frac{\varepsilon}{r}\bar{v}\,F \quad \text{with} \quad F = \int_{-1}^{\zeta} f\, d\zeta \qquad (6.15)$$

The only equation of main flow continuity that is actually incorporated in the model is the depth-averaged equation (5.2), which is exact. In the momentum equations, however, w_m is neglected, indeed.
The admissability of this neglect is verified by investigating whether in the main flow equation

$$w_m \frac{\partial u_m}{\partial \zeta} << \frac{u_m}{r}\frac{\partial u_m}{\partial \phi}, \quad v_m \frac{\partial u_m}{\partial \xi} \qquad (6.16)$$

, which is further reduced to

$$\frac{\bar{u}}{r}\left(f\frac{\partial f}{\partial \phi} - \frac{\partial f}{\partial \zeta}\frac{\partial F}{\partial \phi}\right) << \frac{f^2}{r}\frac{\partial \bar{u}}{\partial \phi} \qquad (6.17)$$

Figure 13 shows that for the LFM-flume this condition holds rather good, except locally near the bend exit, where the range of variation of the

first term is about 25% of the range of variation of the second one. Still assumption (6.16) is thought to be acceptable.

6.3. The similarity hypothesis for the main flow

As far as the influence of diffusion and secondary flow advection is concerned, the applicability of a similarity hypothesis for the main flow was verified for fully developed laminar curved flow (DE VRIEND, 1978a). In developing flow, however, there will be streamwise accelerations of the main flow, which give rise to deformations of the vertical distribution of the main velocity (DE VRIEND, 1976 and 1977; DE VRIEND, 1978b): positive accelerations make the velocity profile flatter, negative accelerations make it more oblique than in fully developed flow. Since in the present approximation (uniform cross-section) the cross-sectional mean velocity is the same everywhere, both positive and negative accelerations will occur in a cross-section. Hence adopting the similarity hypothesis (4.15) for the main flow implies that the effect of the streamwise accelerations is neglected.
The effect of this simplification is investigated for the LFM-flume by carrying out an additional computation step after the normal iteration procedure has been terminated. In this step the vertical distribution functions f and g are calculated in each vertical*), still assuming their horizontal derivatives to be negligible. Subsequently, the depth-averaged quantities and the bottom shear stresses are calculated on the basis of these vertical distribution functions. If the results of this additional computation step differ only slightly from those after the normal iteration, the influence of the streamwise accelerations can be assumed to be small.

Figures 14a and b show the vertical distribution functions to be almost invariable in a cross-section, except near the entrance and the exit of the bend, where small variations occur. The bed shear stress constants k_m and k_s and the constant c, obtained when determining f and g, are represented

*) The only terms in equation (5.7) that are actually varied from vertical to vertical are the main flow acceleration terms. All other terms are calculated on the basis of the quantities in the channel axis.

in figure 14c, showing that k_m is influenced only slightly, whereas k_s and c vary somewhat stronger, especially near the entrance and the exit of the bend.

The results of the depth-averaged computation are shown in figure 15. The variation of the vertical distribution functions due to streamwise accelerations of the main flow appears to have only a minor effect on the mean velocity field (figure 15a) and even the effect on the secondary flow intensity is rather small and of a local kind (figure 15b). Similarly, the magnitude of the bed shear stress (figure 16a), which is dominated by the main component, is hardly influenced, whereas the direction of the bed shear stress vector, in which the secondary flow plays a more important part, is influenced to a somewhat higher extent (see figure 16b). This influence on the direction locally amounts 20% of the overall mean value of ϕ_τ in the bend.

The foregoing comparison leads to the conclusion that the effect of the streamwise accelerations of the main flow on the vertical distribution functions can be neglected when computing the main flow, but has to be taken into account when computing the bed shear stress. In practice, this implies that the similarity hypothesis (4.15) is used during the 'normal' iteration procedure and that an additional iteration step, in which the vertical distribution functions are determined in each vertical, is carried out to determine the bed shear stress (cf. the laminar flow case; DE VRIEND, 1978b).

6.4. The influence of the streamwise inertia of the secondary flow.

On the basis of the conclusions drawn from the equivalent model of developing laminar curved flow (DE VRIEND, 1978b), the streamwise inertia of the secondary flow was incorporated in the equation for $\bar{\psi}$ (see section 5.4). Although these streamwise inertia terms do not give rise to a great deal of extra computational effort, it is interesting to find out how they work out in the results of the model.

Figure 17 gives a comparison between the results for the LFM-flume with and without streamwise inertia of the secondary flow. In contrast with the laminar flow case, the mean velocity distribution is hardly affected (figure 17a). The secondary flow intensity and the direction of the bed shear stress (figures 17b through d) are only affected in two rather small regions, viz. beyond the entrance and the exit of the bend.

Hence it is concluded that the streamwise inertia of the secondary flow needs not be incorporated in the turbulent flow model during the main flow computation. In the bed shear stress computation step, however, the streamwise inertia terms in equation (5.48) have to be accounted for.

6.5. Comparison with experimental data

The flow in curved channels was often investigated experimentally both in the laboratory and in the 'prototype'. Out of the experimental data available a selection was made for the verification of the present model:

1. The experiments carried out in the Laboratory of Fluid Mechanics (LFM) of the Delft University of Technology, in a rather sharply curved ($B/R_c = 0.4$) U-shaped flume with a horizontal bottom and vertical sidewalls (see figures 18)[*]).
2. The experiments carried out at the De Voorst branch of the Delft Hydraulics Laboratory (DHL), in a large flume with a rather gentle ($B/R_c = 0.12$) bend of almost 90^o, a sloping flat bottom and vertical sidewalls (see figure 21). The results, concerning main and secondary velocity distributions and water surface configurations, were reported by DE VRIEND AND KOCH (1977) .
3. The experiments carried out at the Iowa Institute of Hydraulic Research (IIHR), in a flume with two opposite, rather sharp ($B/R_c = 0.25$) bends of 90^o each and a shallow trapezoidal cross-section (see figure 25). The results concern the main and secondary velocity components, the magnitude and the direction of the bed shear stress, and the water surface configuration (B.C. YEN, 1965).
4. One of the experiments (no. 1) carried out at the Institute of Hydrology and Hydraulic Engineering (IHHE) of the Acedemy of Sciences of the USSR, in a sharply curved ($B/R_c = 1.0$) U-shaped flume with a horizontal bottom and vertical sidewalls (see figure 27). The measured data, concerning the main and the secondary velocity components and the water surface configuration, were reported in ROZOVSKII's (1961) book on curved open channel flow.

---

[*]) The measured data gathered during these experiments (main velocity distributions and water surface configurations) have not been reported yet, but they were kindly put at the author's disposal.

It was attempted to simulate each of these experiments by the mathematical model described in this report.

6.5.1. Simulation of the LFM-experiments

Out of the series of experiments carried out in the LFM-flume two cases were selected, one with a rough bottom (C estimated at 30 $m^{\frac{1}{2}}/s$; bottom roughened by a layer of gravel) and one with a smooth bed (C estimated at 60 $m^{\frac{1}{2}}/s$; bare concrete bottom). In both cases the depth to width ratio, based on the depth of flow at the downstream end of the flume, was about 1:10 and the discharge was about 0.19 m^3/s.

Both flow cases were simulated by the mathematical model, on a computational grid consisting of 25 cross-sections situated between a virtual inflow section 6 m ahead of the bend entrance and a virtual outflow section 6 m downstream of the bend, 21 verticals in each cross-section and 21 points in a vertical (see figure 18). The distance between the cross-sections in the straight reaches was 1.00 m and in the bend it was 1.11 m (measured along the axis), which is equivalent to an angle of 15^o enclosed between two subsequent cross-sections. The spacing between the verticals in a cross-section ranged between 0.2d (near the sidewalls) and d (in the central region) and the interval between the grid points in a vertical was constant in the upper half of the vertical (0.1d) and decreased exponentially towards the bottom. The grid points nearest to the fixed boundaries were situated at a distance of 0.01d from these boundaries. The value of C was the only difference between the two cases in the input of the mathematical model. As this value could not be determined very accurately by lack of a long straight reach with uniform flow or velocity measurements close to the bottom, it was estimated and in addition to the simulation on the basis of these estimations, the sensitivity of the model to C was investigated.

Figure 19a shows the mean velocities as they were measured and computed, the latter for three different values of C, ranging from 30 to 60 $m^{\frac{1}{2}}/s$. The differences between the computed distributions appear to be rather small. Only near the sidewalls, especially near the bend exit and in the

downstream straight reach, they are considerable. The measured data for the smooth and the rough bottom differ significantly in the second half of the bend. There the velocity tends to increase towards the outer wall in case of a rough bottom whereas the smooth bottom data show a decreasing tendency.
When comparing the measured and the computed velocities, the smooth bottom case appears to be predicted rather well, except near the sidewalls, where systematically higher velocities were measured: the local influence of the secondary flow seems to be overestimated near the inner wall and underestimated near the outer wall. The prediction of the rough bottom flow, however, is much worse, especially in the second half of the bend, where the theoretical curves lie much closer to those for the smooth bottom than the measured data. Here the effect of the secondary flow seems to be underestimated in the entire cross-section.

The discrepancies between the measured and the computed velocities in case of the smooth bottom can be explained from the assumption that the turbulence viscosity is proportional to the local bottom shear velocity (see chapter 3 and also section 6.1.3). Even in uniform straight channel flow this assumption gives rise to errors near the sidewalls (see figure 4) in that the predicted velocities are too small there and the 'sidewall boundary layer' is too thick. The same occurs in the present case: even in the straight reach before the bend the predicted velocities near the sidewalls are too small. In the bend this will give rise to additional errors in the secondary flow and its effect on the main flow. How this works out is readily illustrated in figure 12: if the horizontal distribution of the turbulence viscosity is made more uniform, the velocities near the sidewalls increase, in the straight reach as well as in the bend.
The same figure, however, shows the model is rather sensitive to the distribution of the turbulence viscosity close to the sidewalls. This implies that a quite accurate description of a should be given there, provided that the turbulence viscosity concept holds good in these regions at all. In principle, it may be possible to find a distribution that gives satisfactory results, but looking for this distribution is thought to be of no use as long as the physical basis is missing. Hence the modelling of

turbulence in the sidewall regions has to be studied before attempting to improve the model predictions there. Regarding the purpose of the present investigations, viz. the prediction of the flow and the bed configuration in alluvial river bends, this is thought to be going too far now.

It could be attempted to explain the differences between the smooth and the rough bottom case from the influence of the sidewall roughness. In the model all fixed boundaries have the same roughness. In the flume, however, the sidewalls in the straight sections and the inner wall in the bend were covered with plaster, the roughness of which was comparable with the roughness of the bare concrete bottom. Moreover, the outer wall in the bend consisted of a series of glass panels that were much smoother than concrete or plaster. The nonuniformity of the boundary roughness introduced in this way was stronger in case of the rough bottom then in case of the smooth one. This could explain why the predictions for the smooth bottom are better than those for the rough bottom. Besides it could provide a qualitative explanation of the stronger outward shift of the rough bottom flow in the second half of the bend, but it is not clear whether this explanation holds good quantitatively. Finding this out would require a modification of the mathematical model and additional measurements of the secondary flow intensity (see also section 6.5.2.).
The predicted pressures and the measured water surface configuration, at a distance of about the depth of flow from the sidewalls, are compared in figure 19b, for the smooth bottom case only. The agreement turns out to be rather poor: the predicted transverse pressure drop is about 1.5 times as large as would correspond with the measured superelevation of the water surface. In contrast with earlier suggestions (DE VRIEND, 1976 and 1977), this difference cannot be explained from a false prediction of the main velocity distribution, the main velocities being predicted rather well in this case.
A quantitative analysis on the basis of a truncated version of equation (5.10), holding for fully developed curved flow,

$$\frac{\partial p}{\partial \xi} \simeq \varepsilon^2 Re_0 \overline{f^2} \frac{\bar{u}^2}{r} \qquad (6.18)$$

leads to a transverse pressure drop given by

$$\frac{p|_{\xi=4} - p|_{\xi=-4}}{\varepsilon Re_0} \simeq 0.35 \qquad (6.19)$$

, which agrees with the model predictions. Besides, this way of estimation leads to appropriate predictions of the transverse pressure drop in many other curved flow experiments (C.L. YEN AND B.C. YEN, 1971; ROZOVSKII, 1961; DE VRIEND AND KOCH, 1977), which raises doubt against the measured data in the LFM-flume.

The LFM-experiments were simulated using the partially-parabolic main flow computation model. To find out to what extent the simpler and more economic parabolic model (see chapter 5) is applicable here, an additional run was made using this parabolic model.

The essential difference between the two models is readily illustrated by the pressure distributions represented in figure 19b: upstream influencing is incorporated in the partially-parabolic model, so that the pressure distribution starts changing before the bend entrance or the bend exit is reached; the parabolic model, however, takes no account of upstream influencing, so that the pressure distribution starts changing at the entrance and at the exit of the bend.

According to figure 20, the use of the parabolic model leads to important errors, both in the main velocity distribution (figure 20a) and in the secondary flow intensity (figure 20b). Hence this parabolic model is not suited to predict this rather sharply curved flow (see also PRATAP, 1975 and PRATAP AND SPALDING, 1975).

6.5.2. Simulation of the DHL-experiments

The experiments in the rectangular DHL-flume*) (DE VRIEND AND KOCH, 1977) concern velocity and water level measurements for two discharges, viz. 0.610 and 0.305 m^3/s, with a depth of flow near the outflow boundary of about 0.25 m in either case. The magnitude and the direction of the horizontal velocity component were measured in a three-dimensional grid covering the whole flume and the water surface elevation was measured in

*) In a later stage experiments were carried out in the same flume with a non-rectangular cross-section (DE VRIEND AND KOCH, 1978).

each vertical of this grid.
To determine the vertical distributions of the main and the secondary flow, a rather fine vertical spacing of the grid points was used in the channel axis and in one of the cross-sections in the bend (at 55^{o}). In the other parts of the flume only the depth-averaged velocity was determined and the grid was taken coarser.
The two flow cases were simulated numerically, with the partially-parabolic as well as with the parabolic model. The computational grid (see figure 21) consisted of 25 cross-sections, lying between a vertical inflow section 24 m ahead of the bend entrance and a virtual outflow section at 82.5^{o}, 29 verticals in each cross-section and 21 points in a vertical. When measured along the channel axis, the distance between two adjacent verticals ranged from 0.2d near the sidewalls to 2.0d in the central region. The vertical spacing was the same as for the LFM-flume (see section 6.5.1) and the wall distance of the grid points nearest to the bottom or the sidewalls was 0.01d.

As the discharge plays no role in the mathematical system to be solved, the two flow cases were covered by one run of the model. Consequently, the results of the numerical simulation are represented in the figures by only one curve.

Figure 22a shows the measured and the computed mean velocities for $C = 60\ m^{\frac{1}{2}}/s$. In contrast with the LFM-flume, the results obtained by the parabolic model closely approximate those from the partially-parabolic model now. Both theoretical distributions, however, show systematic discrepancies with the measured data: near the inner wall the thickness of the wall layer increases too little when proceeding through the bend, whereas the velocities near the outer wall remain too small. It looks as if the effect of the secondary flow were underestimated.
This is a rather unexpected conclusion, regarding the fair agreement with the measured data obtained when simulating this turbulent flow using the laminar version of the present model (DE VRIEND, 1978b). Moreover, the kind of discrepancies is not in accordance with those found for the LFM-flume, where the influence of the secondary flow was rather overestimated, at least near the inner wall (see figure 19a).

An important step towards the explanation of the discrepancies in figure 22a is made when considering the secondary flow intensity represented in figure 22b and c. Although the measured data are rather scarce (the intensity could only be determined with reasonble accuracy in the verticals with the finer grid), they clearly show that the predicted intensities are far too small.
If the secondary flow intensity in the model is multiplied by a factor 1.5, the main flow predictions are much better, as is shown in figure 22a. The remaining discrepancies near the sidewalls (too small predicted velocities close to the walls) are consistent with those in the LFM-flume and can be explained in the same way (see section 6.5.1). Hence it is concluded that the main flow is described fairly well if the secondary flow intensity is correct.

Thus the problem is shifted from the main velocity distribution to the secondary flow intensity: how is it possible that the actual secondary flow intensity is so much larger than the predicted one? The discrepancy occurs throughout the flow field, without any preference for the sidewall regions*) or the first part of the bend. Hence the explanation must be looked for in the truncated version of the stream function equation (5.48), holding for fully developed curved flow far from the sidewalls:

$$c\, f^2|_{\zeta=0}\, \bar{u}\, \bar{\psi} = -\frac{r\bar{u}^2}{k_m r_s} f^2|_{\zeta=0} \quad , \text{ whence } \bar{\psi} = \frac{\bar{u}}{k_m c} \tag{6.20}$$

If the secondary flow intensity is characterized by $\bar{\psi}Re_0$, the differences between the measured data and the model predictions have to be explained on the basis of the relationship

$$\bar{\psi}Re_0 = Re_0 \frac{\bar{u}}{k_m c} \tag{6.21}$$

This implies that the source of these differences lies either in the vertical distribution of the main velocity, influencing k_m and c,

*) The deviant values of the measured secondary flow intensity near the outer wall are caused by a locally deviating secondary flow pattern there (see DE VRIEND AND KOCH, 1977).

or in the turbulence model.
The influence of the vertical distribution of the main velocity can be shown by calculating the fully developed secondary flow far from the sidewalls on the basis of the measured distribution of u (see figure 23a). As this distribution is more uniform than the theoretical one, k_m and c are larger and the secondary flow intensity is considerably smaller than when using the theoretical distribution of u (fugure 23c). Hence the explanation of the underestimated secondary flow intensity can certainly not be found in the vertical distribution of the main velocity alone.
Consequently, this underestimation must be attributed to the turbuelence model. As was shown in sections 6.1.1 and 6.1.2, the secondary flow intensity tends to increase if γ is raised and if the almost-parabolic distribution of a' (equation 6.8) is replaced by the k-ε-approximation (6.9). The factor γ is related directly to Von Karman's constant κ and to the constant of proportionality in equation (6.2). Neither κ nor the constant, however, are known very accurately: for both quantities a great variety of values is suggested in the literature (see section 6.1.1). Hence the possible values of γ vary within wide bounds and raising the value from 5 to 6, for instance, seems to be allowable. For C = 60 $m^{\frac{1}{2}}/s$, raising γ from 5 to 6 and replacing (6.8) by (6.9) lead to an increase of the secondary flow intensity of about 50%.
Regarding the important role of the secondary flow in the direction of the shear stress, this strong dependence on the turbulence model emphasizes the need of further investigations on the modelling of turbulence in this type of flow.

In contrast with the simulation of the LFM-experiments, the present simulation yields transverse pressure distributions that agree fairly well with the measured water surface configuration (see figure 24): the differences between the measured and the computed values lie within the range of accuracy of the former.

6.5.3. Simulation of the IIHR-experiments

The flow case selected out of the series of experiments carried out in

the IIHR-flume (YEN, 1965) concerns 'Run 3', i.e. a mean depth of flow of 0.512 ft (0.16 m), a mean velocity of 2.27 fps (0.69 m/s) and a channel slope of $7.2 * 10^{-4}$. For the numerical simulation of the cross-section was assumed to be rectangular, with $B = B_{bed} + d \simeq 6.5$ ft (1.99 m) and the bottom was taken horizontal. The Chezy-factor was estimated at 127 $ft^{\frac{1}{2}}/s$ (70 $m^{\frac{1}{2}}/s$).

The magnitude and the direction of the horizontal velocity component were measured in a three-dimensional grid covering the straight section between the two bends and the second bend (see figure 25). In addition, the water surface elevation and the bed shear stress were measured in each vertical of this grid.

The flow was simulated numerically in the entire flume since the flow in the second part of the flume, where the measurements were taken, was expected to be influenced by the preceding bend. The computational grid consisted of 25 cross-sections, lying between an inflow section 7 ft ahead of the first bend and an outflow section 7 ft beyond the second bend. The cross-section was divided into 22 (horizontal) x 20 (vertical) meshes, the size of which decreased near the fixed boundaries, as shown in figure 25.

According to figure 26a, the depth-averaged main velocity field is reasonbly well predicted, except near the sidewalls and in the exit sections of the bends, where the outward shift of the measured flow is stronger. As in the other simulations (see sections 6.5.1 and 6.5.2), the wall discrepancies must be attributed to the horizontal distribution of the turbulence viscosity. The deviations at the bend exits can be explained from the underestimation of the secondary flow intensity that becomes evident from figures 26b through d.

Figure 26b shows the outward and inward radial discharges in the channel axis, defined as

$$\int_{-1}^{\zeta} v \, d\zeta \quad \text{and} \quad \int_{\zeta}^{0} v \, d\zeta \tag{6.22}$$

in which ζ denotes the level at which the radial velocity component changes

sign. These definitions can further be elaborated to

$$\int_{-1}^{\zeta} v\,d\zeta = \bar{v} \int_{-1}^{\zeta} f\,d\zeta - Re_0 \bar{\psi}\, g(\zeta) \tag{6.23}$$

$$\int_{\zeta}^{0} v\,d\zeta = \bar{v}\{1 - \int_{\zeta}^{0} f\,d\zeta\} + Re_0 \bar{\psi}\, g(\zeta) \tag{6.24}$$

When comparing the predicted values of these quantities with the measured ones, they appear to be too small. Despite of great local differences, however, the net radial velocity $\bar{v}$ has the correct order of magnitude (figure 26c), so that it must be the secondary flow that is underestimated. This becomes even more evident from figure 26d, showing the radial component of the secondary flow v_s in the channel axis*).
Not only the intensity of the secondary flow in the bend is underestimated, however, but also the 'memory effect' of the preceding bend. In the model predictions, the secondary flow generated in the first bend has damped out before the second bend is entered, whereas the measured data show the secondary flow of the first bend to the perceptible even in the first part of the second bend, not only in the intensity, but also in the vertical distribution of v_s (cf. MOSONYI AND GÖTZ (1973) and GÖTZ (1975), who conducted experiments in subsequent, rather sharp ($B/R_c = 0.25$) 180^o bends with small ($L = 2B$) straight sections in between).
The predicted magnitude of the bed shear stress is about 20% larger than the measured one (figure 26e) and the transverse distribution is not quite correct, not only near the sidewalls (turbulence model), but also in the central region, where the predicted curves have a somewhat smaller slope. It should be noted, however, that the bed shear stress was measured

*) The 'measured values' of this quantity were obtained from

$$v_s = v - \bar{v} f \tag{6.25}$$

in which the actually measured v and $\bar{v}$ were used and f was taken logarithmic.

using a Preston tube, which is not quite suited for this skewed type of flow (NISHI, SENOO AND TERAZONO, 1974).
The direction of the bed shear stress in the present model coincides with the direction of the velocity near the bottom (cf. VAN DEN BERG a.o. (1975), stating that in skewed boundary layers this is not quite correct). Therefore the computed bed shear stress angles are considerably larger than the predicted ones (see figure 26f).
The transverse pressure distribution corresponds quite well with the measured water surface configuration (figure 26g), which is in accordance with the conclusion to be drawn for the DHL-flume, but not for the LFM-flume (see sections 6.5.2 and 6.5.1, respectively).

6.5.4. Simulation of the IHHE-experiments

There are different reasons why it is interesting to try and simulate the IHHE-experiment 'no. 1' (ROZOVSKII, 1961):

- it concerns the flow in a sharp bend ($B/R_c = 1.0$), which provides the possibility to test the performance of the model under extreme conditions (high Dean-numbers),
- ROZOVSKII states that his secondary flow predictions, which are quite similar to the present ones, are rather good, especially for this experiment (see also DE VRIEND, 1976 and 1977),
- the same experiment was simulated numerically with a fully three-dimensional model (LESCHZINER AND RODI, 1978), which provides another testing possibility for the present 'two-plus-one'-dimensional model.

All attempts to carry out this simulation, however, failed because of ill-convergence of the main flow iteration procedure. Apparently, the equivalent Dean number, amounting about 66 here, was too high to make the similarity procedure underlying the model convergence (cf. fully developed laminar flow (DE VRIEND, 1978a), where the procedure converged for Dean numbers up to about 40).
In spite of this failure in the main flow prediction, some other tests are possible, considering that

- far from the sidewalls and from the transitions between the bend and the straight reaches, the predicted secondary flow can be approximated as if it were fully developed, i.e.

$$v_s = - Re_0 \frac{\bar{u}}{k_m cr} \frac{\partial g}{\partial \zeta} \tag{6.26}$$

- the predicted transverse pressure distribution far from the transitions is fairly well approximated by

$$\frac{\partial p}{\partial \xi} \simeq \varepsilon^2 \frac{\bar{u}^2}{r} Re_0 \overline{f^2} \tag{6.18}$$

, so that the transverse pressure drop follows from

$$\frac{p_{outer} - p_{inner}}{\varepsilon Re_0} \simeq \frac{B}{R_c} \tag{6.27}$$

The secondary flow in the IHHE-experiments is adequately described by Rozovskii's formula for a smooth bottom

$$v_s = \frac{\bar{u}}{r} \frac{1}{\kappa^2} \{2F_1(\zeta) + \frac{\sqrt{g}}{\kappa C} F_2(\zeta) + 2(1 - \frac{\sqrt{g}}{\kappa C})\} \tag{6.28}$$

in which $F_1 = \int_{-1}^{\zeta} \frac{\ln(1+\zeta)}{\zeta} d\zeta$ and $F_2 = \int_{-1}^{\zeta} \frac{\ln^2(1+\zeta)}{\zeta} d\zeta$.

If the secondary flow intensity is characterized by $\bar{\psi} Re_0$, this yields

$$\bar{\psi} Re_0 = - \int_{-1}^{0} d\zeta \int_{-1}^{\zeta} v_s d\zeta = \frac{\bar{u}}{r} (1 - \frac{1}{2} \frac{\sqrt{g}}{\kappa C}) \frac{1}{4\kappa^2} \tag{6.29}$$

For $C = 60\ m^{\frac{1}{2}}/s$ and $\kappa = 0.5$, as Rozovskii suggests, the intensity amounts $0.95 \frac{\bar{u}}{r}$. The intensity predicted by the present model, for $\kappa = 0.4$, $\gamma = 5$ and $C = 60\ m^{\frac{1}{2}}/s$ is $0.82 \frac{u}{r}$, i.e. about 15% smaller. If γ is kept equal to 5 and the k-ε-approximation (6.9) is used for a' instead of the almost-parabolic distribution (6.8), however, the intensity becomes $0.96 \frac{u}{r}$, which is almost correct. So in contrast with the simulation of the DHL- and IIHR-experiments, $\gamma = 5$ leads to

satisfactory results here, provided that (6.9) is used as a vertical distribution of the turbulence viscosity.
The transverse pressure drop following from (6.27) equals 1.0 and the measured superelevation in the second part of the bend, where it was almost constant, is about $7.5 * 10^{-3}$ m, at a Froude number $\frac{V^2}{gd}$ of about 0.11, which corresponds with 1.1 as a result of (6.27). So even in this sharp bend the model describes the transverse configuration of the water surface fairly well.

6.6. Discussion

The experimental verification of the mathematical model developed here makes clear that the turbulence model is a most crucial part of it, having a great influence on the main flow (near the sidewalls), but especially on the secondary flow and hence on the bed shear stress direction. This turbulence model, however, is also the most important source of uncertainty in the model. On the basis of theoretical (HINZE, 1975) and practical (RODI, 1978; VAN DEN BERG, 1975) arguments, the fundamental hypotheses of the model, viz. the applicability of a scalar turbulence viscosity and especially of an algebraic relationship between this viscosity and mean flow quantities, are subject to doubt. Besides, the present verification of the complete mathematical model has raised doubt against the assumed vertical distribution of the turbulence viscosity, its overall mean value and its exclusive dependence on the bottom friction velocity. Verification and improvement of the turbulence model, however, requires more and also more accurate experimental data, both for simple uniform shear flow and for curved channel flow.
It seems that the rather poor prediction of the secondary flow intensity in the DHL- and the IIHR-flume can for the greater part be attributed to the turbulence model, but as turbulence quantities were not (DHL) or insufficiently (IIHR) investigated in these experiments, this can be no more than a hypothesis. Besides, if this hypothesis holds good, it is not clear why the secondary flow intensity in the IHHE-flume is predicted much better. Therefore it would be most interesting to have secondary flow measurements in the LFM-flume, which is sharper than the DHL- and the IIHR-flumes, but not as sharp as the IHHE-flume.

Another point concerning the secondary flow that needs further study is the poorly described 'memory effect' (see section 6.5.3). This aspect of the model is likely to become even more important in channels with a non-flat bottom, where much stronger streamwise variations occur than in channels with a flat bed. So far, it has not become clear whether the false prediction of this 'memory effect' is due to the turbulence model or to the simplifications in the secondary flow computation. Here, too, secondary flow data from the LFM-flume, especially of the damping beyond the bend, would be of interest.

More experimental data are also needed in the matter of the magnitude of the bed shear stress. If this quantity is measured at all, the accuracy of the results allows at best for a qualitative verification of the calculated bed shear stress.

Finally, the present verification emphasizes the important role of the sidewall regions in the flow process in rectangular channels. In channels with non-rectangular cross-sections resembling those in curved alluvial rivers, however, this influence of the sidewalls, if present at all, is likely to be much less important. As the modelling in the sidewall regions requires a lot of extra effort, this raises the question whether a model for rectangular channel flow is quite efficient as an intermediate step in the development of a mathematical model of the flow in curved alluvial rivers. It should be noted, however, that a great deal of most important experimental information on curved channel flow concerns rectangular channels and that extending the rectangular channel model to more arbitrary cross-sectional shapes makes it possible to investigate the importance of the sidewalls (banks).

7. Recapitulation and conclusions

The investigations reported here have led to a mathematical model of steady turbulent low Froude number flow in curved open channels with a shallow rectangular cross-section. In the present chapter the most important features of this model and the most important conclusions drawn from the investigations will be summarized.

7.1. The turbulence model

The modelling of turbulence, i.e. establishing a relationship between the Reynolds stresses and the turbulence-averaged flow properties, is an important part of the model. The turbulence model adopted here is based on the Boussinesq-hypothesis, stating that the Reynolds stress tensor can be related to the rate-of-strain tensor of the turbulence-averaged flow through a scalar turbulence viscosity. This turbulence viscosity is assumed to be related to the mean flow through the bottom friction velocity only; it is taken proportional to this quantity. Its vertical distribution is taken similar throughout the flow field, independent of the local flow conditions. The prescribed spatial distribution of the turbulence viscosity was subject to a closer investigation, which led to the following conclusions:

- the mean value of the turbulence viscosity strongly influences the secondary flow intensity and hence the direction of the bed shear stress; its influence on the vertical distribution of the main flow and on the magnitude of the bed shear stress factor is rather small.
- the literature gives no decisive answer regarding the mean turbulence viscosity, not even for fully developed straight channel flow;
- the literature gives no decisive experimental or theoretical evidence for the vertical distribution of the turbulence viscosity in the upper half of the vertical, either;
- this distribution hardly influences the main flow and even its influence on the secondary flow is rather small;
- the secondary flow intensity tends to increase slightly if the turbulence viscosity distribution in the upper half of the vertical becomes more uniform;
- the assumption that the bottom friction velocity is the only mean flow quantity influencing the turbulence viscosity is certainly not correct near the sidewalls; in the central region the assumption seems to hold good;
- prescribing a horizontal distribution of the turbulence viscosity independent of any mean flow quantity may give rise to important local errors near the sidewalls.

7.2. Simplification of the mathematical system

The complete mathematical system describing this case of turbulent flow consists of the conservation laws for mass and momentum, a turbulence model and a number of boundary conditions (see chapters 2 and 3). In order to reduce the computational effort, some simplifications were introduced into this system, making use of the limitation to shallow channels. The most important of these simplifications were verified, which yielded the following conclusions:

- the vertical component of the main velocity, which arises from variations in the shape of the vertical distribution of the streamwise velocity, is negligible in all equations of the system;
- adopting a similarity hypothesis for the main flow in a whole cross-section implies that the effect of streamwise accelerations on the vertical distribution of the main flow is neglected;
- this neglect is allowable when calculating the depth-averaged main velocity field, but it is not when calculating the secondary flow and the magnitude and direction of the bed shear stress;
- the streamwise inertia of the secondary flow needs not be incorporated in the main flow computation, but it has to in the secondary flow and bed shear stress computations.

Taking account of these conclusions, the computational procedure was split up into two subsequent steps, viz. the main flow computation step and the bed shear stress computation step. In the main flow computation step the similarity hypothesis for the main and the secondary flow is carried through completely: in any vertical of a cross-section the velocity distributions are taken similar to those in the channel axis. In the bed shear stress computation step the similarity hypothesis is dropped in that the velocity distributions may vary slightly from vertical to vertical in a cross-section.

The main flow computation step can be summarized as an iterative procedure, in which the depth-averaged main velocity and pressure fields, the horizontal distribution of the secondary flow intensity and the vertical distributions of the main and the secondary flow in the channel axis are calculated alternately. In the bed shear stress computation step the distributions of the main and the secondary flow are calculated in all verticals of the computational grid, making use of the depth-averaged main velocities and the secondary flow

intensities resulting from the main flow computation step. Subsequently, the distribution of the secondary flow intensity is corrected and the magnitude and direction of the bed shear stress are calculated.

7.3. Computation of the depth-averaged main velocity field

The only part of the mathematical model that requires a rather complicated computational procedure is the determination of the depth-averaged main velocity field, where a complicated system of three partial differential equations, viz. two momentum equations and an equation of continuity, has to be solved simultaneously. All other parts of the model come down to the solution of one ordinary differential equation allowing for rather simple and straightforward computational methods.
The investigations concerning the depth-averaged main flow computations involved two essentially different methods, viz.

- a method based on the stream function/vorticity concept for two-dimensional flows, solving for the stream function and the vorticity of the flow rather than for the velocity components and the pressure; thus the number of differential equations to be solved is reduced from three to two;
- a two-dimensional version of Spalding's method, calculating the velocity components and the pressure directly from the momentum and continuity equations; both the parabolic mode, discarding all upstream influencing, and the partially-parabolic mode, in which upstream influencing through the pressure is taken into account, were considered.

The conclusions drawn from these investigations are:

. in contrast with the equivalent model computational method in the model for laminar curved flow (DE VRIEND, 1978b), the stream function/vorticity concept gives rise to ill-convergence of the iteration procedure in the main flow computation step,
. the two modes of Spalding's method do not give rise to convergence problems,
. Spalding's method is much more efficient than the stream function/vorticity method,
. the most economic mode of the method, the parabolic one, is only applicable in mildly curved flows,
. the partially-parabolic mode of the method gives reliable results even in sharply curved flows, provided that no flow separation occurs.

7.4. Performance of the model

The performance of the model was tested by simulating a number of laboratory experiments carried out in various curved flumes. The conclusions drawn from these tests can be summarized as follows:

- the main velocity redistribution in a curved channel with almost uniform roughness is predicted reasonably well if the correct secondary flow intensity is introduced; only locally near the sidewalls considerable deviations from the measured data occur, most likely as a consequence of the inadequate modelling of turbulence there;
- the transverse distribution of the pressure and hence the transverse configuration of the water surface is predicted fairly well;
- the longitudinal distribution of the pressure does not correspond everywhere with the longitudinal configuration of the water surface as a consequence of backwater effects;
- the often observed velocity reduction near the water surface, both in straight and in curved channels, is not reproduced by the model; this velocity reduction can certainly not be explained entirely from the influence of the secondary flow due to the main flow curvature;
- even in mildly curved flows the intensity of the secondary flow is underestimated considerably, probably as a consequence of an erroneous turbulence model; the overall mean value of the turbulence viscosity is of great importance in this respect;
- the damping of the secondary flow beyond a bend is poorly described by the model; it is not clear whether this failure must be attributed to simplifications in the mathematical system or to an inappropriate turbulence model;
- the vertical distribution of the secondary flow agrees rather well with the measured data, except for regions where the 'memory effect' is important;
- the magnitude of the bed shear stress can hardly be verified by lack of reliable experimental data for rectangular channels; the comparison with the measured data from the IIHR-flume suggests the magnitude of the shear stress to be overestimated;
- the direction of the velocity vector close to the bed is related directly to the secondary flow intensity, so that the deviation from the direction

of the channel axis is underestimated; in not too sharply curved flows this implies that the predicted direction of the bed shear stress is in error, as well;

- the model does not work at all for sharply curved flows with relatively high effective Dean numbers.

7.5. Further research

Apart from the extension of the present model to shallow channels with a more arbitrary cross-section (arbitrary cross-sectional shape; more arbitrary channel pattern), the investigations reported herein have raised the need for further research at the following points;

- the modelling of turbulence in this type of flow; what is the answer to questions as:
  - to what extent does the Boussinesqu-hypothesis apply?
  - how is the turbulence influenced by the streamline curvature and how important is this influence?
  - how is the turbulence influenced by the free surface and how can this influence be accounted for?
  - if a scalar turbulence viscosity is applicable, what is the simplest acceptable way to relate it to the mean flow?
  - what should this turbulence viscosity look like in uniform rectilinear shear flow?
- the 'memory effect' in the secondary flow, both theoretically and experimentally;
- the magnitude and direction of the bed shear stress, on which little experimental information is available; in this context it is worthwhile to find out to what extent the direction of the bed shear stress coincides with the direction of the velocity close to the bottom.

Besides, it would be most interesting to carry out additional experiments in the LFM-flume, with special attention to the secondary flow.

REFERENCES

1 BERG, B. VAN DEN, ELSENAAR, A., LINDHOUDT, J.P.V. and WESSELING, P., (1975)
Measurements in an incompressible three-dimensional turbulent boundary layer, under infinite swept wing conditions, and comparison with theory,
Journal of Fluid Mechanics, 70, part 1, p. 127

2 BÖSS, P., (1938)
Die Berechnung der Wasserbewegung in gekrümmten Fluszstrecken mittels der Potentialtheorie und ihre Ueberprüfung durch Modell-versuche,
in: "Wasser- und Geschiebebewegung in gekrümmten Fluszstrecken", H. Wittmann und P. Böss, Springer, Berlin

3 BRADSHAW, P., (1973)
Effect of streamline curvature on turbulent flow,
AGARDograph 169 (see also: lecture notes of VKI-Course 56, 'Advances in turbulent shear layers', 1973)

4 BRADSHAW, P., (1976)
Complex turbulent flows,
in: 'Theoretical and applied mechanics', W.T. Koiter (ed.), North-Holland Publ. Comp., Amsterdam

5 CHOW, V.T., (1959)
Open channel hydraulics,
Mc.Graw-Hill, New York

6 COLEMAN, N.L., (1970)
Flume studies of the sediment transfer coefficient,
Water Resources Research, 6, no. 3, p. 801

7 ENGELUND, F., (1964)
A practical approach to self-preserving turbulent flows,
Acta Polytechnica Scandinavica, Ci 27

8 ENGELUND, F. (1974)
Flow and bed topography in channel bends,
Proc. ASCE, Jnl. Hydr. Div., 100, no. HY 11, p. 1631

9 GERARD, R., (1978)
Secondary flow in noncircular conduits,
Proc. ASCE, Jnl. Hydr. Div., 104, no. HY 5, p. 755

10 GESSNER, F.B. and JONES, J.B., (1965)
On some aspects of fully-developed turbulent flow in rectangular channels,
Jnl. Fluid Mech., 23, part 4, p. 689

11 GOSMAN, A.D. and PUN, W.M., (1973)
Calculation of recirculating flow,
Imperial College, London, Heat-transfer report no. HTS/74/2

12 GÖTZ, W., (1975)
Sekundärströmungen in aufeinander folgenden Gerinnekrümmungen,
Universität Fredericiana Karlsruhe, Mitt. Theodor-Rehbock-Flussbaulaboratorium, Heft 163

13 HINZE, J.O., (1975)
Turbulence,
Mc.Graw-Hill, New York

14 HUNT, I.A. and JOUBERT, P.N. (1979)
Effect of small streamline curvature on turbulent duct flow,
Jnl. Fluid Mech., 91, part 4, p. 633

15 JOBSON, H.E. and SAYRE, W.W., (1970)
Vertical transfer in open channel flow,
Proc. ASCE, Jnl. Hydr. Div., 96, no. HY 3, p. 703

17 KARAUSHEV, A.V., (1946)
Distribution of velocities and coefficients of turbulent exchange along the vertical,
GCI-Proceedings, 56, no. 2 (ref. from: ROZOVSKII, 1961)

18 LAUNDER, B.E. and SPALDING, D.B., (1972)
Mathematical models of turbulence,
Academic Press, London

19 LAUNDER, B. E. and SPALDING, D.B., (1974)
The numerical calculation of turbulent flows,
Computer Methods in Appl. Mech. and Eng., 3, p. 269

20 LESCHZINER, M. and RODI, W., (1978)
Calculation of three-dimensional turbulent flow in strongly curved open channels,
Universität Karlsruhe, Sonderforschungsbereich 80,
Report SFB 80/T/126

21 McGUIRK, J., (1978)
Numerische Verfahren für dreidimensionale Strömungen,
in: 'Numerische Berechnung turbulenter Strömungen in Forschung und Praxis', Hochschulkursus Univ. Karlsruhe, April 1978, Vorlesung 9

22 MOSONYI, E. and GÖTZ, W., (1973)
Secondary currents in subsequent model bends,
IAHR, Int. Symp. on River Mechanics, Bangkok, Thailand

23 NAKAGAWA, H., NEZU, I. and UEDA, H., (1975)
Turbulence of open channel flow over smooth and rough beds,
Proc. JSCE, no. 241, September 1975, p. 155

24 NISHI, M., SENOO, Y. and TERAZONO, M., (1974)
Measurements of local wall friction force exerted by skewed turbulent boundary layers by means of an improved Preston tube,
Bull., of the JSME, 17, no. 113, p. 1447

25 PATANKAR, SV, (1975)
Numerical prediction of three-dimensional flows,
in: 'Studies in convection; theory, measurements and applications', B.E. Launder (ed.), Academic Press, London

26 PATANKAR, S.V. and SPALDING, D.B., (1972)
A calculation procedure for heat, mass and momentum transfer in three-dimensional parabolic flows,
Int. Jnl. Heat and Mass Transfer, 15, p. 1787

27 PRATAP, V.S., (1975)
Flow and heat transfer in curved ducts,
Imperial College London, Dept. Mech. Eng., Ph. D. thesis HTS/75/25

28 PRATAP, V.S. and SPALDING, D.B., (1975)
Numerical computations of the flow in curved ducts,
Aeronautical Quarterly, 26, part 3, p. 219

29 PRATAP, V.S. and SPALDING, D.B. (1976)
Fluid flow and heat transfer in three-dimensional duct flows,
Int. Jnl. Heat and Mass Transfer, 19, p. 1183

30 RASTOGI, K., and RODI, W., (1978)
Predictions of heat and mass transfer in open channels,
Proc. ASCE, Jnl. Hydr. Div., 104, no. HY3, p. 397

31 RODI, W., (1978)
Turbulence models and their application in hydraulics - A state of the art review,
Universität Karlsruhe, Sonderforschungsbereich 80, Report SFB80/T/127

32 RODI, W., (1978'), Private communication

33 RODI, W. a.o., (1978)
Numerische Berechnung turbulenter Strömungen in Forschung und Praxis,
Hochschulkursus an der Universität Karlsruhe, April 1978

34 ROZOVSKII, I.L., (1961)
Flow of water in bends of open channels,
Israel Program for Scientific Translation, Jerusalem
(original publication in Russian, 1957)

35 TRACY, H.J., (1965)
Turbulent flow in a three-dimensional channel,
Proc. ASCE, Jnl. Hydr. Div., 91, no. HY6, p. 9

36 VANONI, V.A., (1946)
Transportation of suspended sediment by water,
Transactions of the ASCE, 111, p. 67

37 VRIEND, H.J. DE, (1976)
A mathematical model of steady flow in curved shallow channels,
Delft University of Technology, Dept. of Civil Engng.,
Communications on Hydraulics, no. 76-1

38 VRIEND, H.J. DE, (1977)
A mathematical model of steady flow in curved shallow channels,
Jnl. Hydr. Res., 15, no. 1, p. 3

39 VRIEND, H.J. DE (1978a)
Fully developed laminar flow in curved ducts,
Delft University of Technology, Dept. of Civil Engng,
Laboratory of Fluid Mechanics, Int. report 2-78

40 VRIEND, H.J. DE, (1978b)
Developing laminar flow in curved rectangular channels,
Delft University of Technology, Dept. of Civil Engng.,
Laboratory of Fluid Mechanics, Int. report 6-78

41 VRIEND, H.J. DE AND KOCH, F.G., (1977)
Flow of water in a curved open channel with a fixed plane bed,
Delft Hydraulics Laboratory/Delft University of Technology,
TOW-report R657-V/M1415 I

42 VRIEND, H.J. DE AND KOCH, F.G., (1978)
Flow of water in a curved open channel with a fixed uneven bed,
Delft Hydraulics Laboratory/Delft University of Technology,
TOW-report R657-VI/M1415 II

43 YEN, B.C., (1965)
Characteristics of subcritical flow in a meandering channel,
Institute of Hydraulic Research, Univ. of Iowa, Iowa City

44 YEN, C.L. and YEN, B.C., (1971)
Water surface configuration in channel bends,
Proc. ASCE, Jnl. Hydr. Div., 97, no. HY2, p. 303

Figures

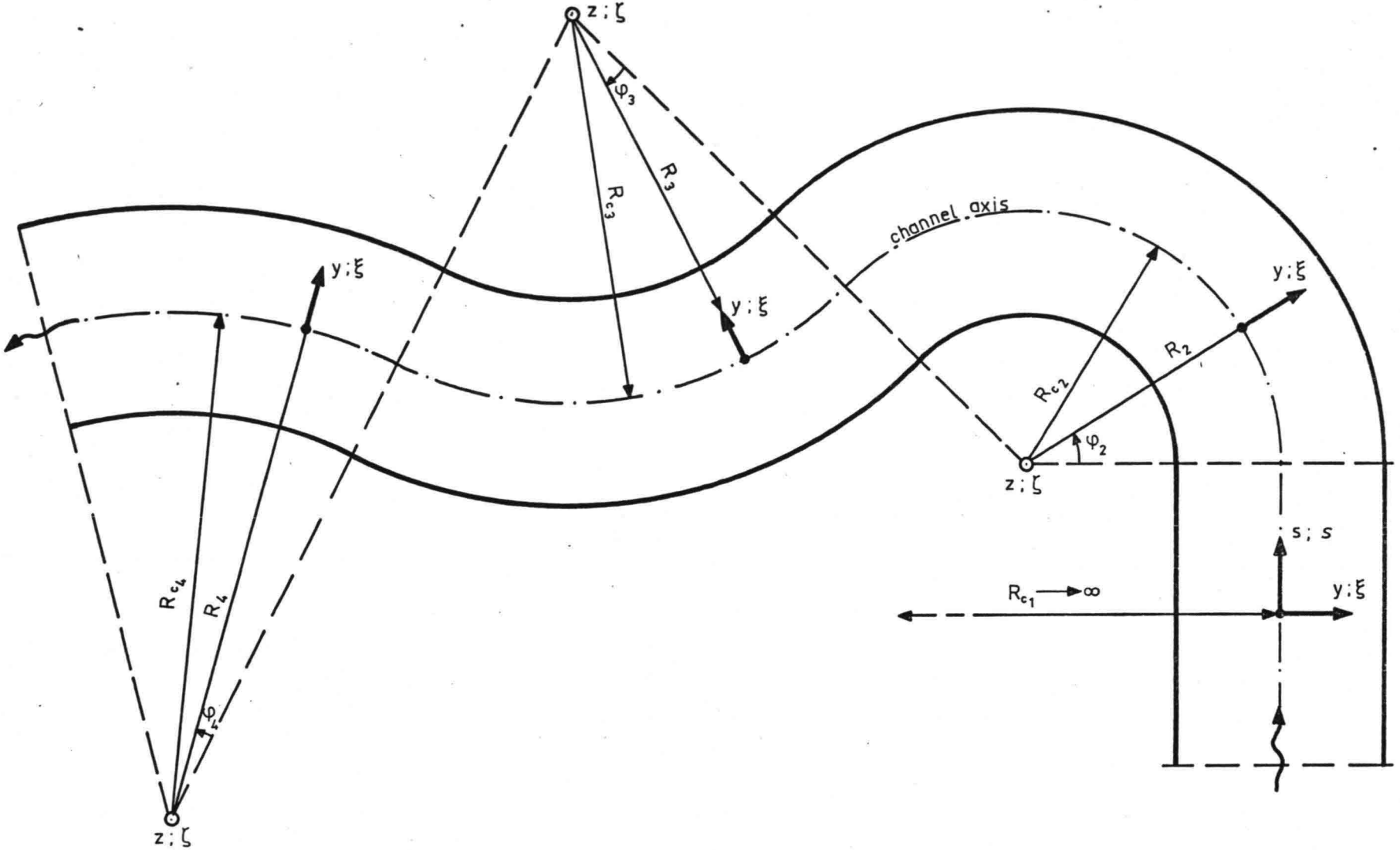

Figure 1. Combined cylindrical coordinate system

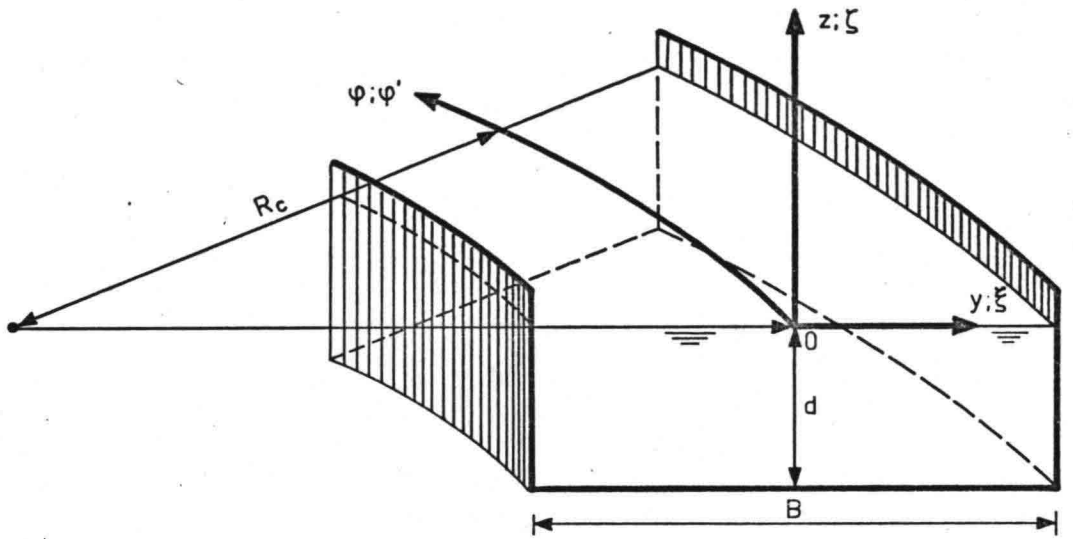

Figure 2. Definition sketch

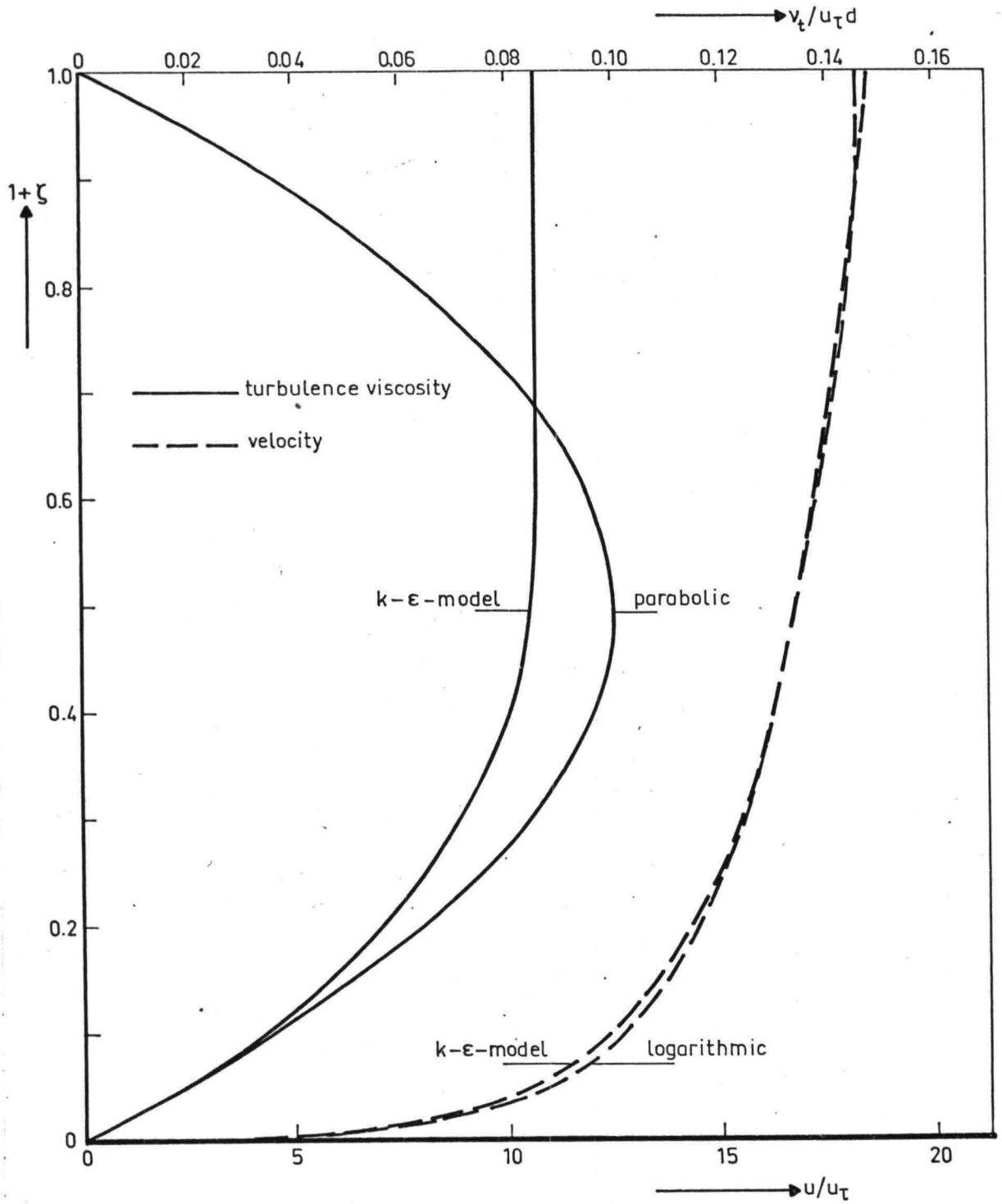

Figure 3. The k-ε-model in uniform straight channel flow

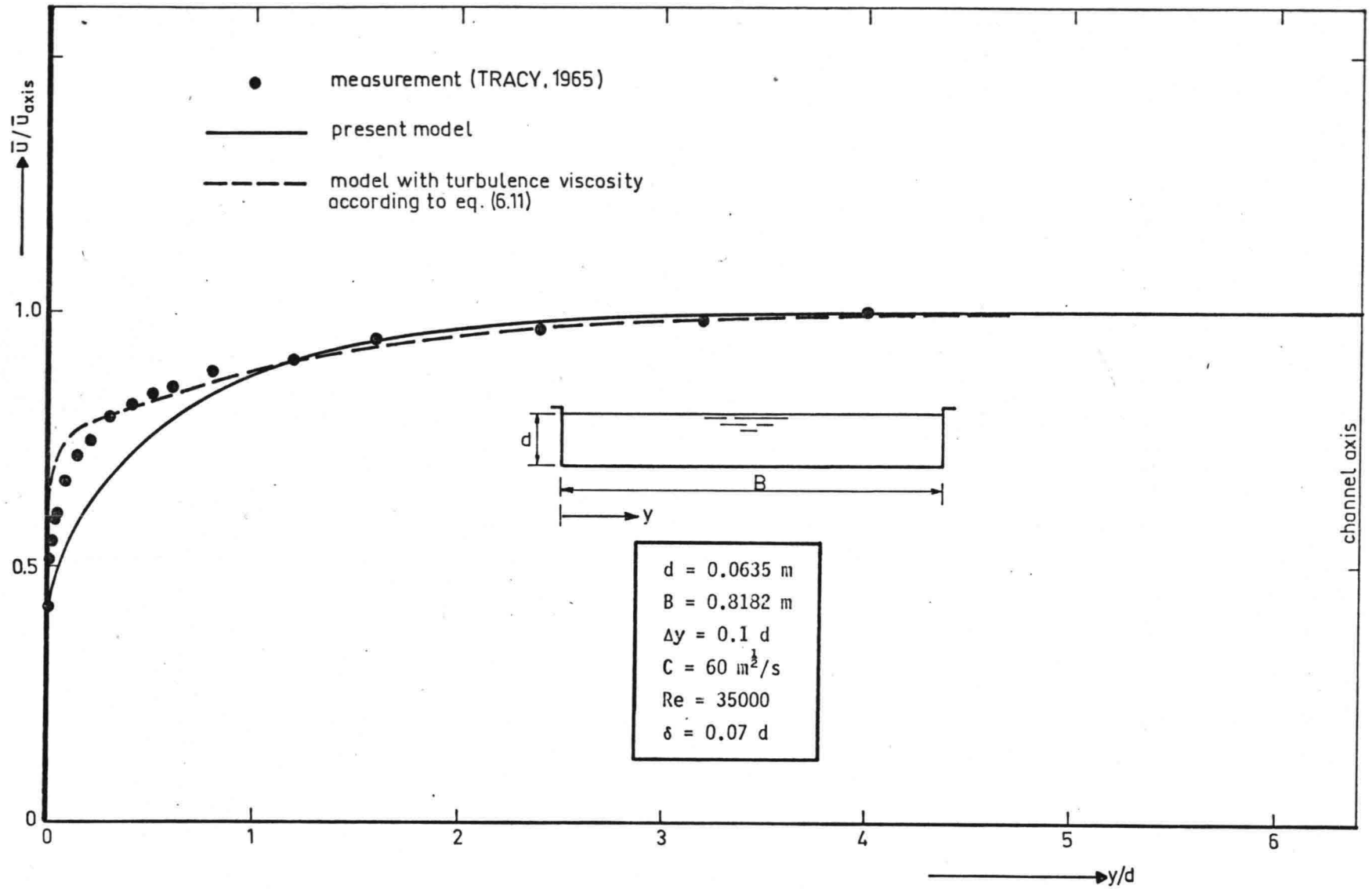

Figure 4. Fully developed flow in a straight channel of finite width

(a) Comparison with Tracy's measurements

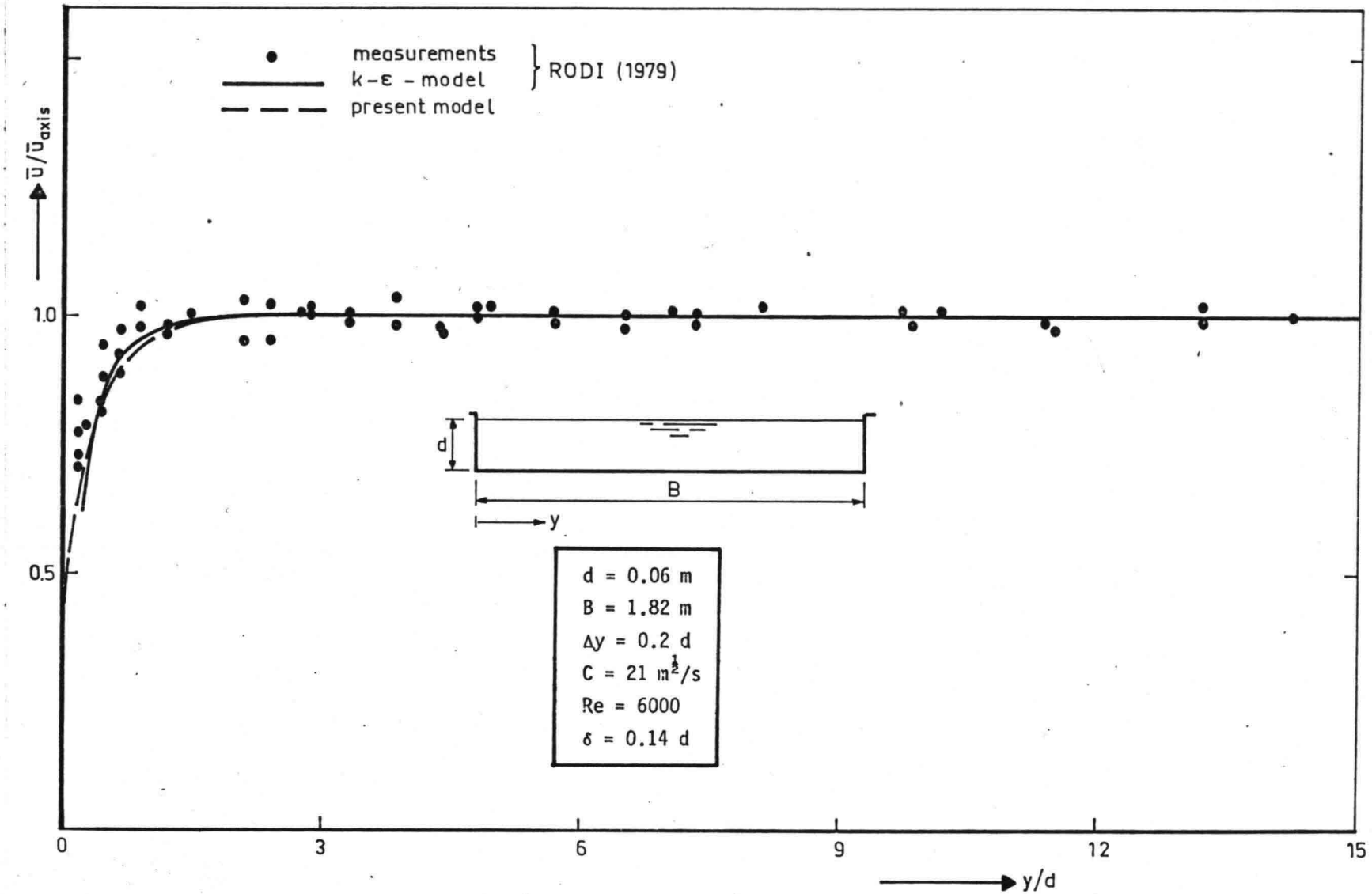

Figure 4. Fully developed flow in a straight channel of finite width

(b) Comparison with the depth-averaged k-ε-model

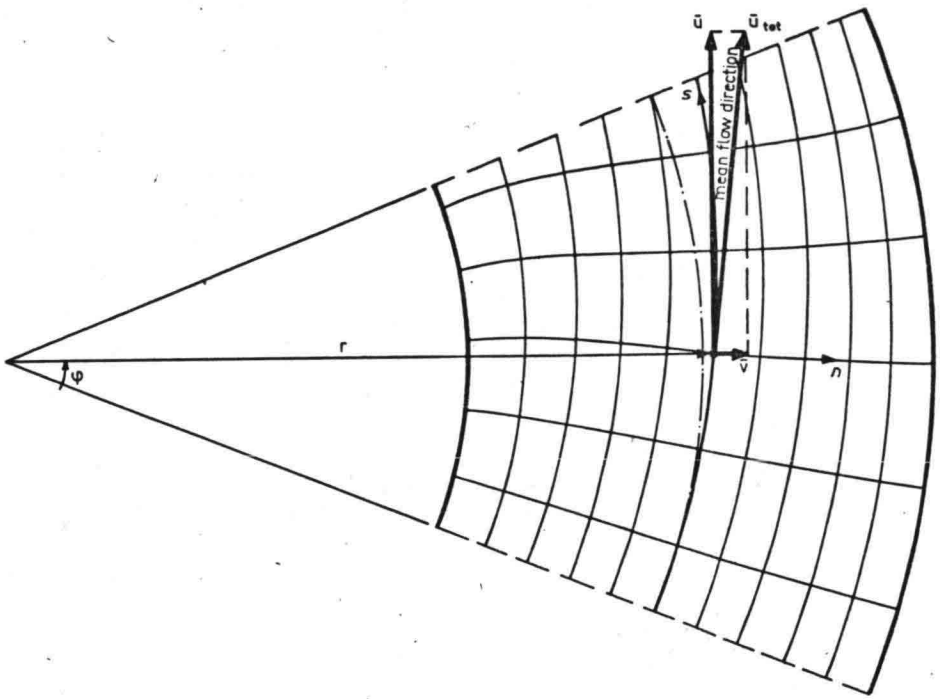

Figure 5. Streamwise coordinates

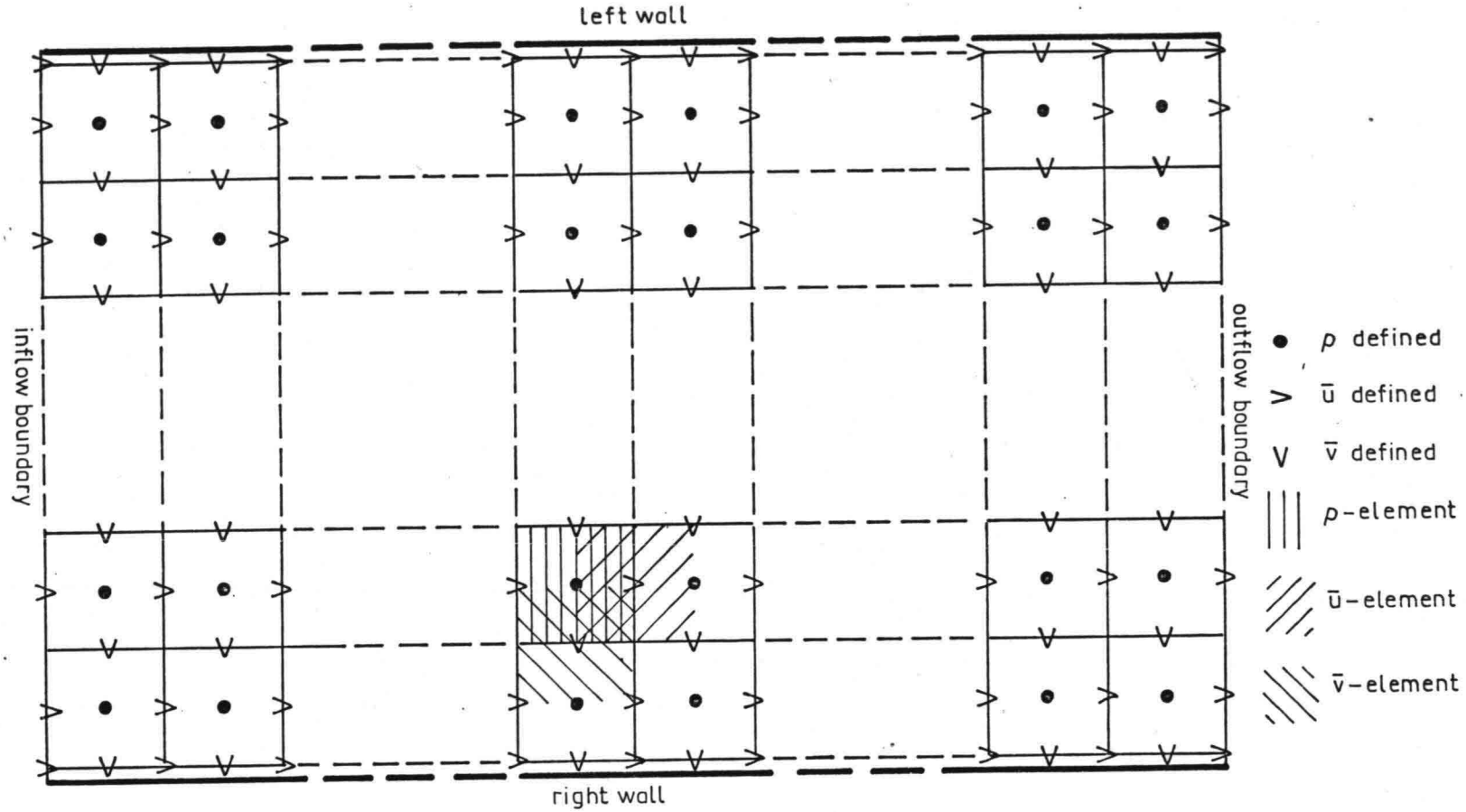

Figure 6. Computational grid for calculation of the depth-averaged flow

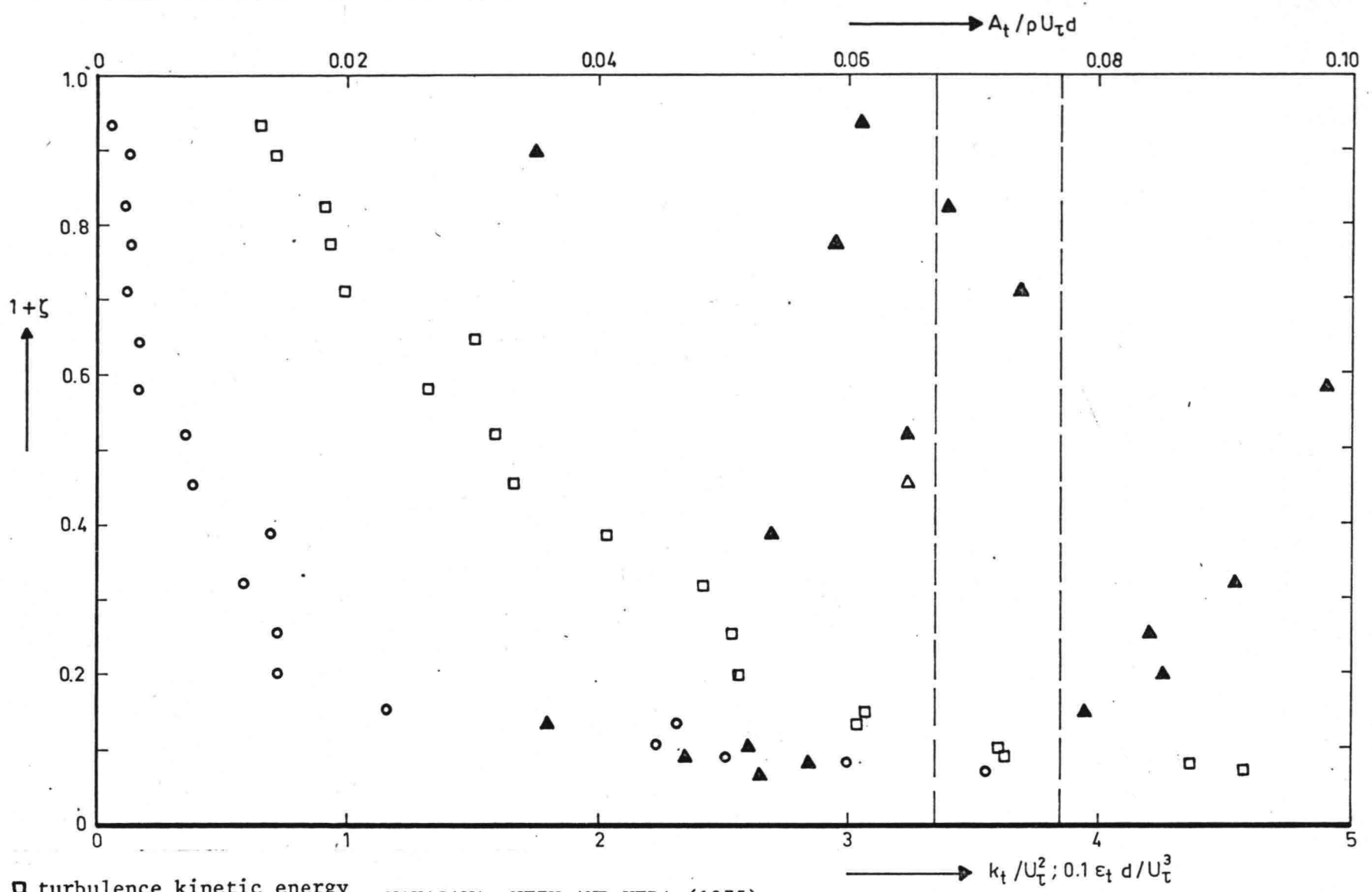

Figure 7. Turbulence viscosity based on measured turbulence data

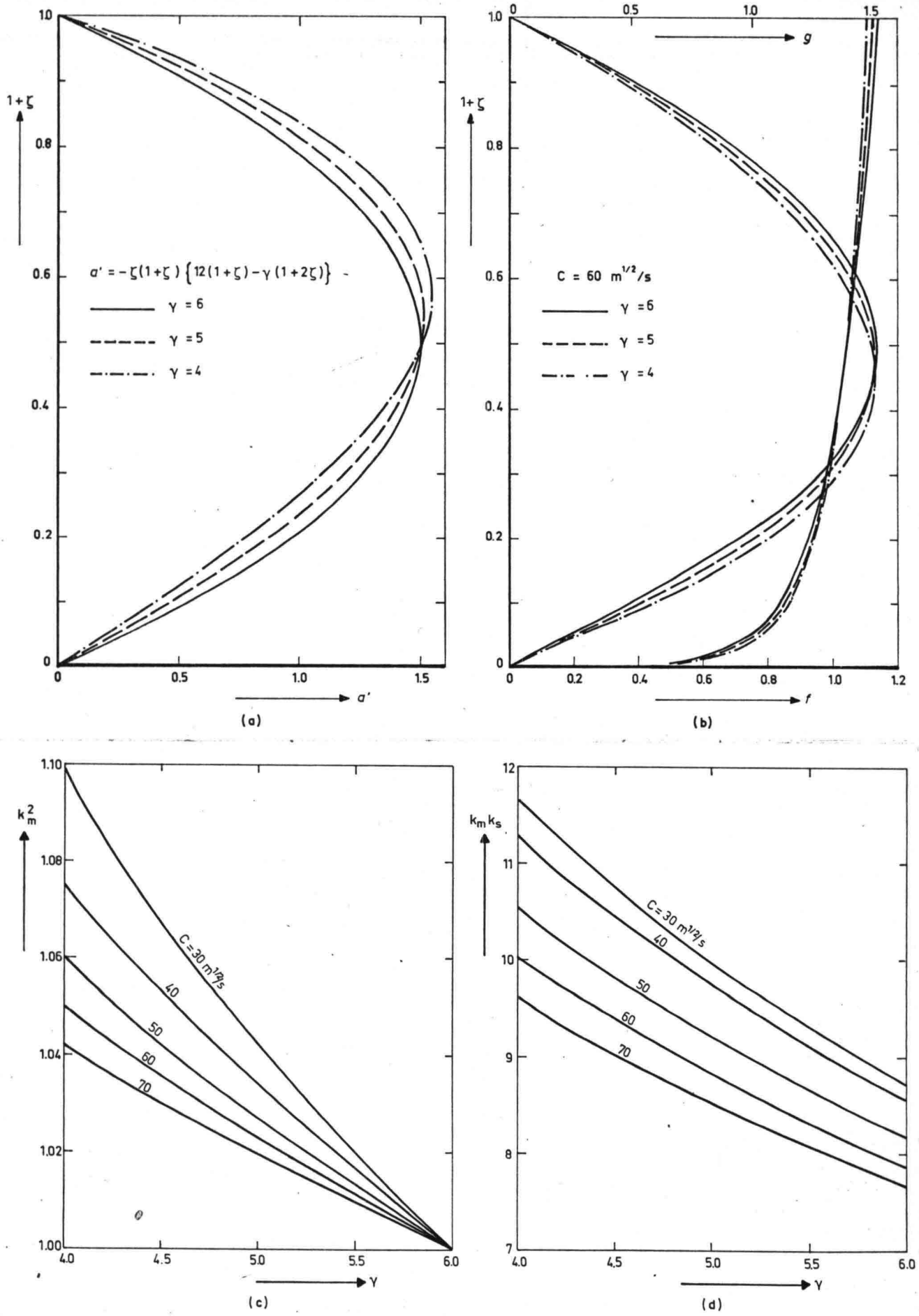

Figure 8. Influence of the mean value of the turbulence viscosity
(a) Turbulence viscosity (b) Main and secondary velocity
(c)-(d) Bed shear stress factors

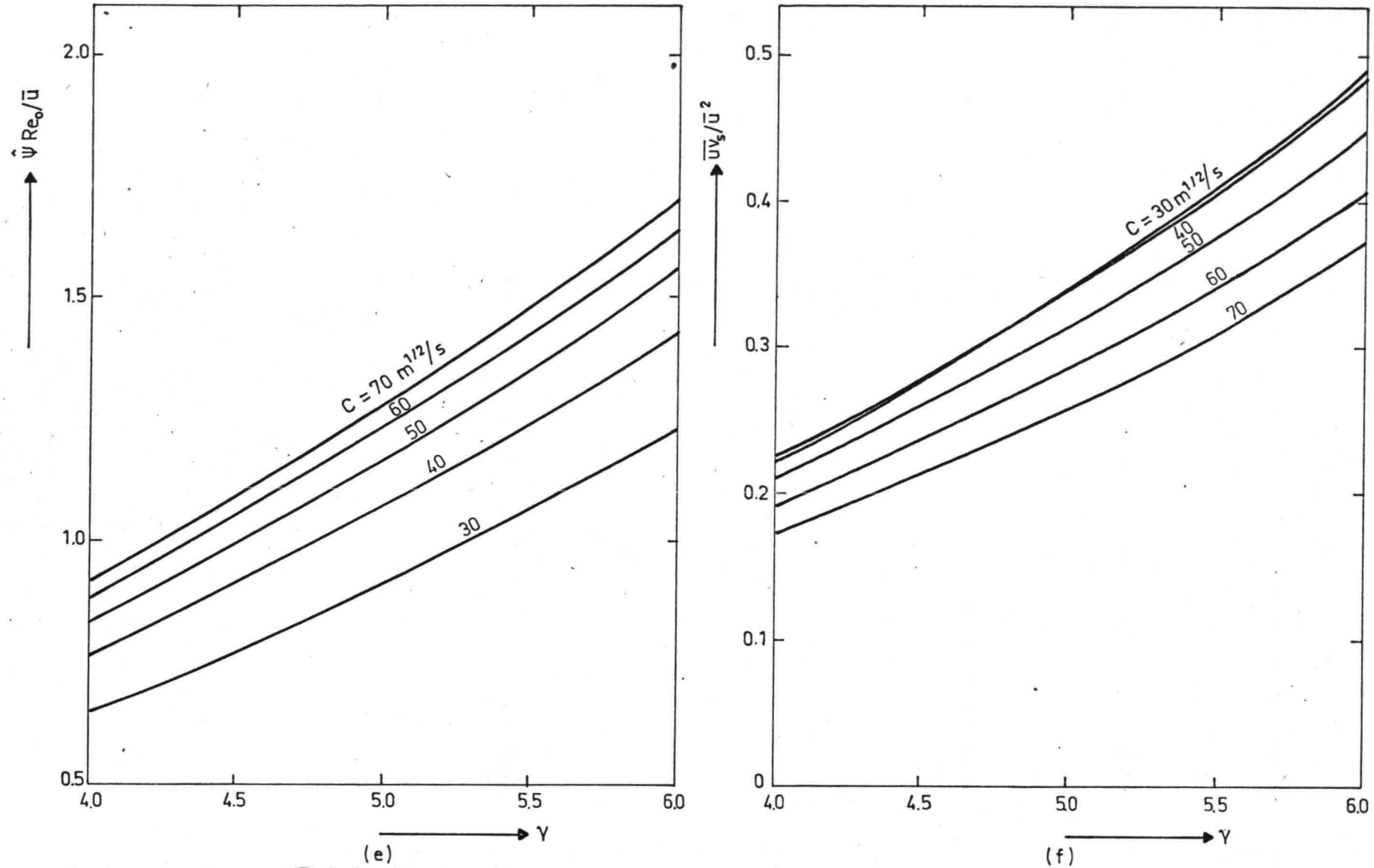

Figure 8. Influence of the mean value of the turbulence viscosity

(e) Secondary flow intensity

(f) Secondary flow advection factor

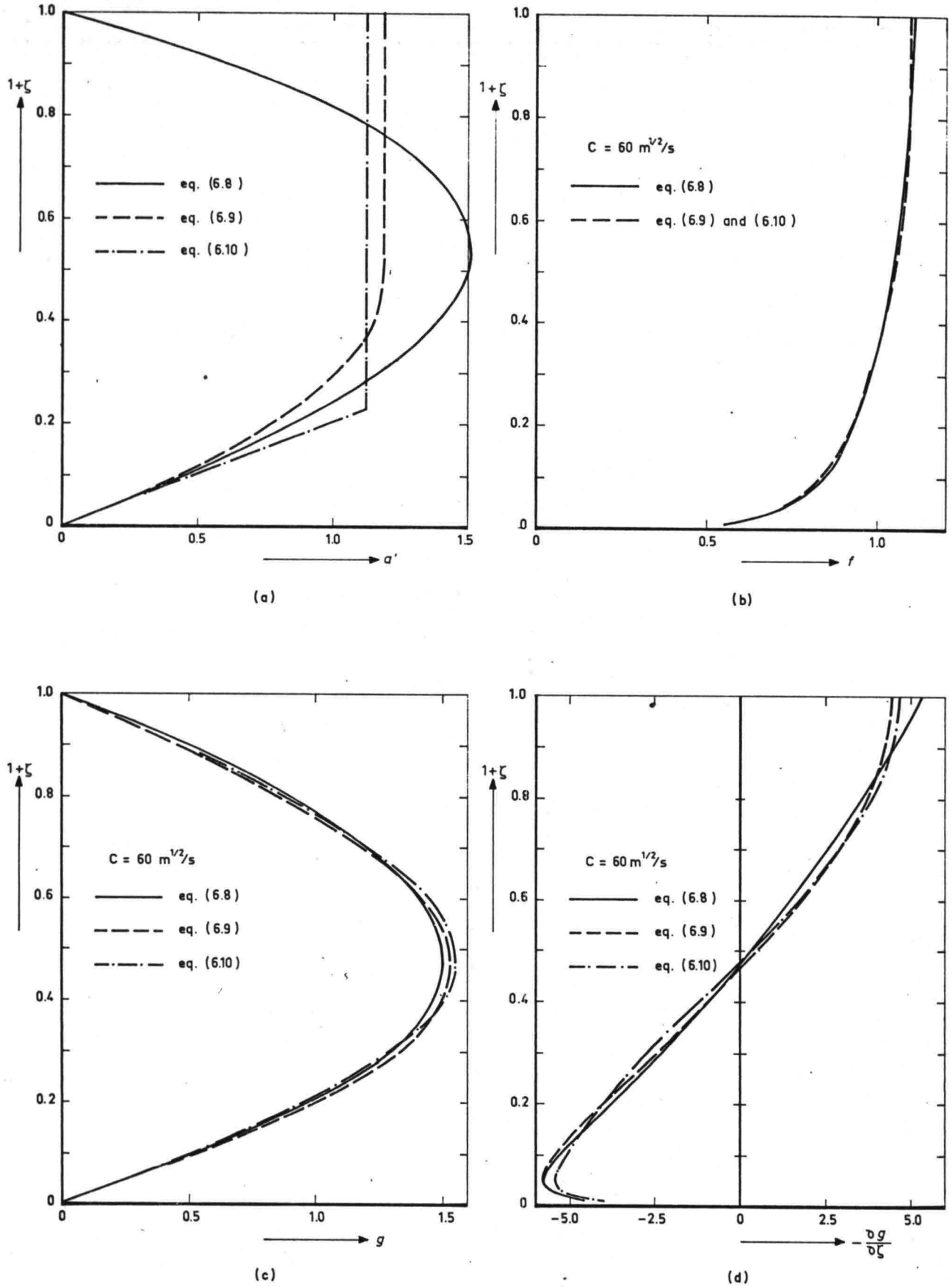

Figure 9. Influence of the vertical distribution of the turbulence viscosity on the vertical velocity distributions

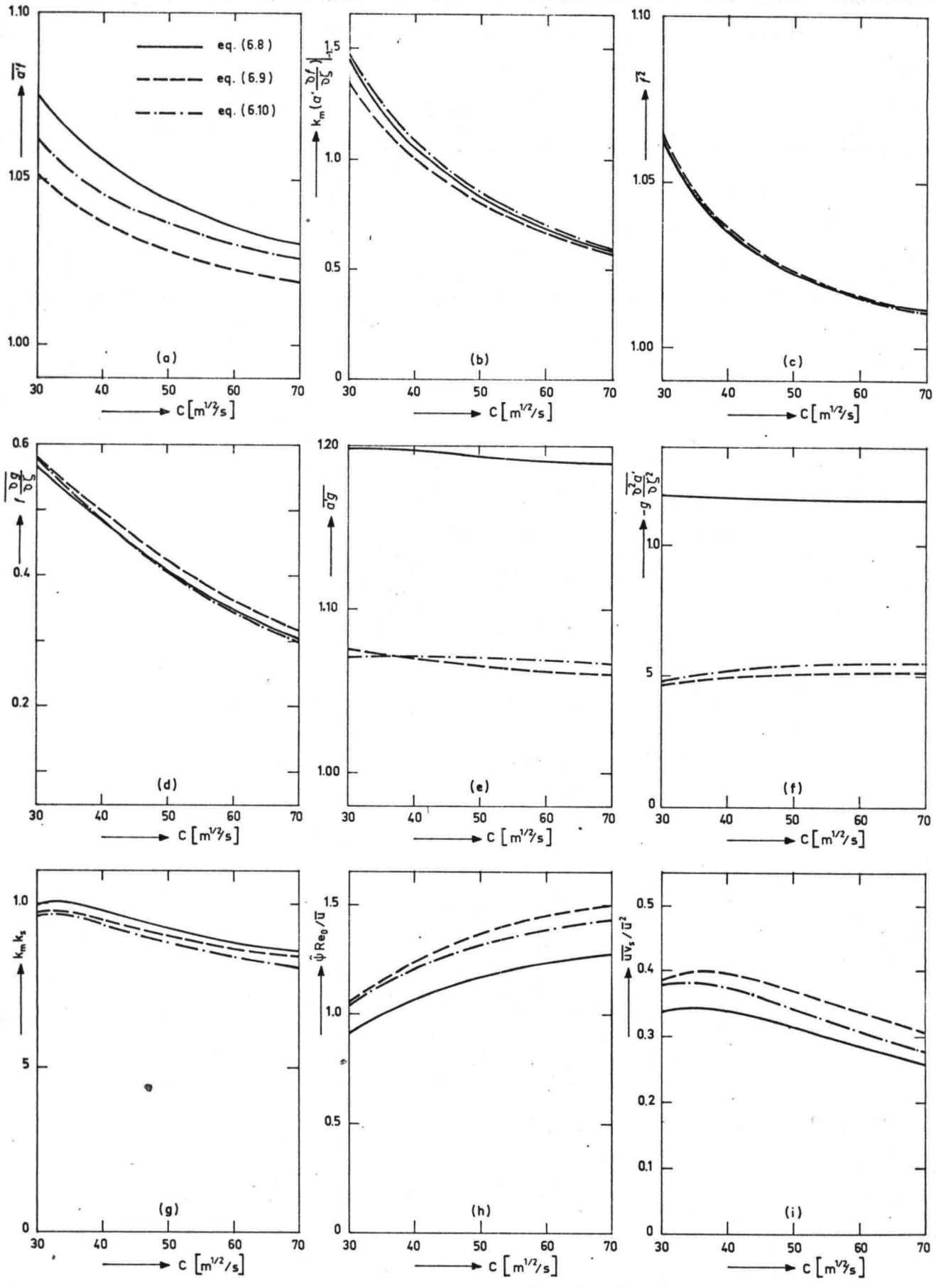

Figure 10. Influence of the vertical distribution of the turbulence viscosity on the coefficients in the depth-averaged system

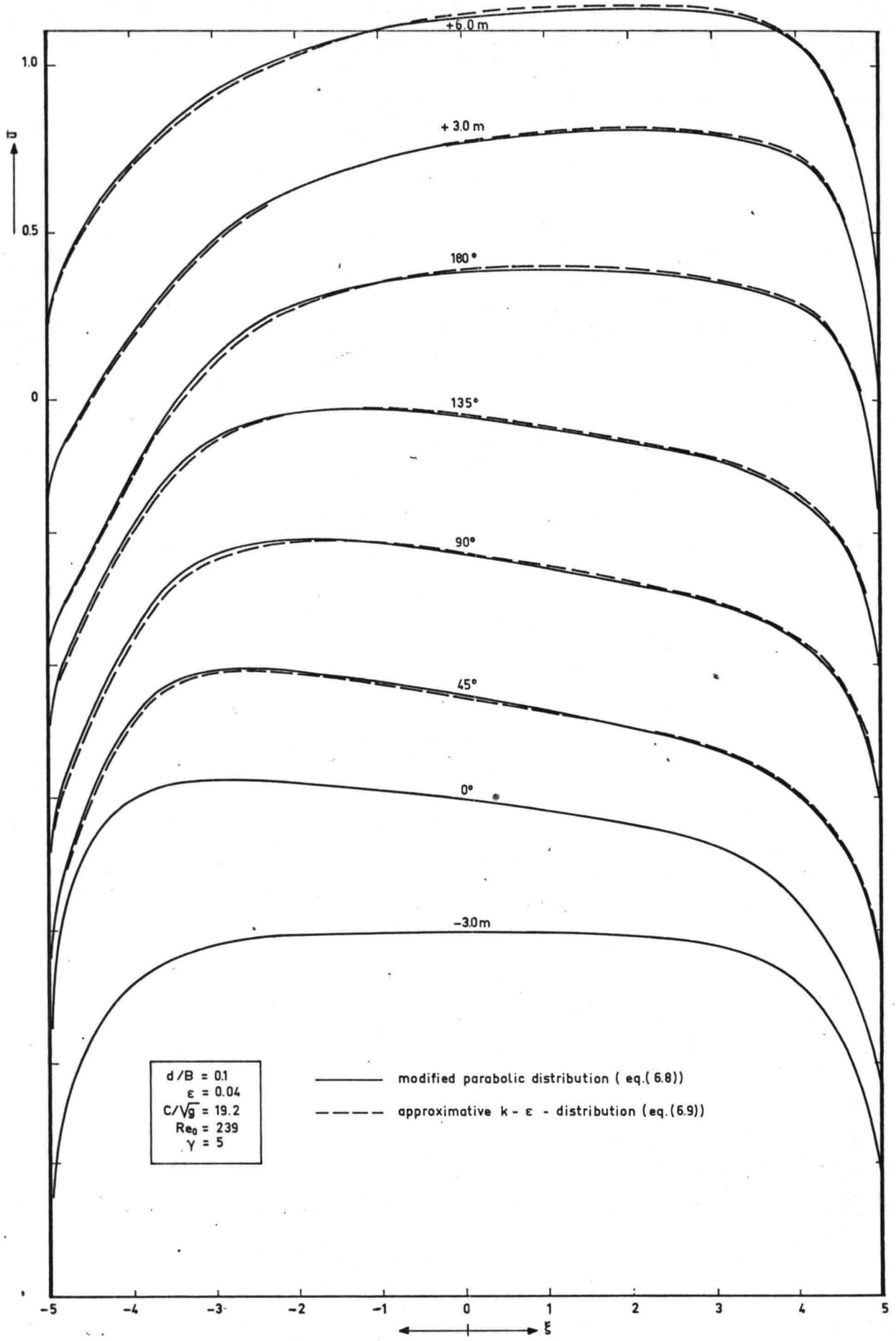

Figure 11. Influence of the vertical distribution of the turbulence viscosity on the flow in the LFM-flume

(a) Main velocity distribution

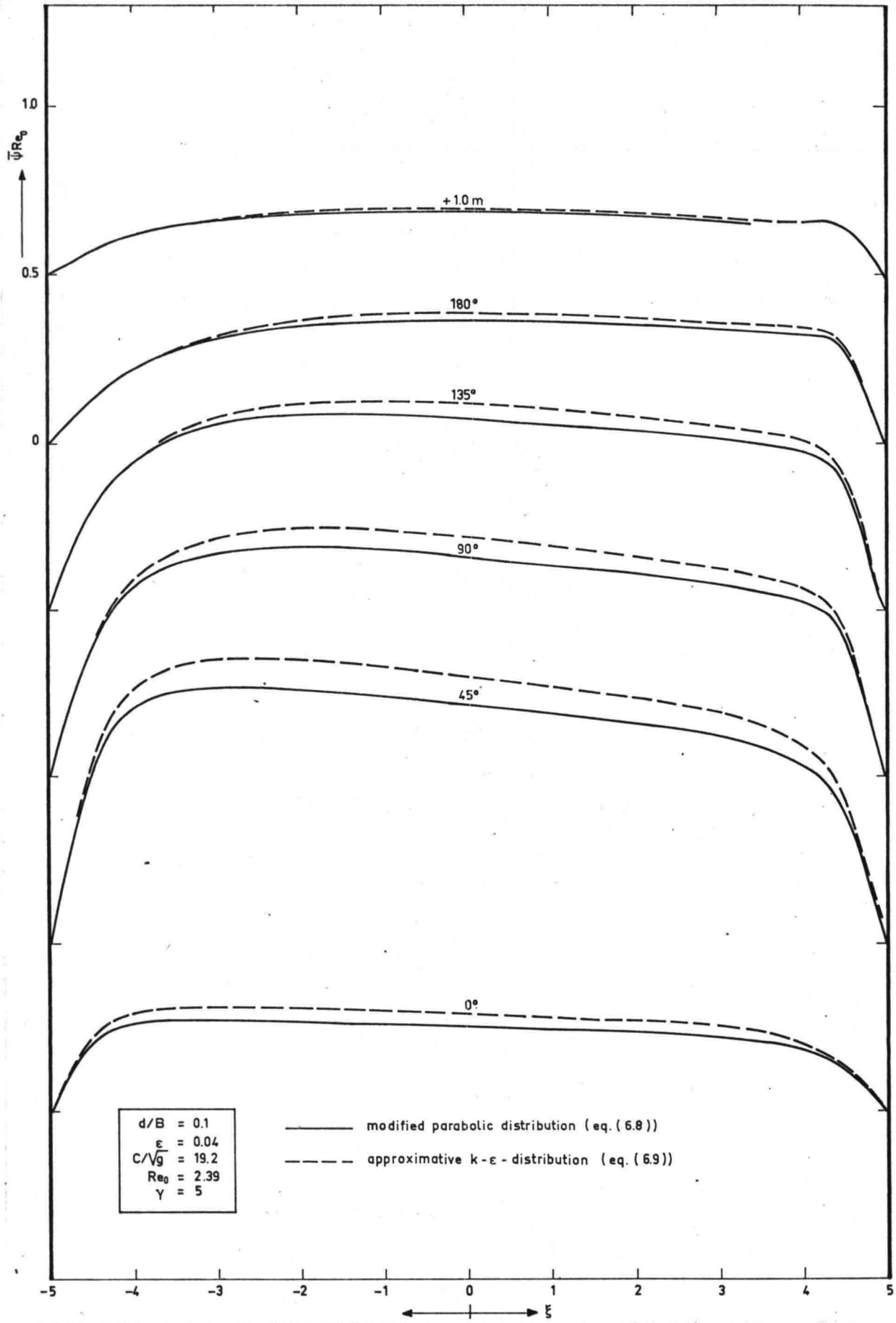

Figure 11. Influence of the vertical distribution of the turbulence viscosity on the flow in the LFM-flume

(b) Stream function of the secondary flow

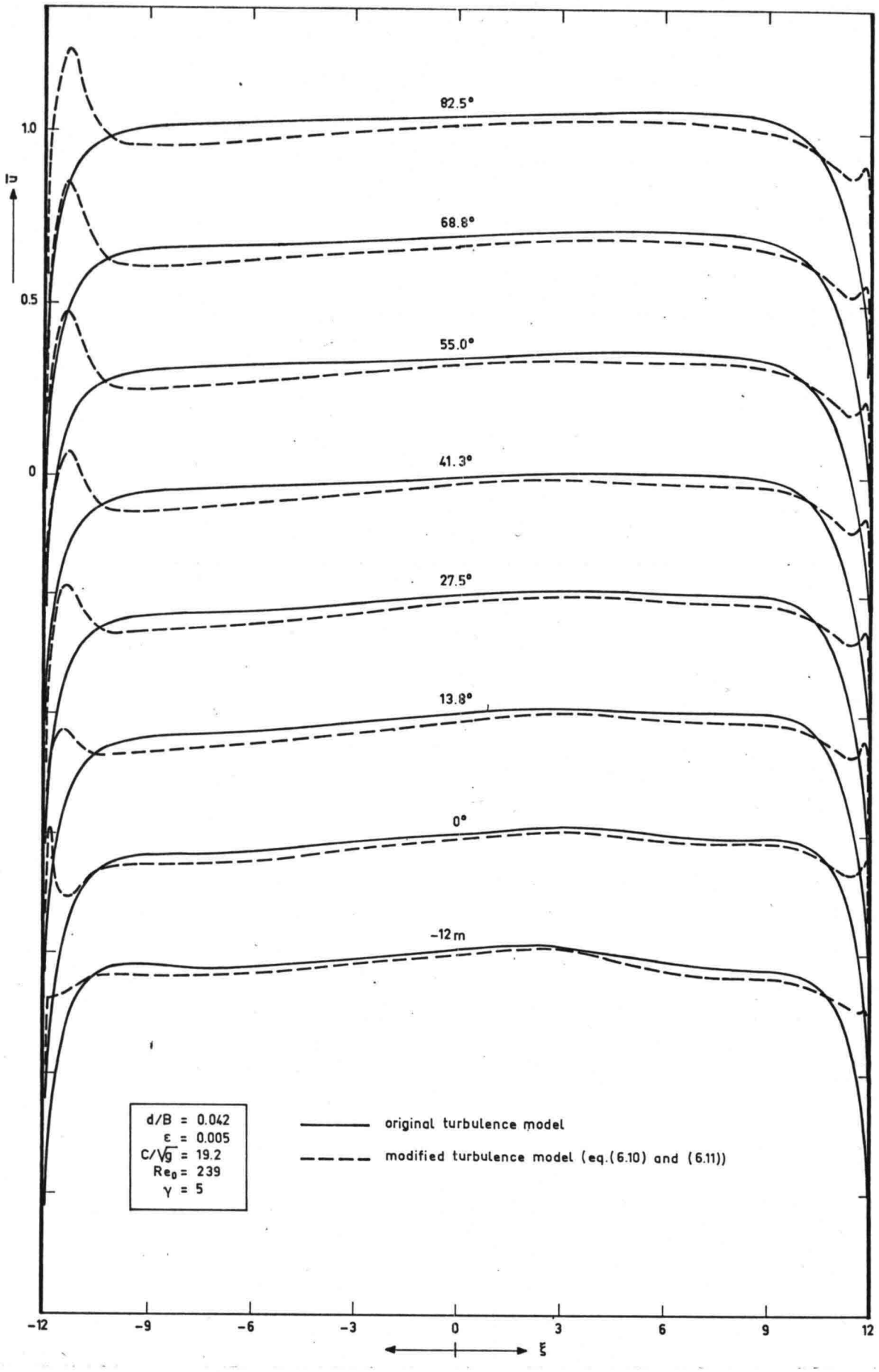

Figure 12. Influence of the horizontal distribution of the turbulence viscosity

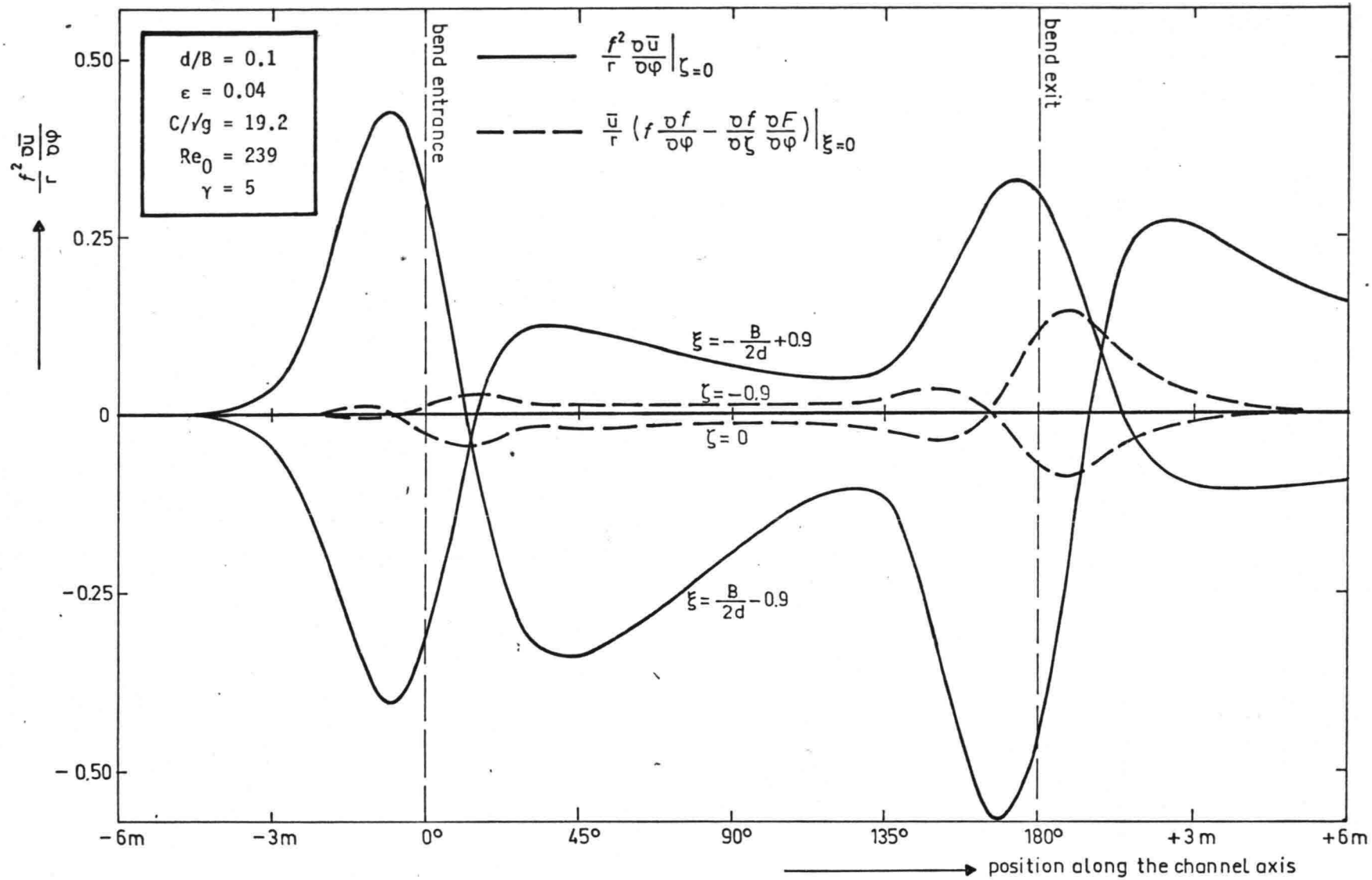

Figure 13. Influence of the vertical component of the main velocity in the main flow momentum equation

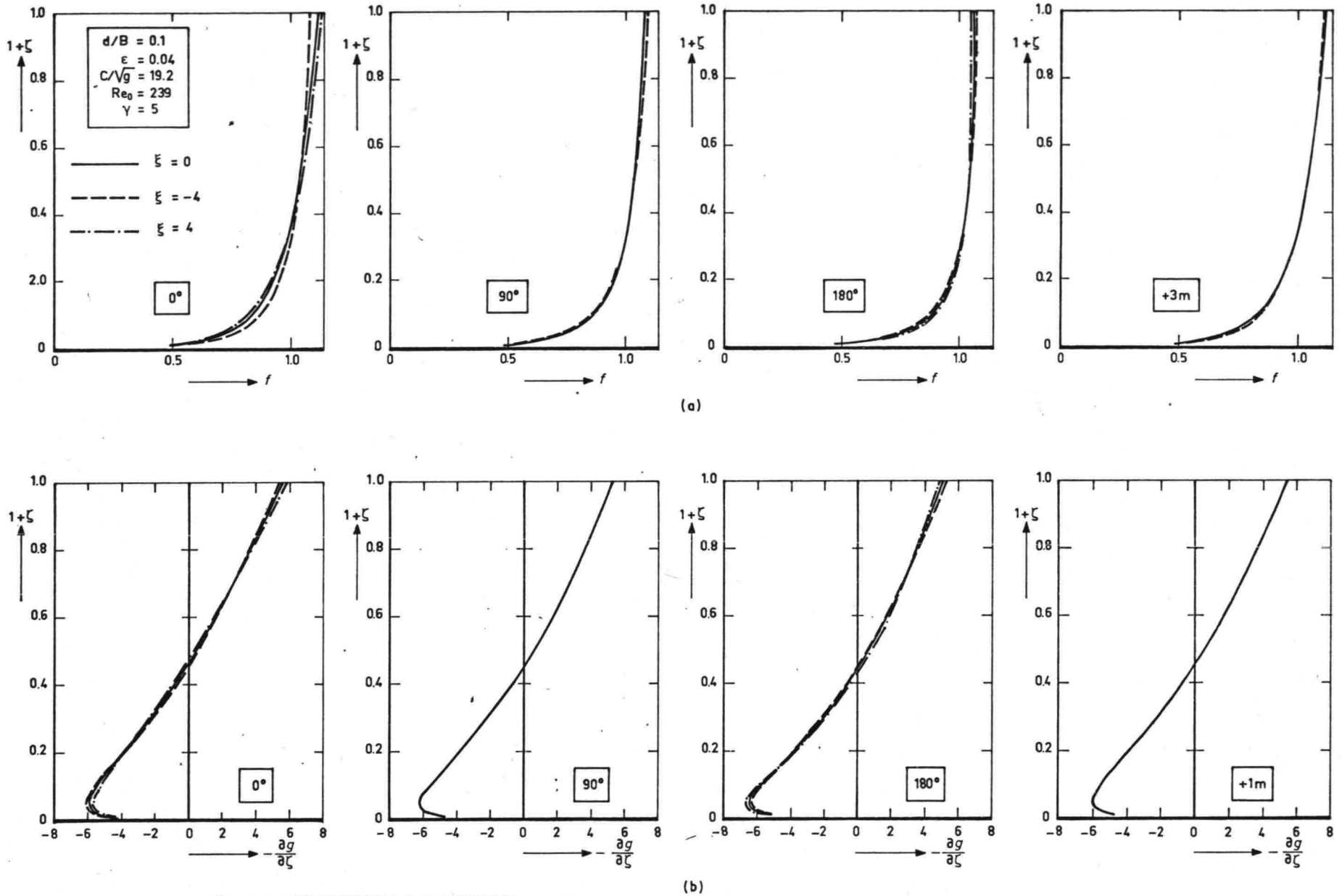

Figure 14. Influence of the streamwise accelerations of the main flow on the vertical distribution functions

(a) Main velocity (b) Horizontal component of the secondary flow

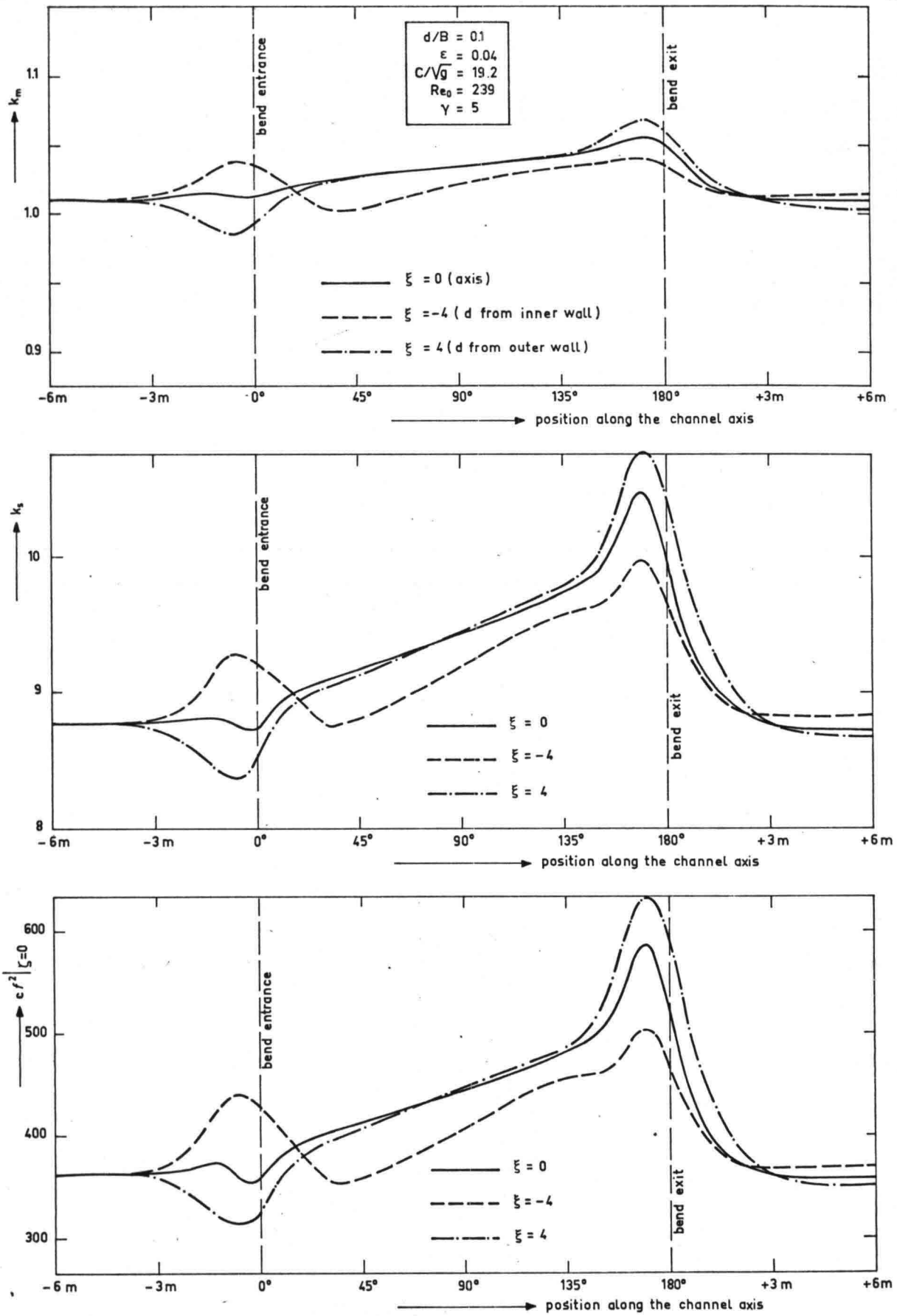

Figure 14. Influence of the streamwise accelerations of the main flow on the vertical distribution functions

(c) Constants

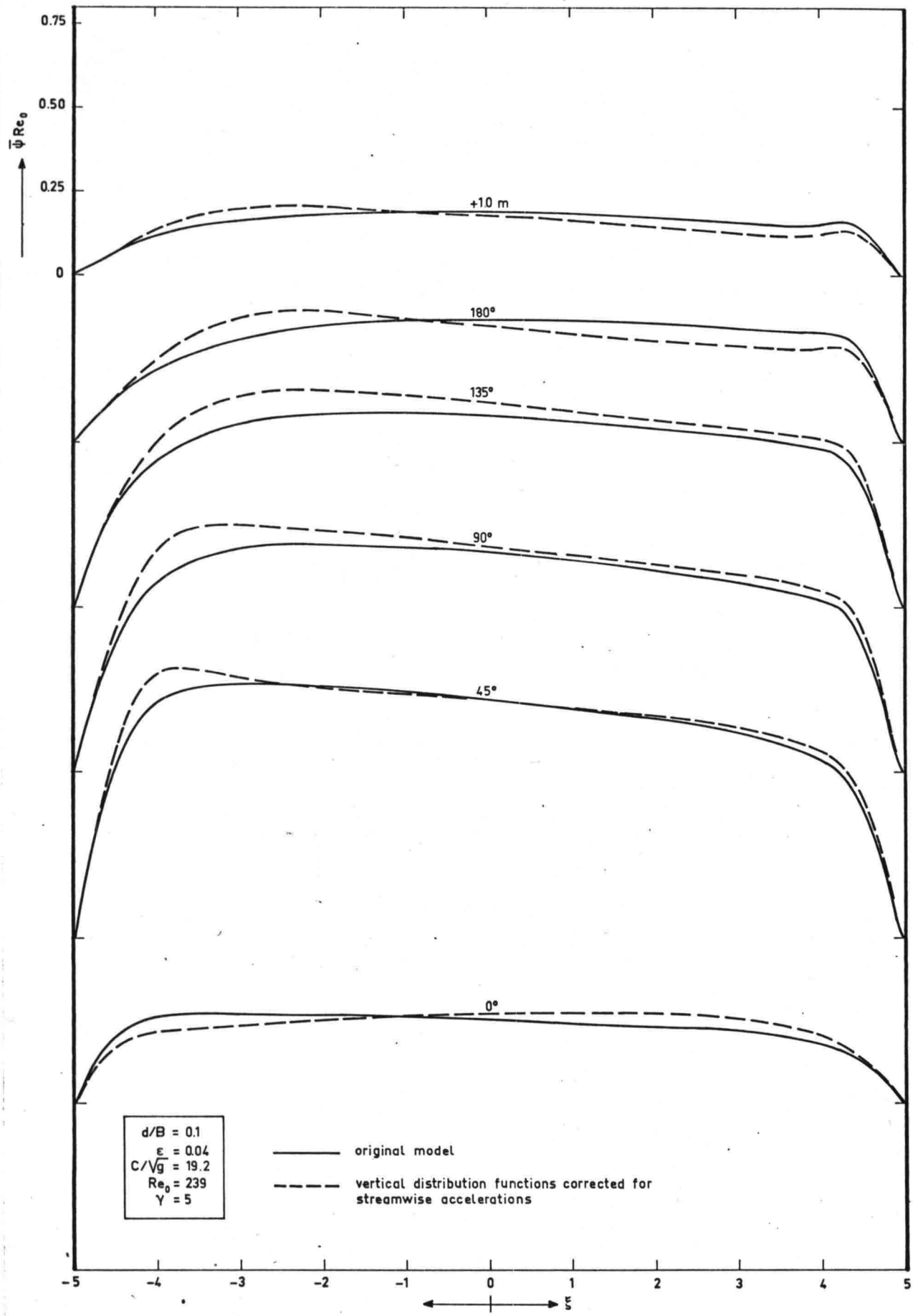

Figure 15. Influence of the streamwise accelerations of the main flow on the depth-averaged flow

(b) Secondary flow intensity

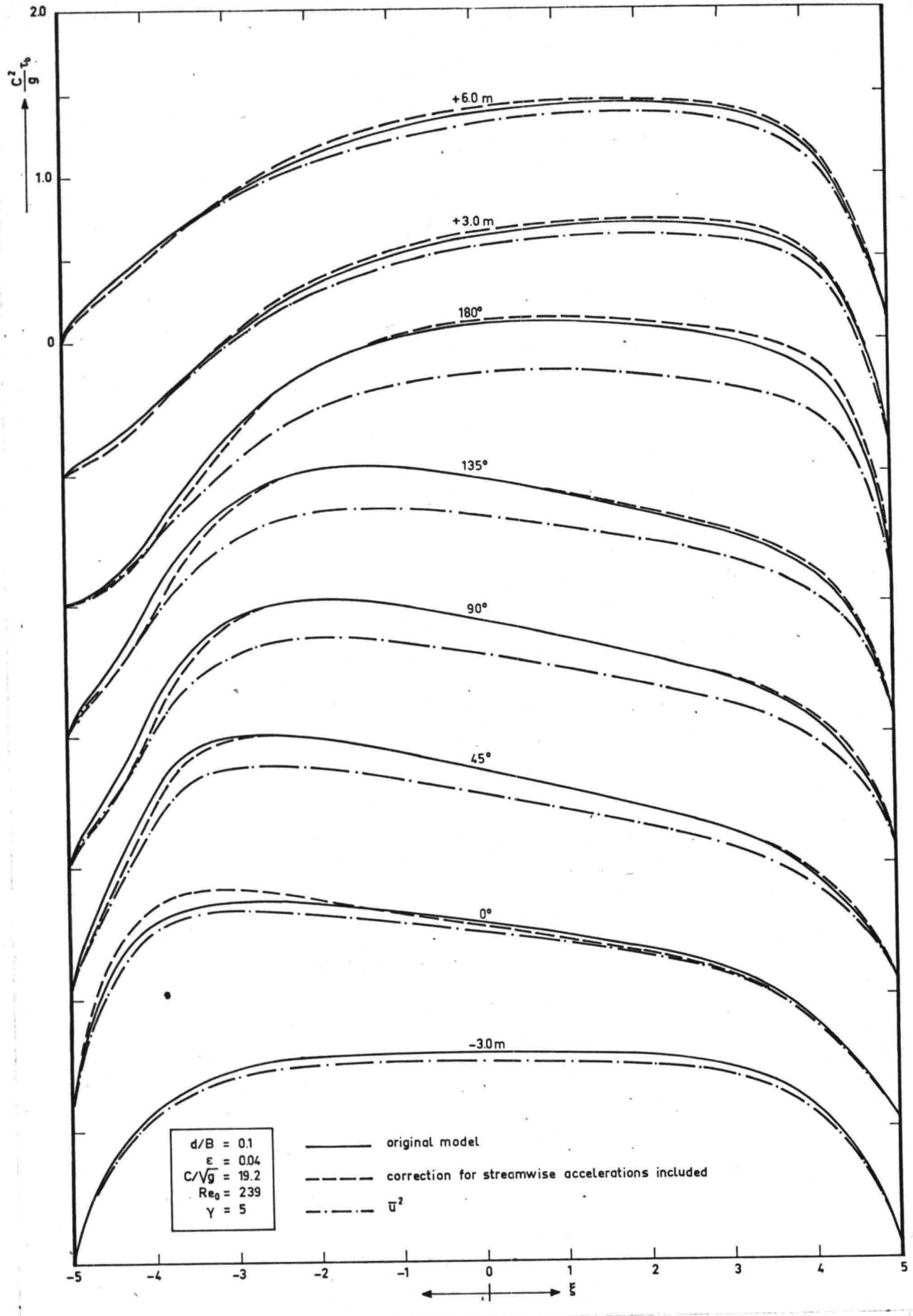

Figure 16. Influence of the streamwise accelerations of the main flow on the bed shear stress

(a) Magnitude of the total bed shear stress

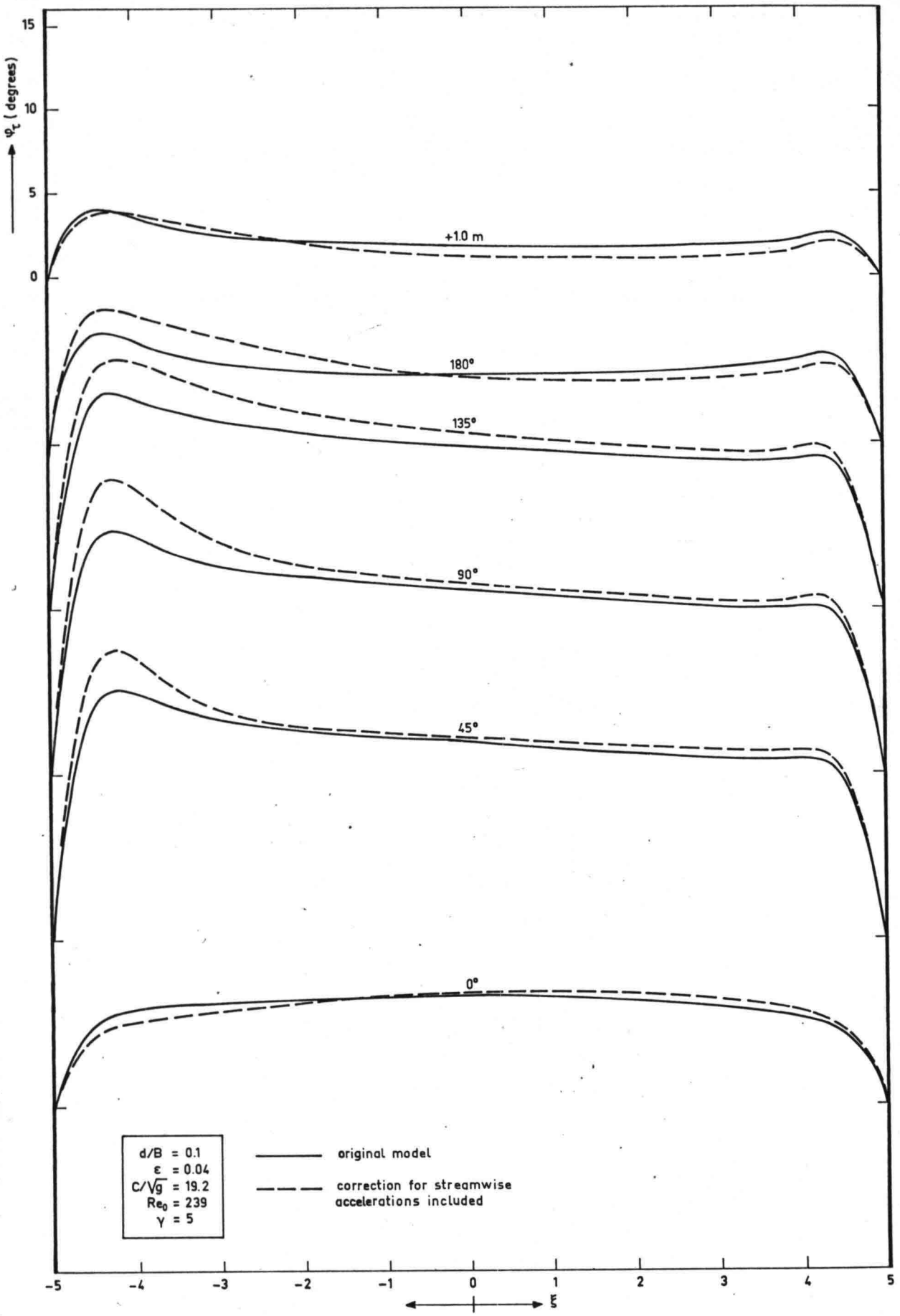

Figure 16. Influence of the streamwise accelerations of the main flow on the bed shear stress

(b) Direction of the total bed shear stress

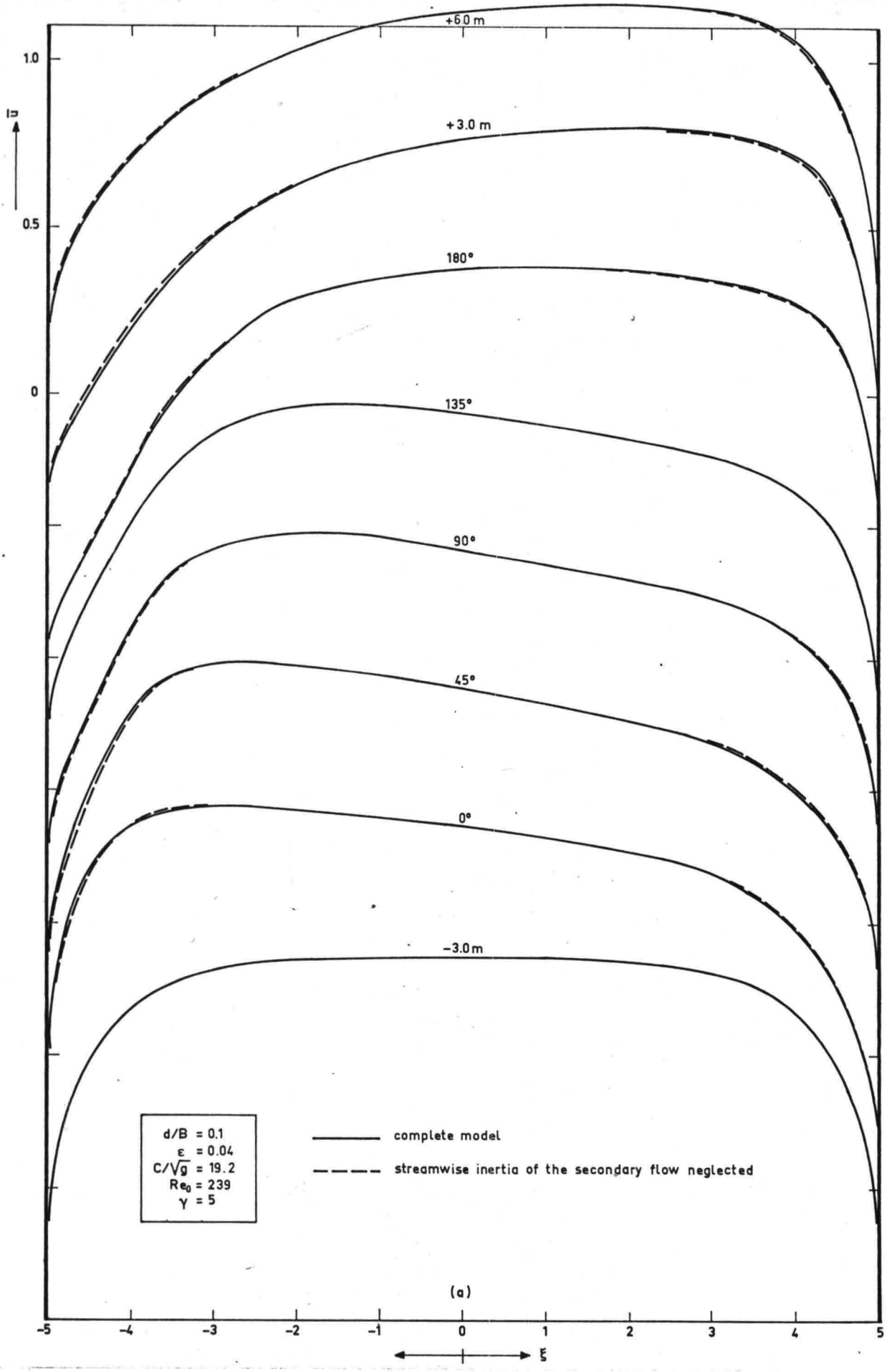

Figure 17. Influence of the streamwise inertia of the secondary flow

(a) Depth-averaged main velocity

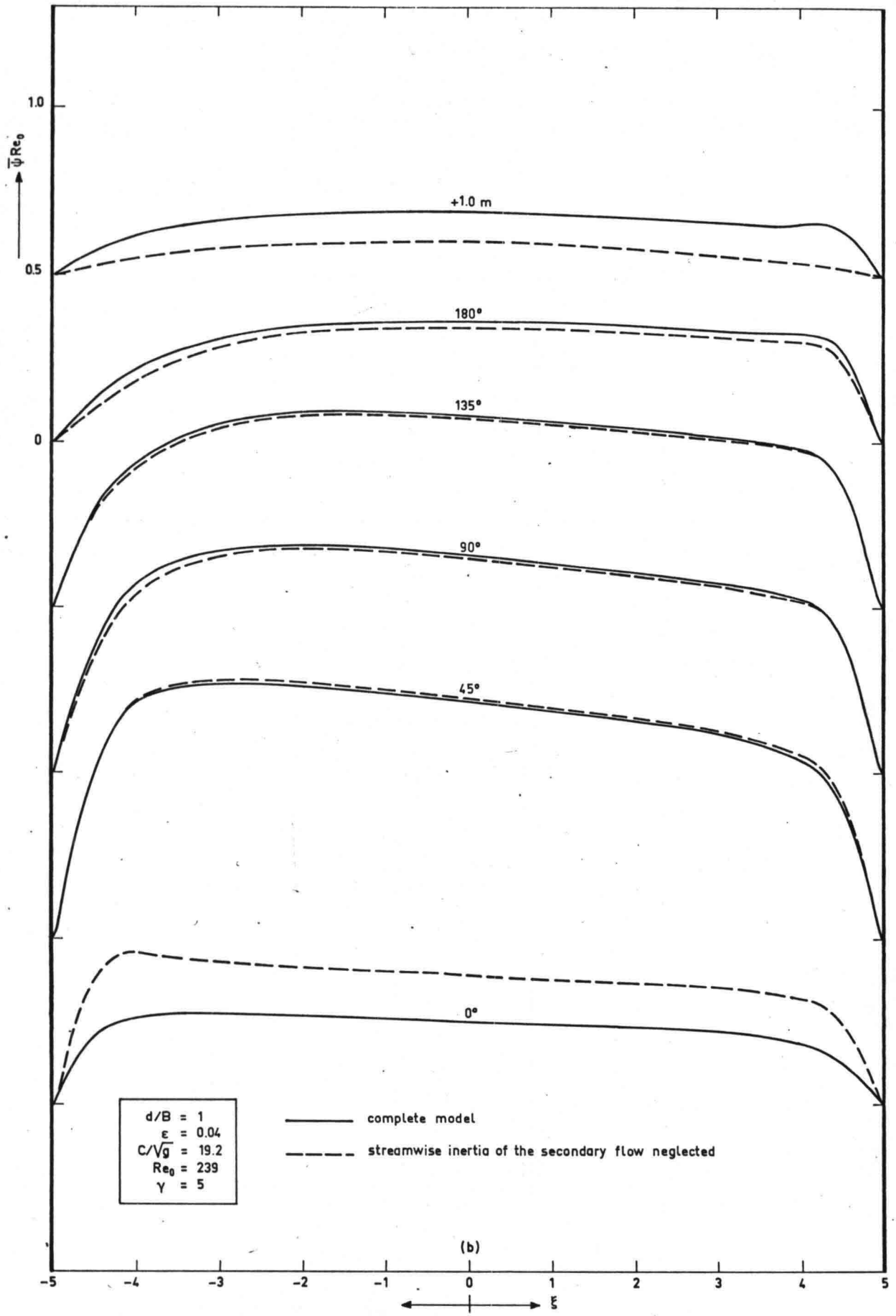

Figure 17. Influence of the streamwise inertia of the secondary flow
(b) Secondary flow intensity

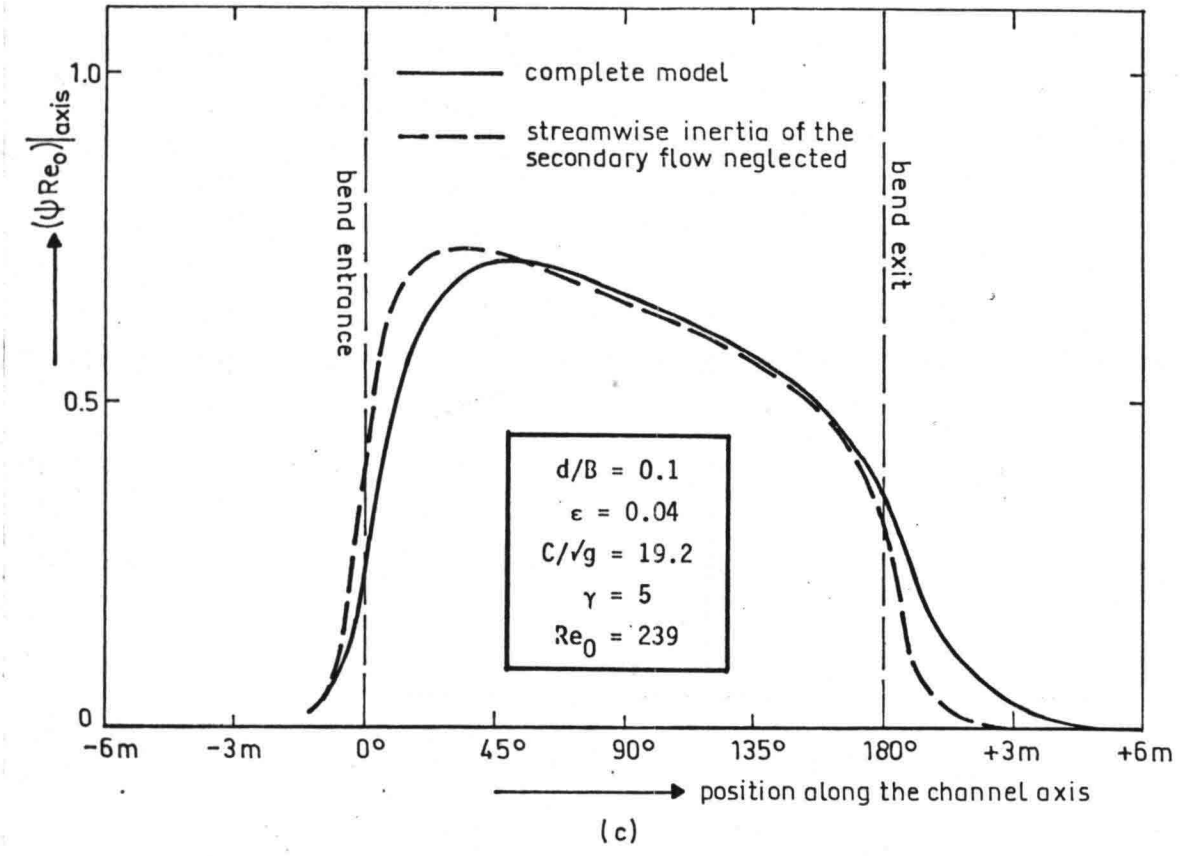

(c)

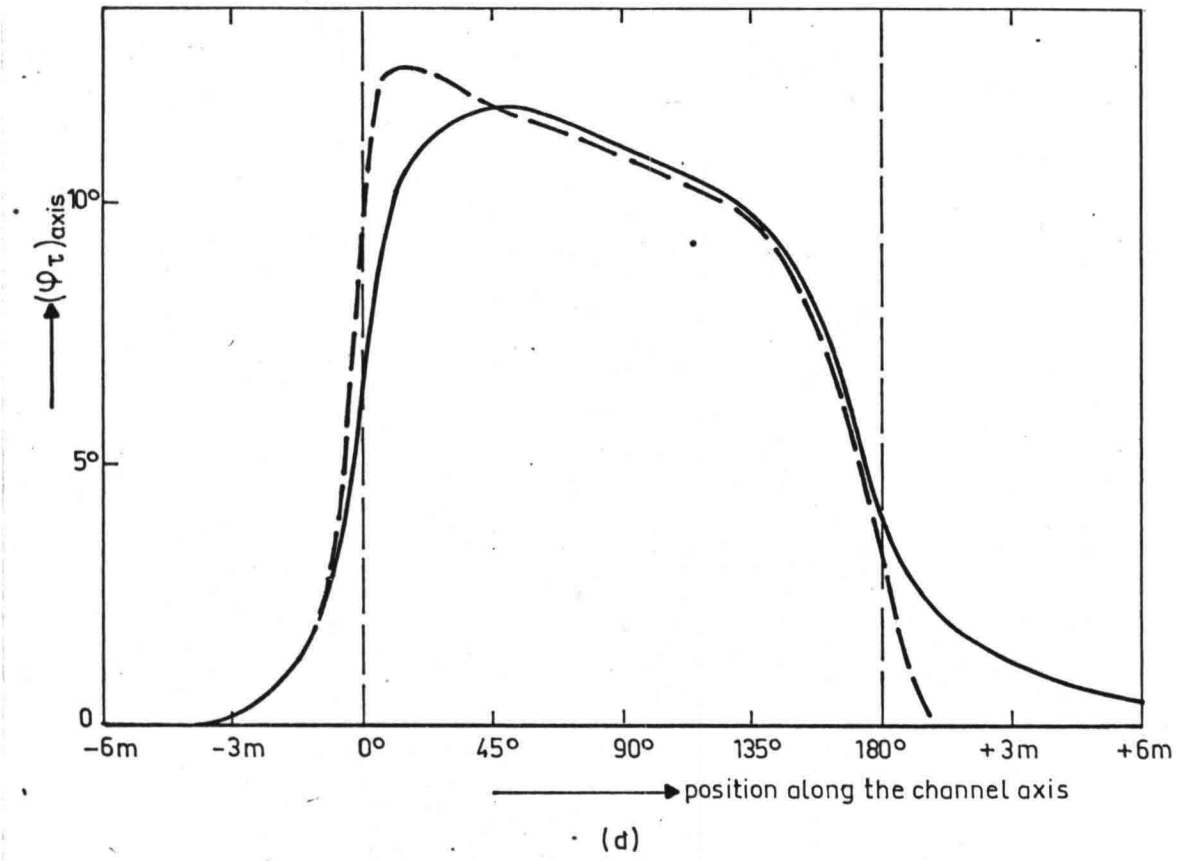

(d)

Figure 17. Influence of the streamwise inertia of the secondary flow

(c) Secondary flow intensity in the channel axis

(d) Direction of the bed shear stress in the channel axis

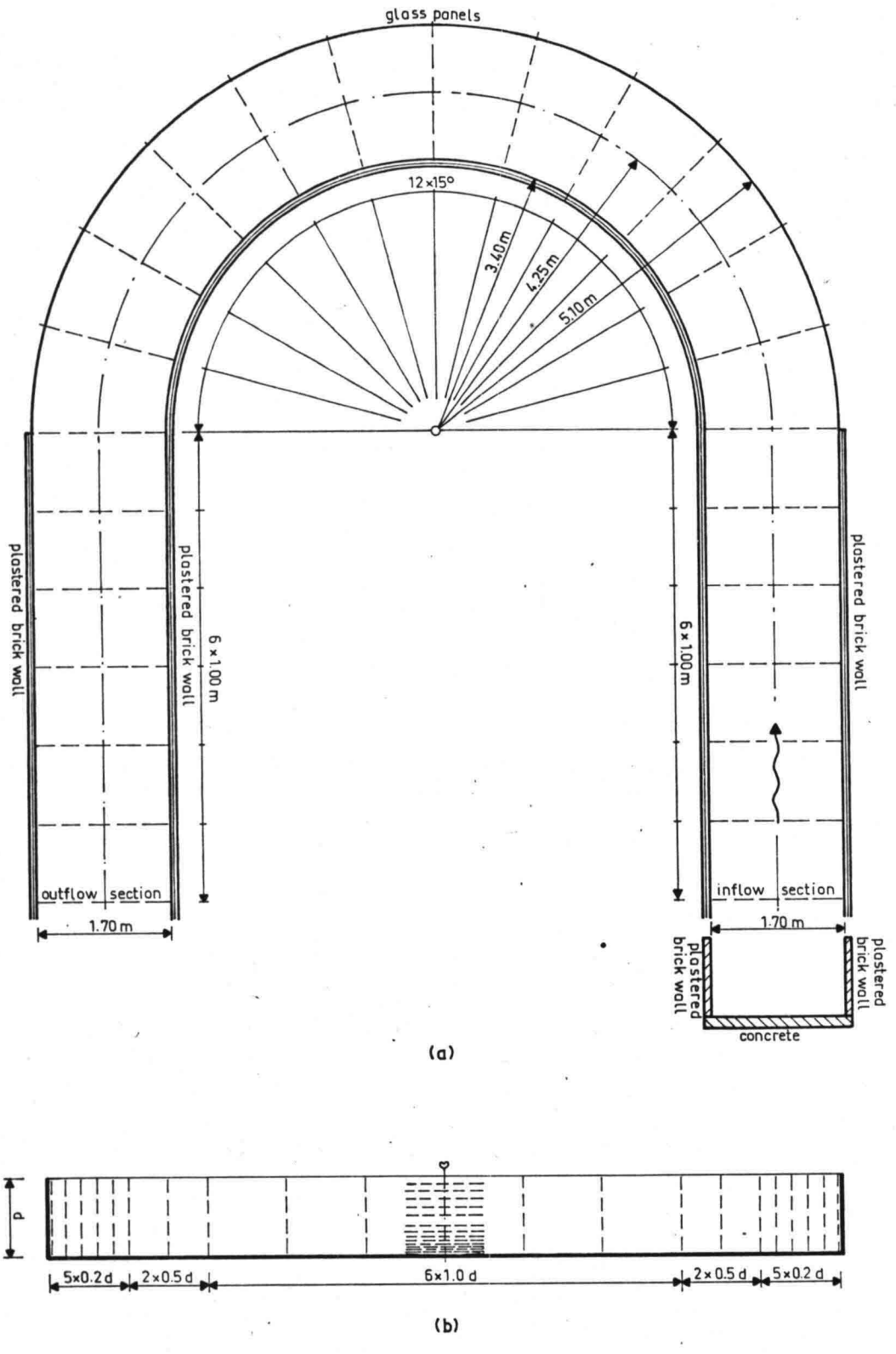

Figure 18. Simulation of the LFM-experiments

(a) Flume and cross-sections of the computational grid

(b) Transverse configuration of the computational grid

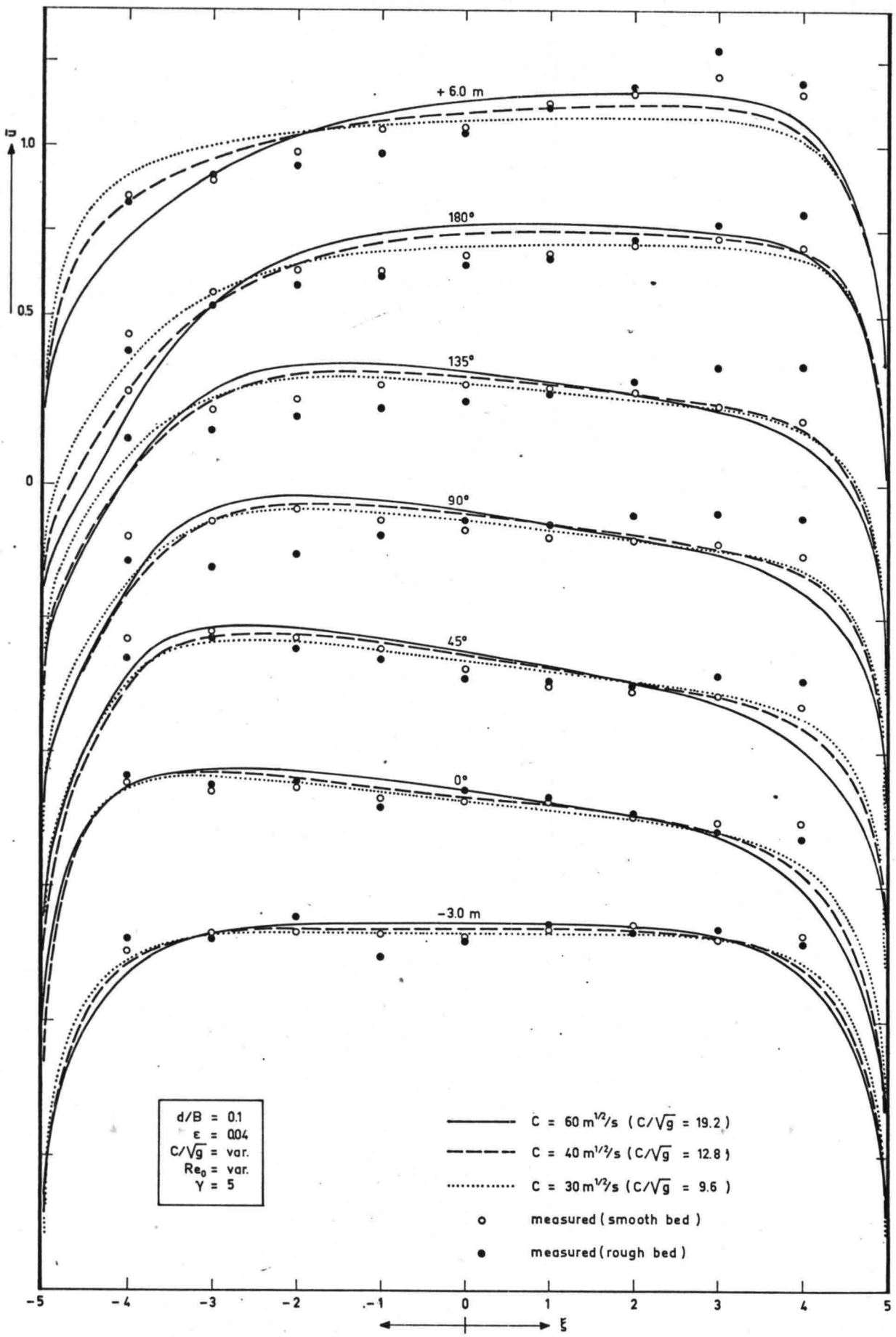

Figure 19. Results of the simulation of the LFM-experiments

(a) Depth-averaged main velocity

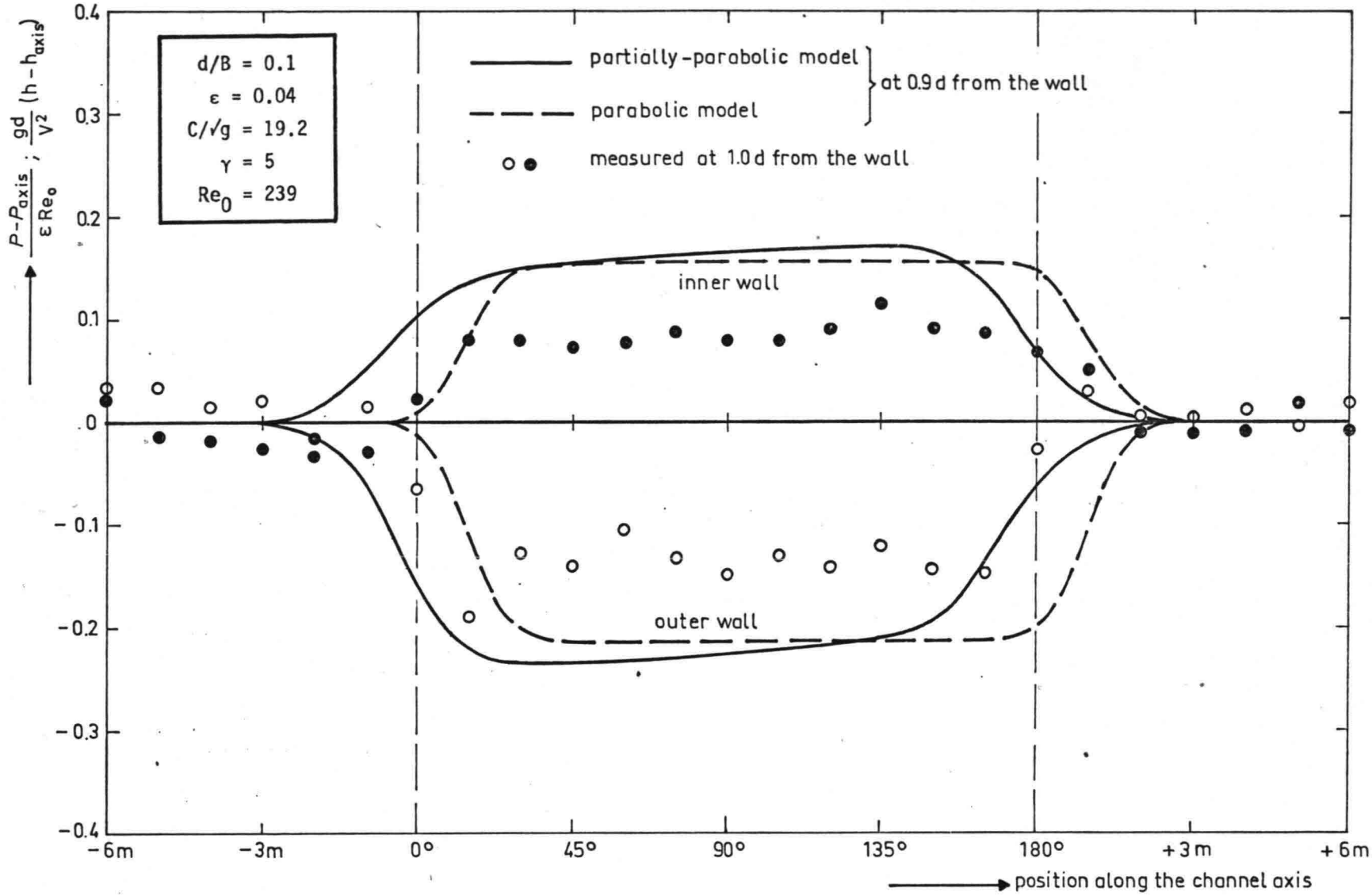

Figure 19. Results of the simulation of the LFM-experiments

(b) Transverse pressure drop

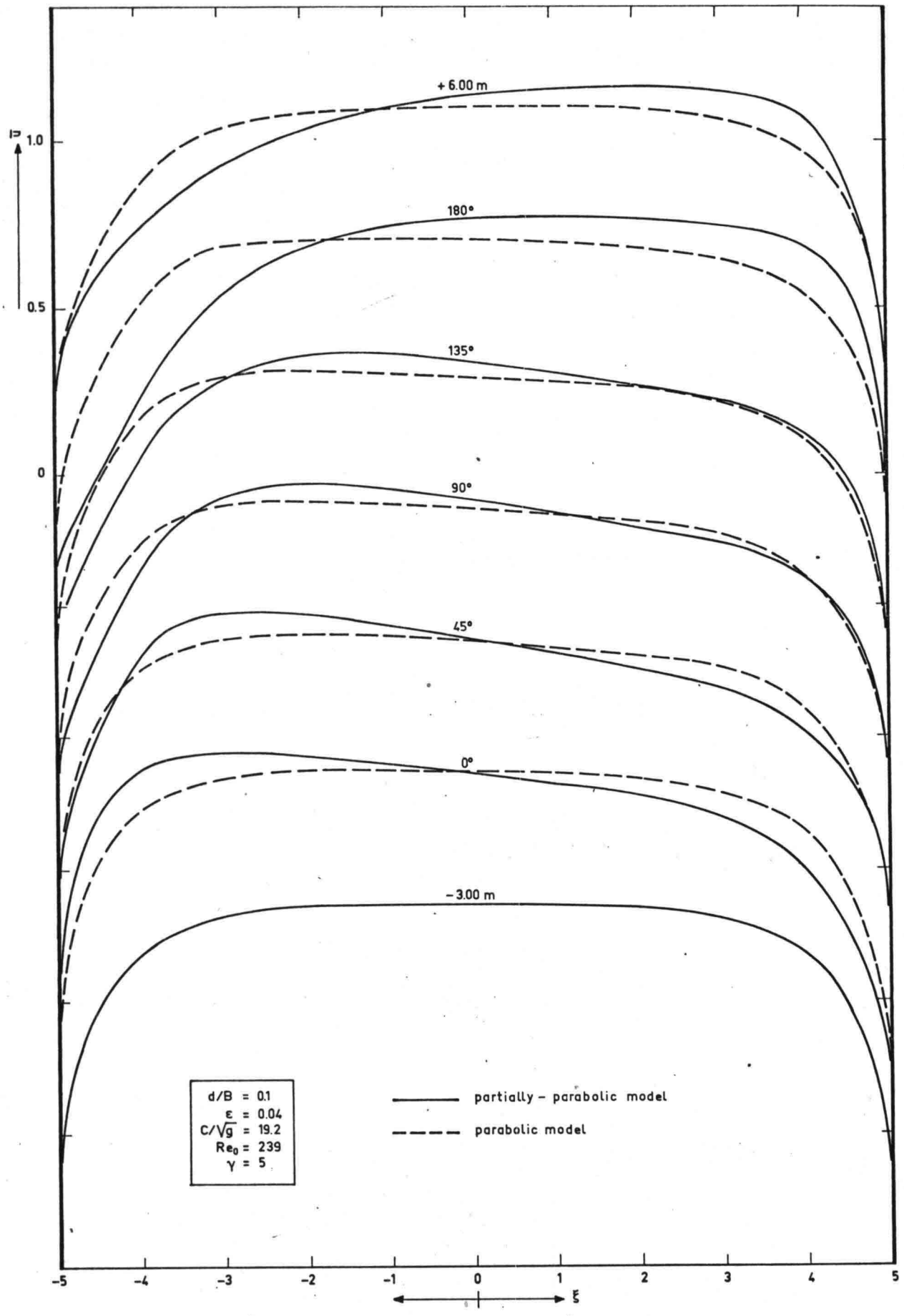

Figure 20. Parabolic vs. partially-parabolic model in the LFM-simulation

(a) Depth-averaged main velocity

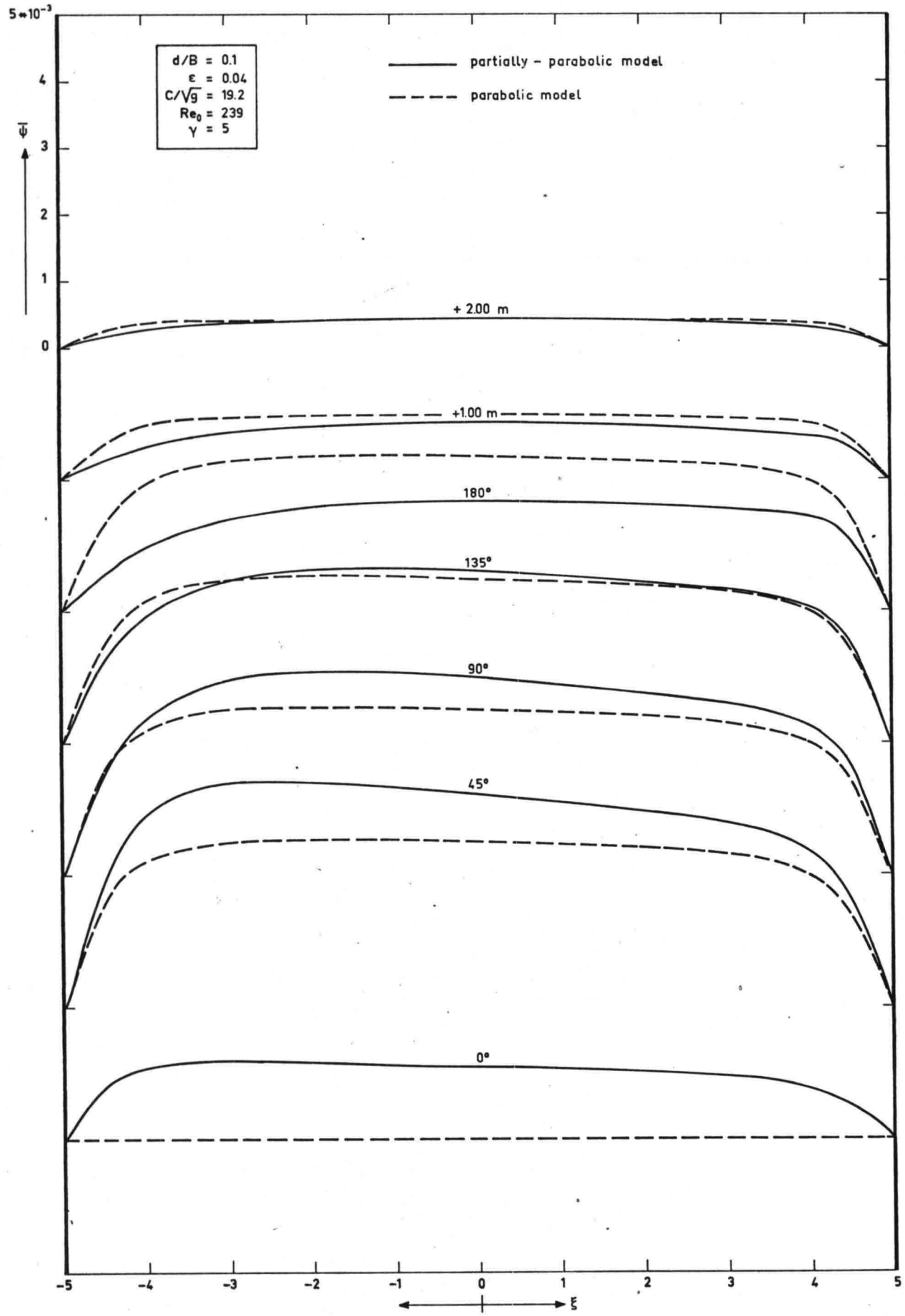

Figure 20. Parabolic vs. partially-parabolic model in the LFM-simulation

(b) Secondary flow intensity

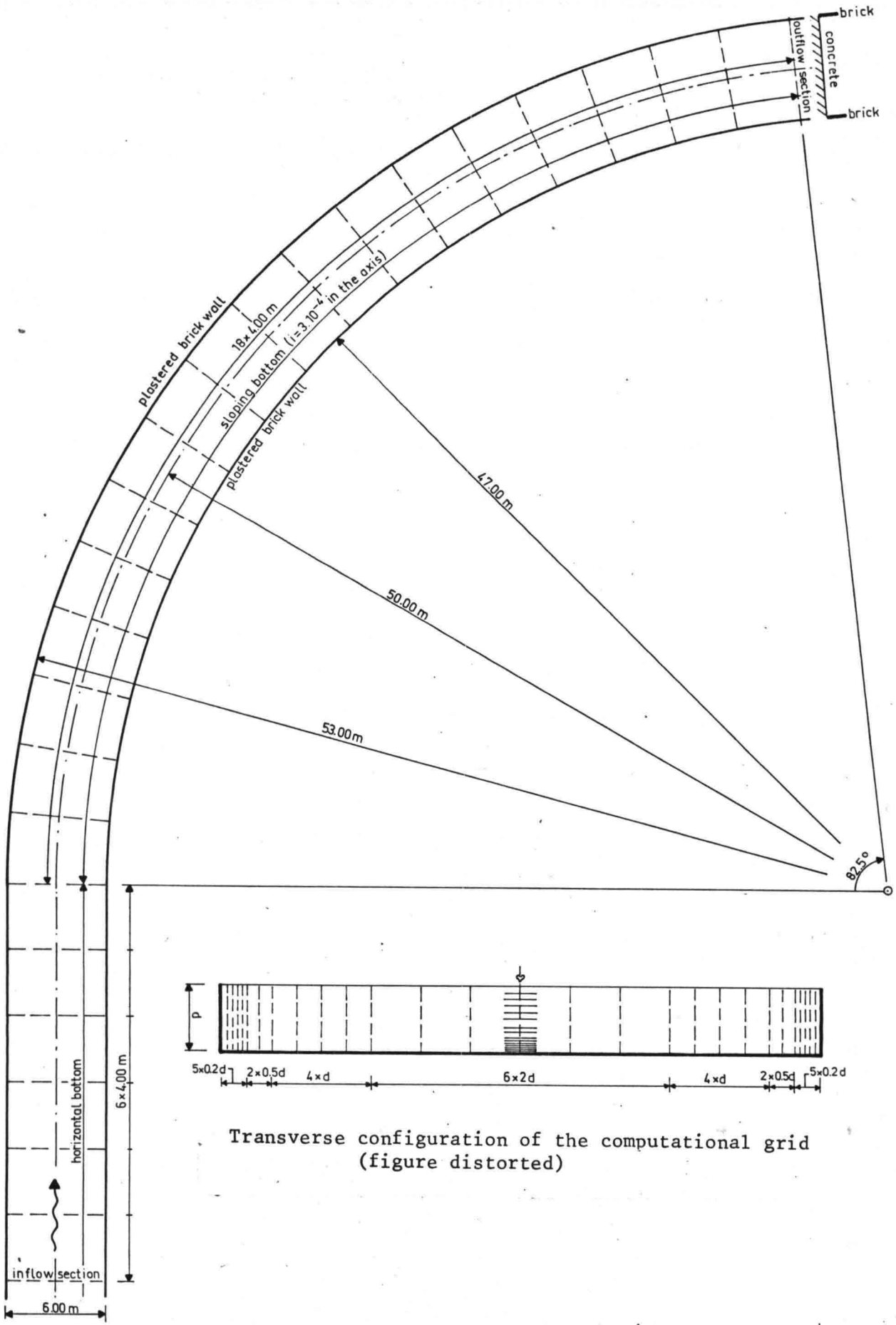

Transverse configuration of the computational grid
(figure distorted)

Figure 21. Simulation of the DHL-experiments: flume geometry and computational grid

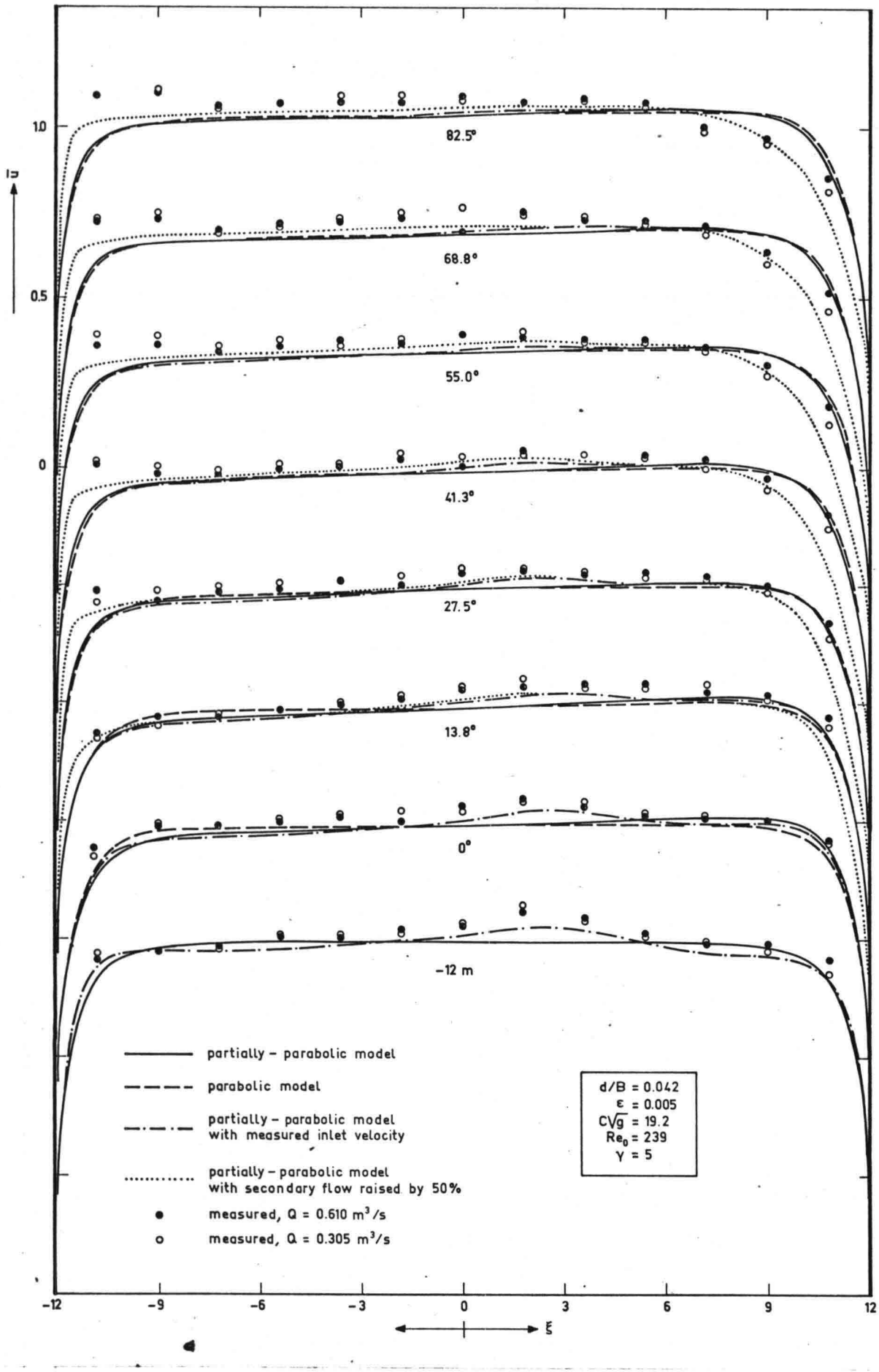

Figure 22. Results of the simulation of the DHL-experiments

(a) Depth-averaged main velocity

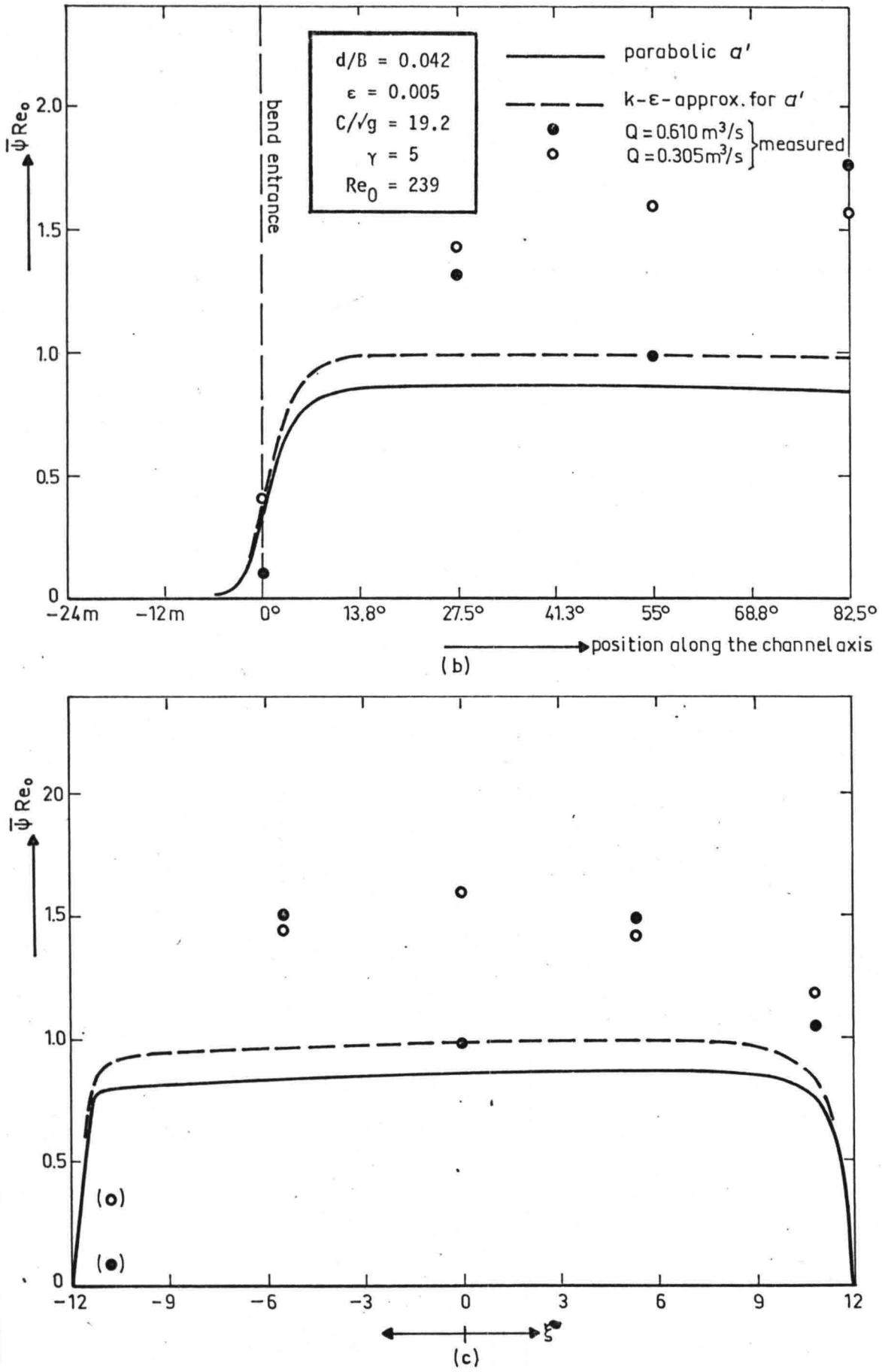

Figure 22. Results of the simulation of the DHL-experiments
Secondary flow intensity (b) in the axis (c) at 55°

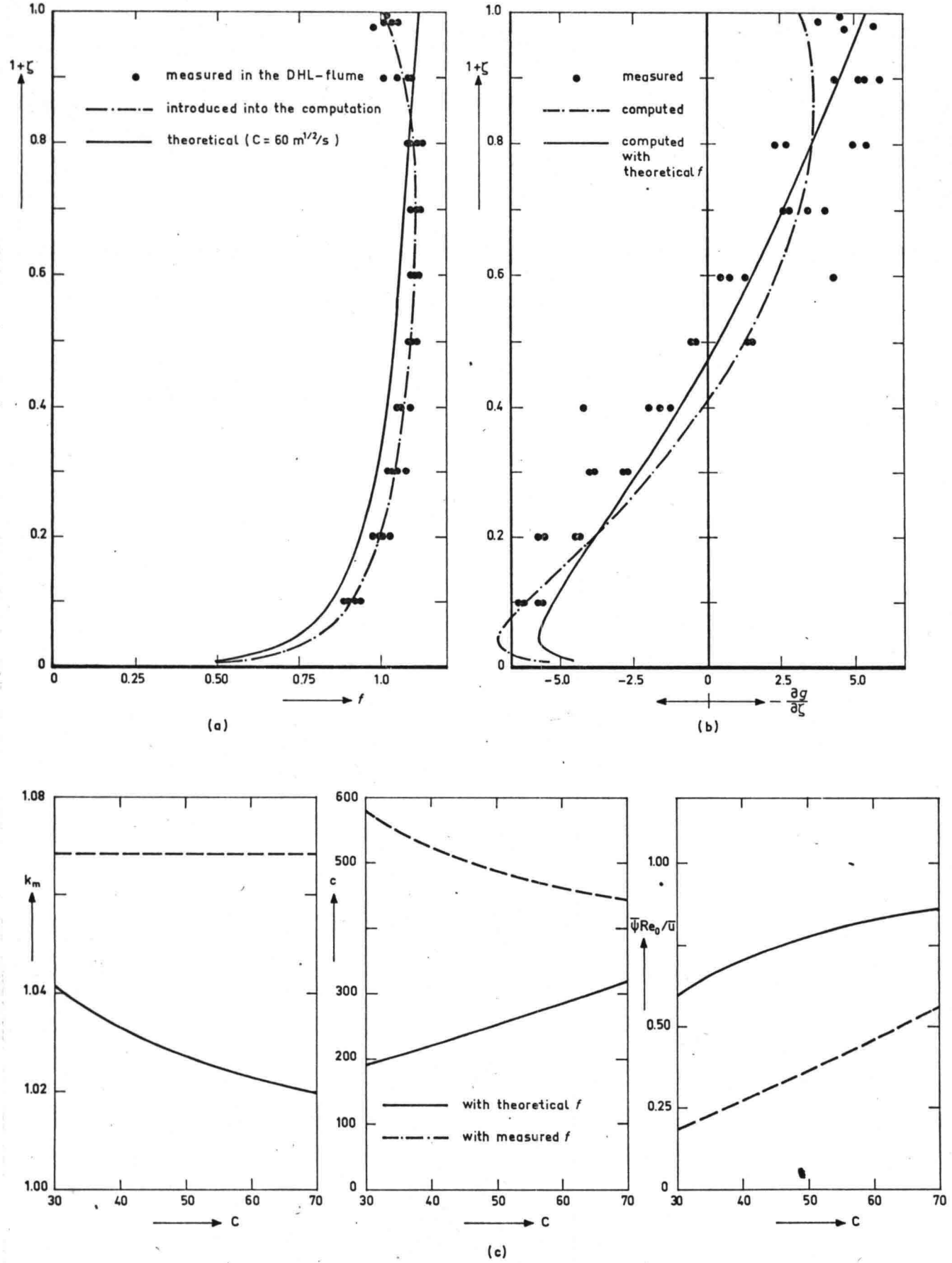

Figure 23. Influence of the main velocity distribution on the secondary flow intensity

(a) Vertical distribution of the main velocity

(b) Vertical distribution of the radial component of the secondary flow

(c) Constants and secondary flow intensity

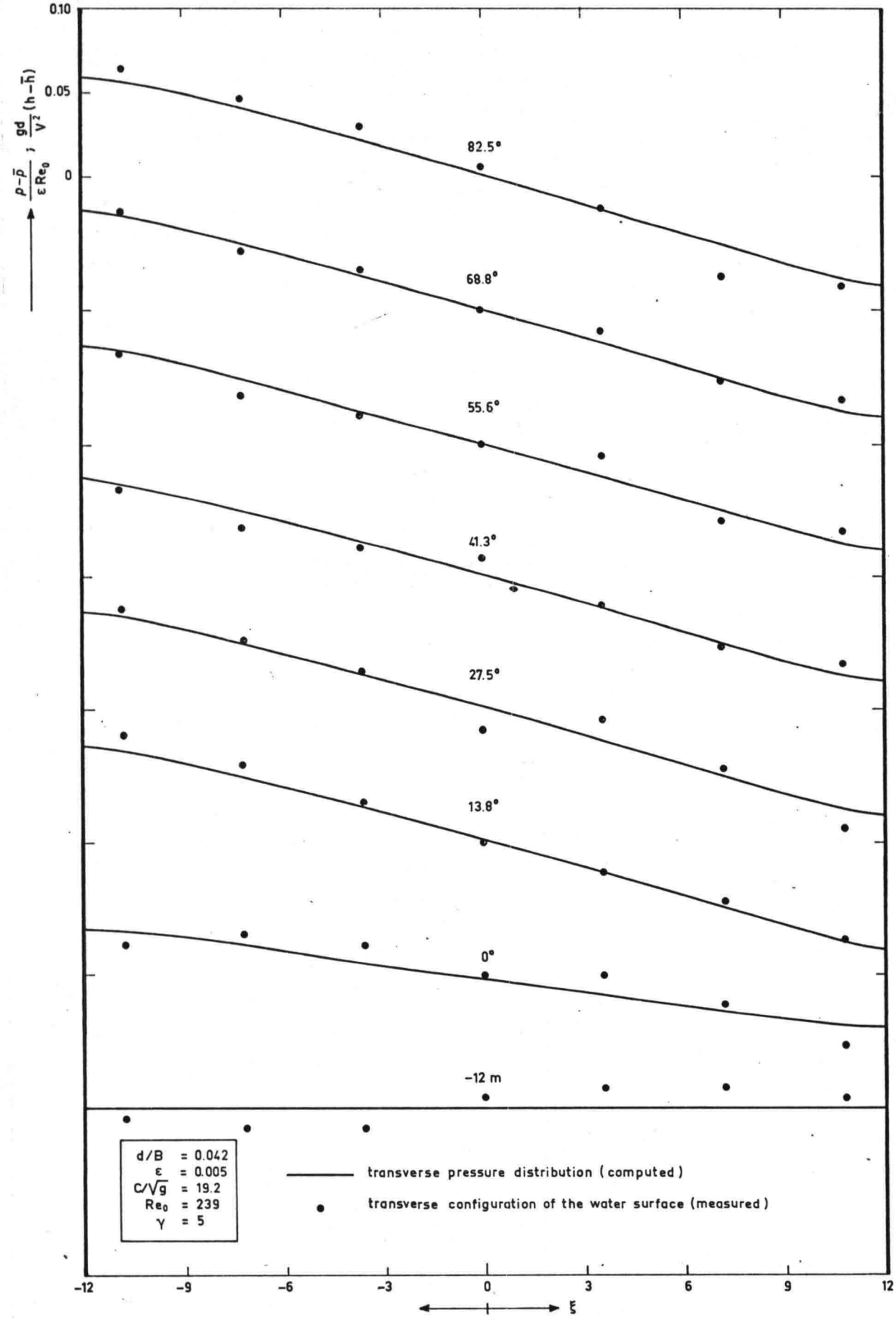

Figure 24. Transverse configuration of the water surface during the DHL-experiments (higher discharge only)

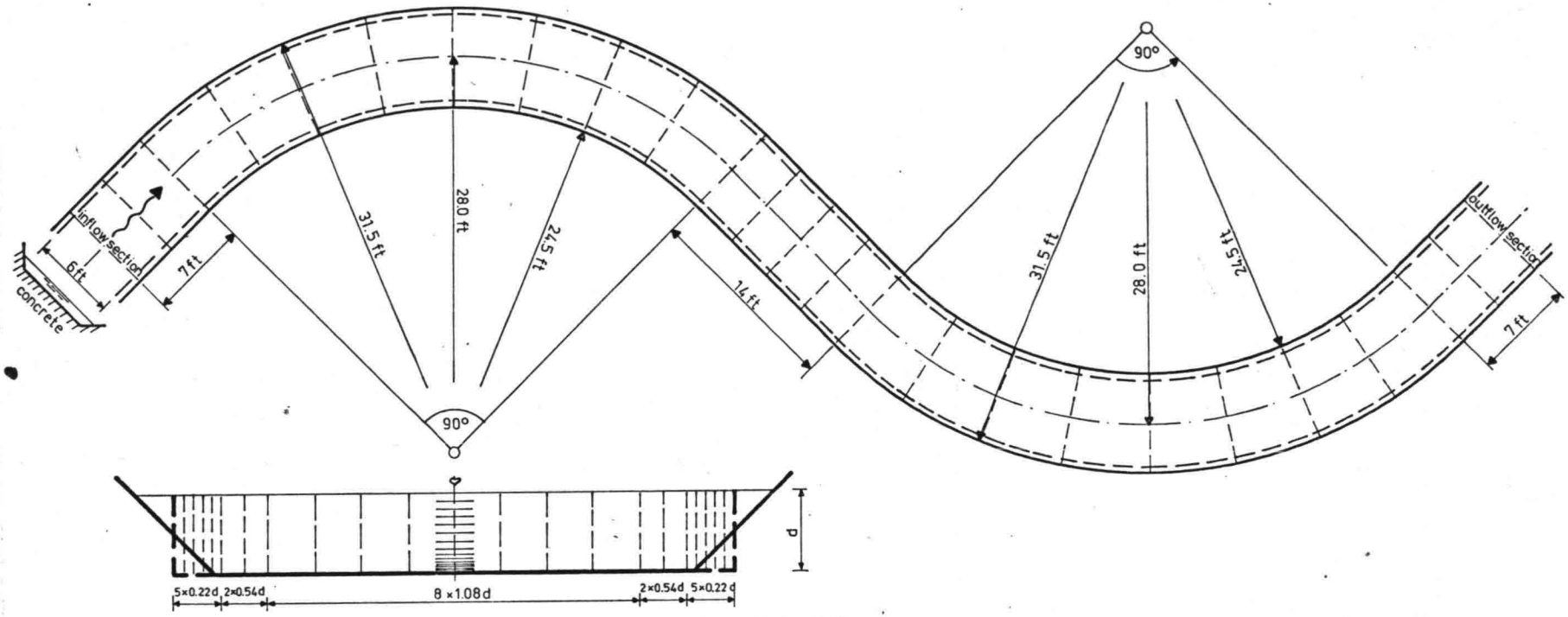

Transverse configuration of the computational grid
(figure distorted)

Figure 25. Simulation of the IIHR-experiments: flume geometry and computational grid

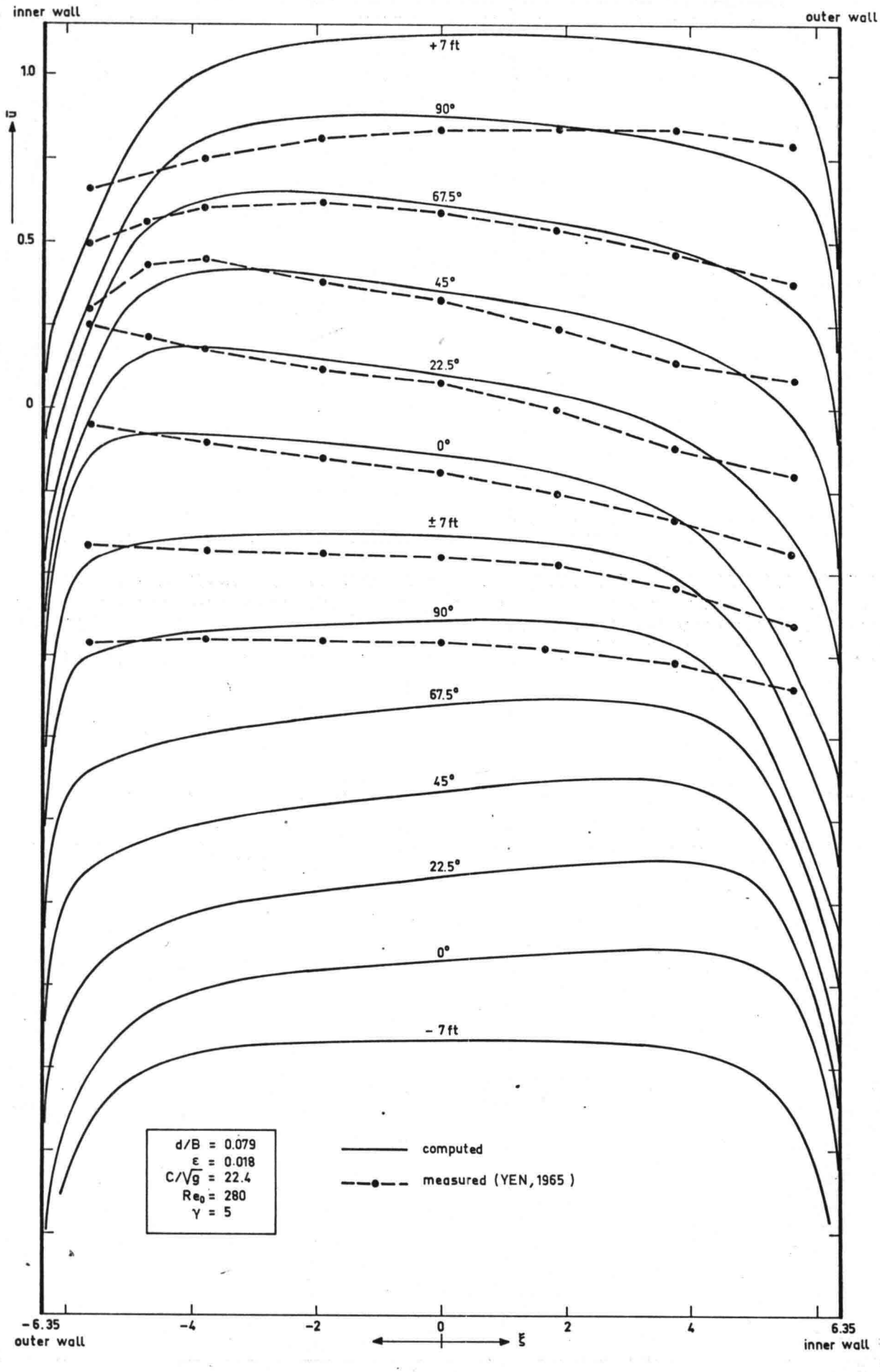

Figure 26. Results of the simulation of the IIHR-experiments

(a) Depth-averaged main velocity

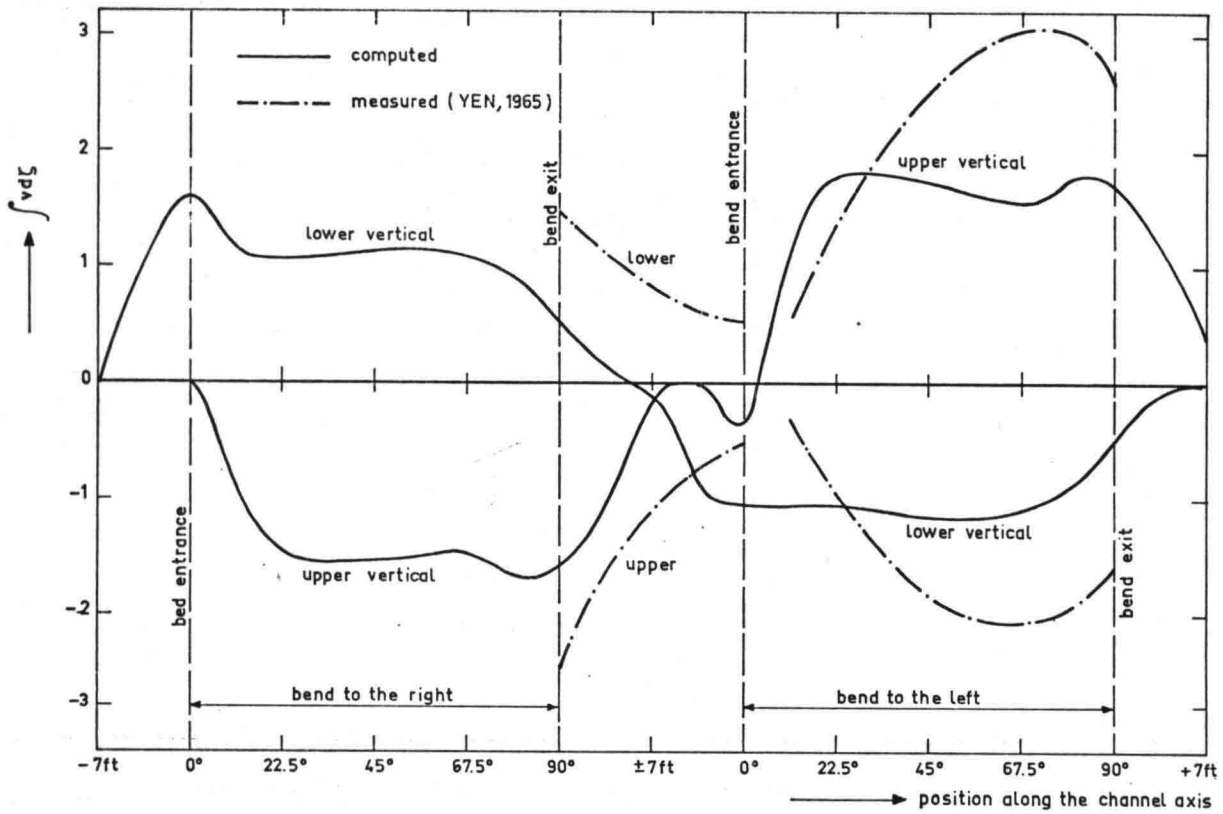

(b)

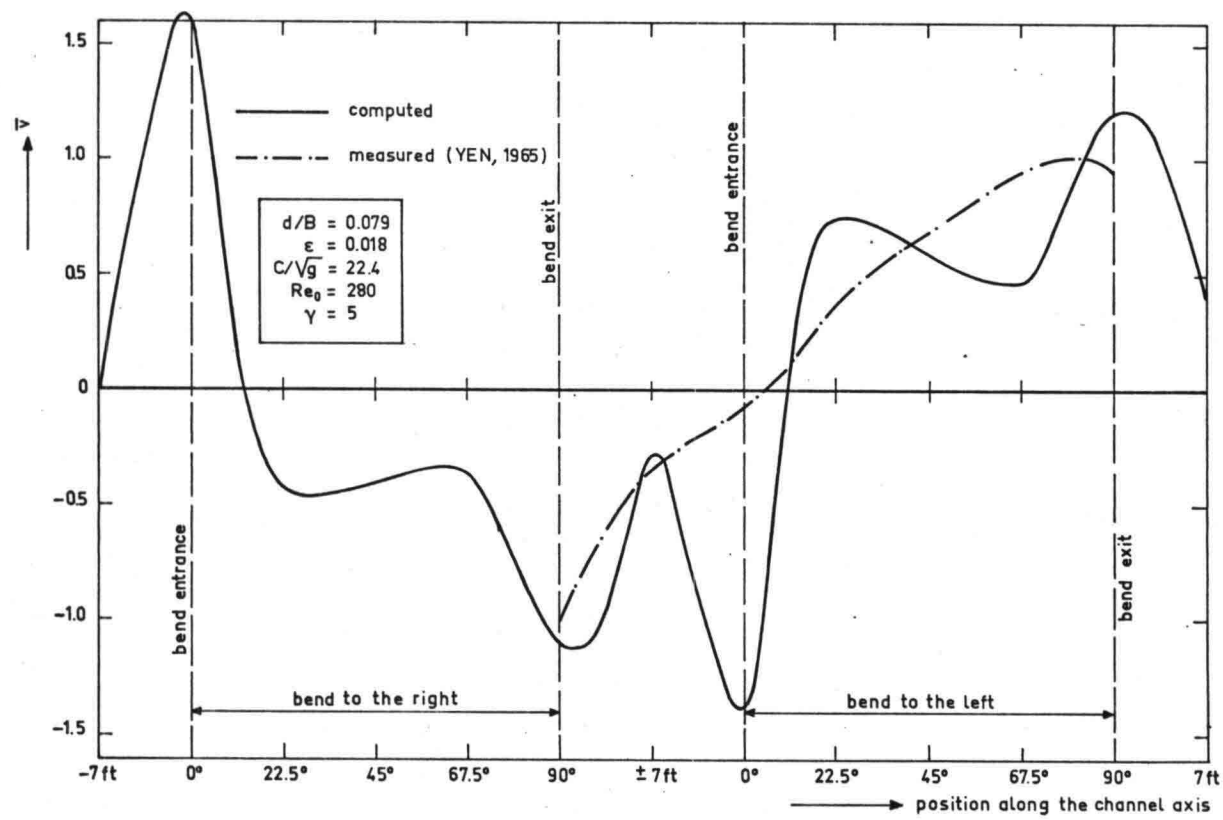

(c)

Figure 26. Results of the simulation of the IIHR-experiments

(b) Inward and outward radial discharge in the channel axis

(c) Net radial discharge in the channel axis

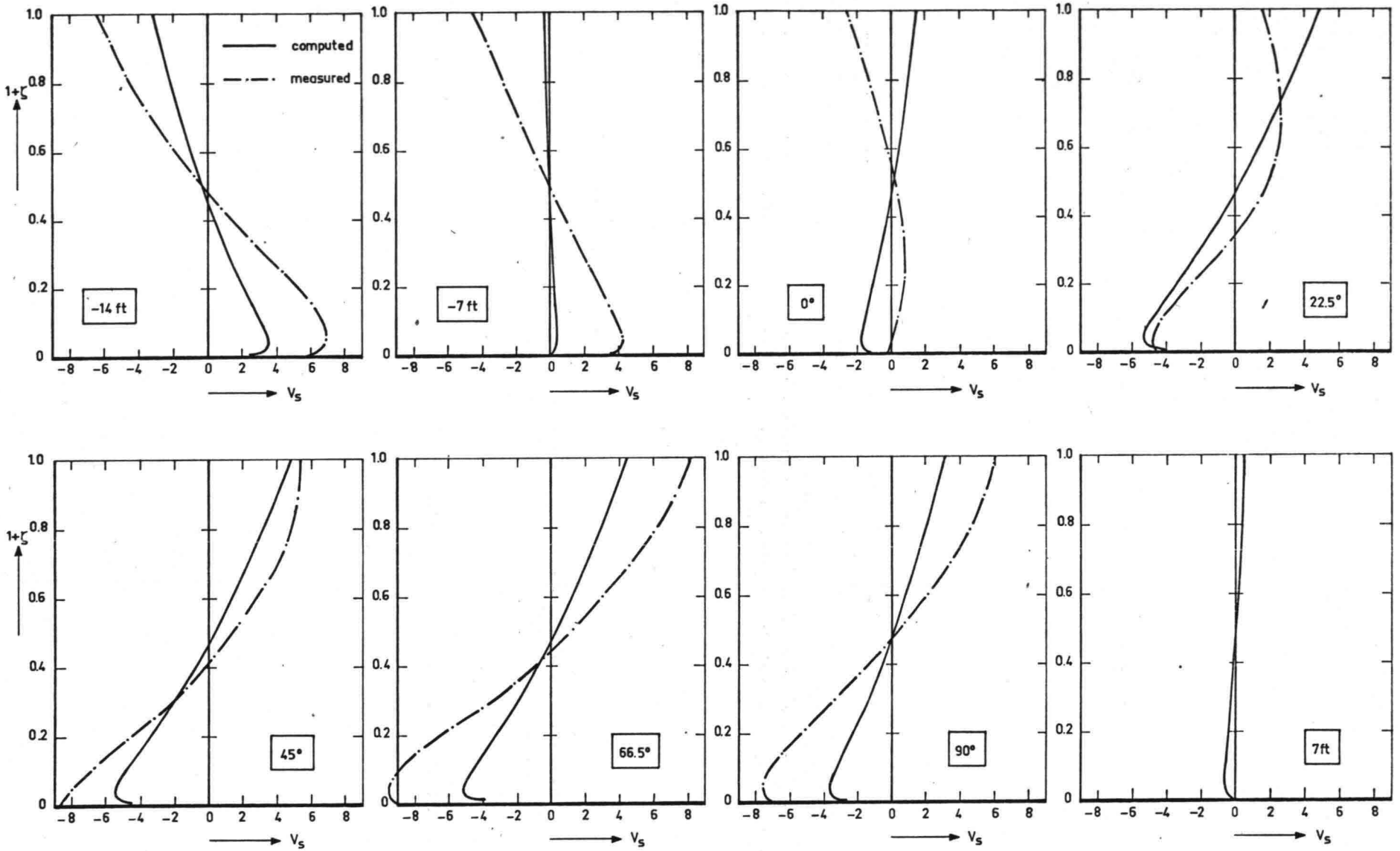

Figure 26. Results of the simulation of the IIHR-experiments

(d) Secondary flow

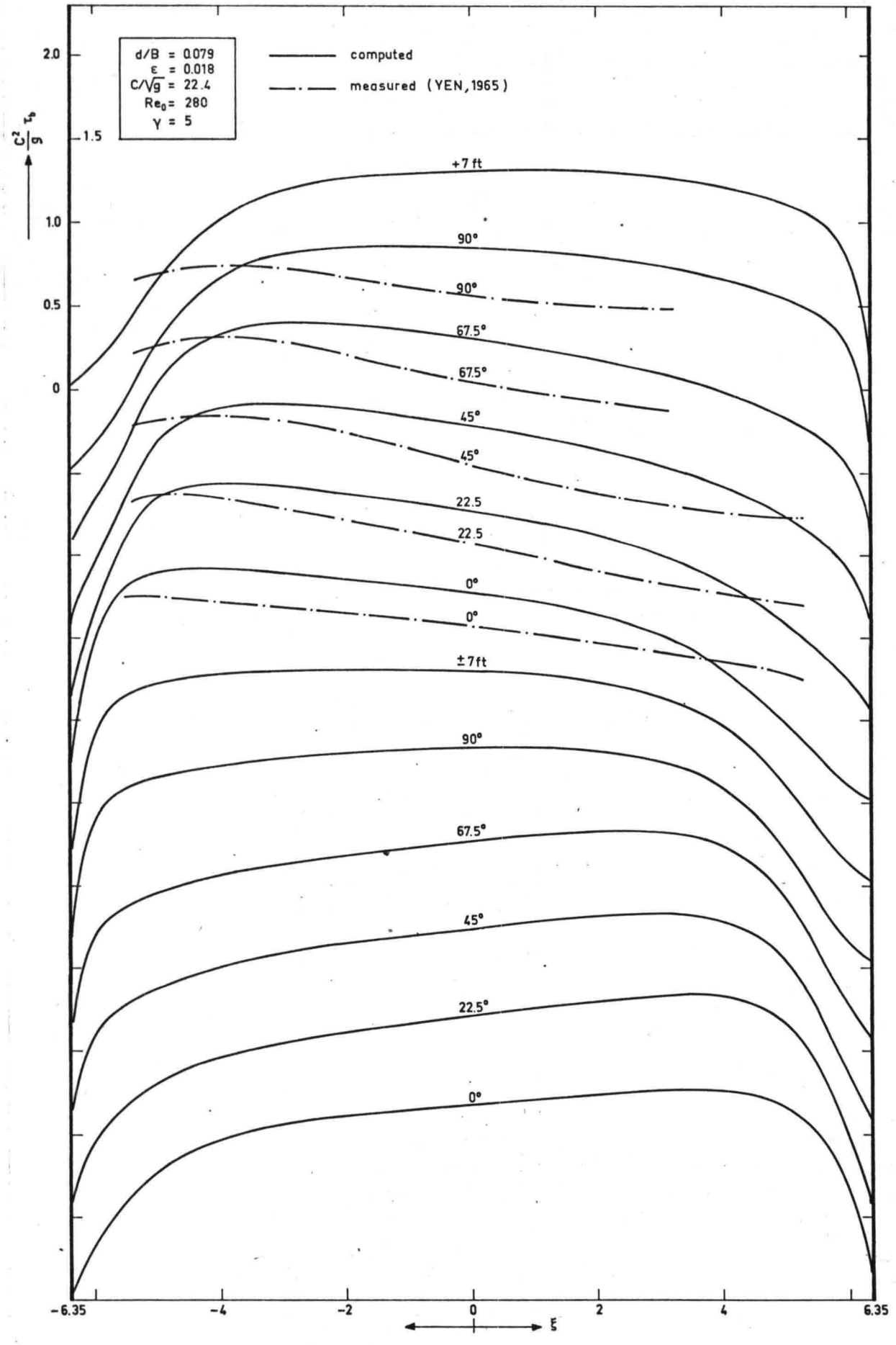

Figure 26. Results of the simulation of the IIHR-experiments

(e) Magnitude of the total bed shear stress

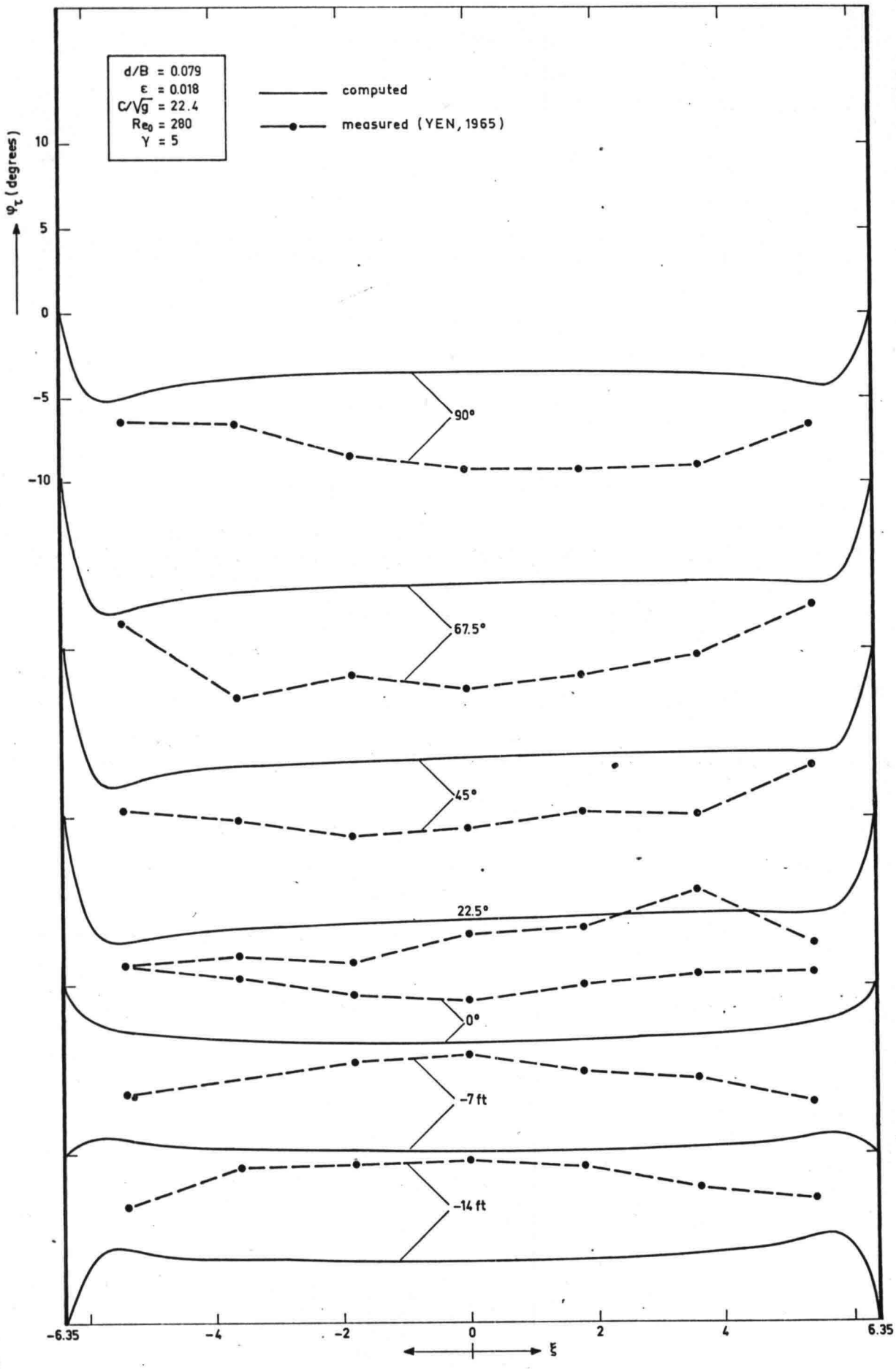

Figure 26. Results of the simulation of the IIHR-experiments

(f) Direction of the velocity and the shear stress at the bottom

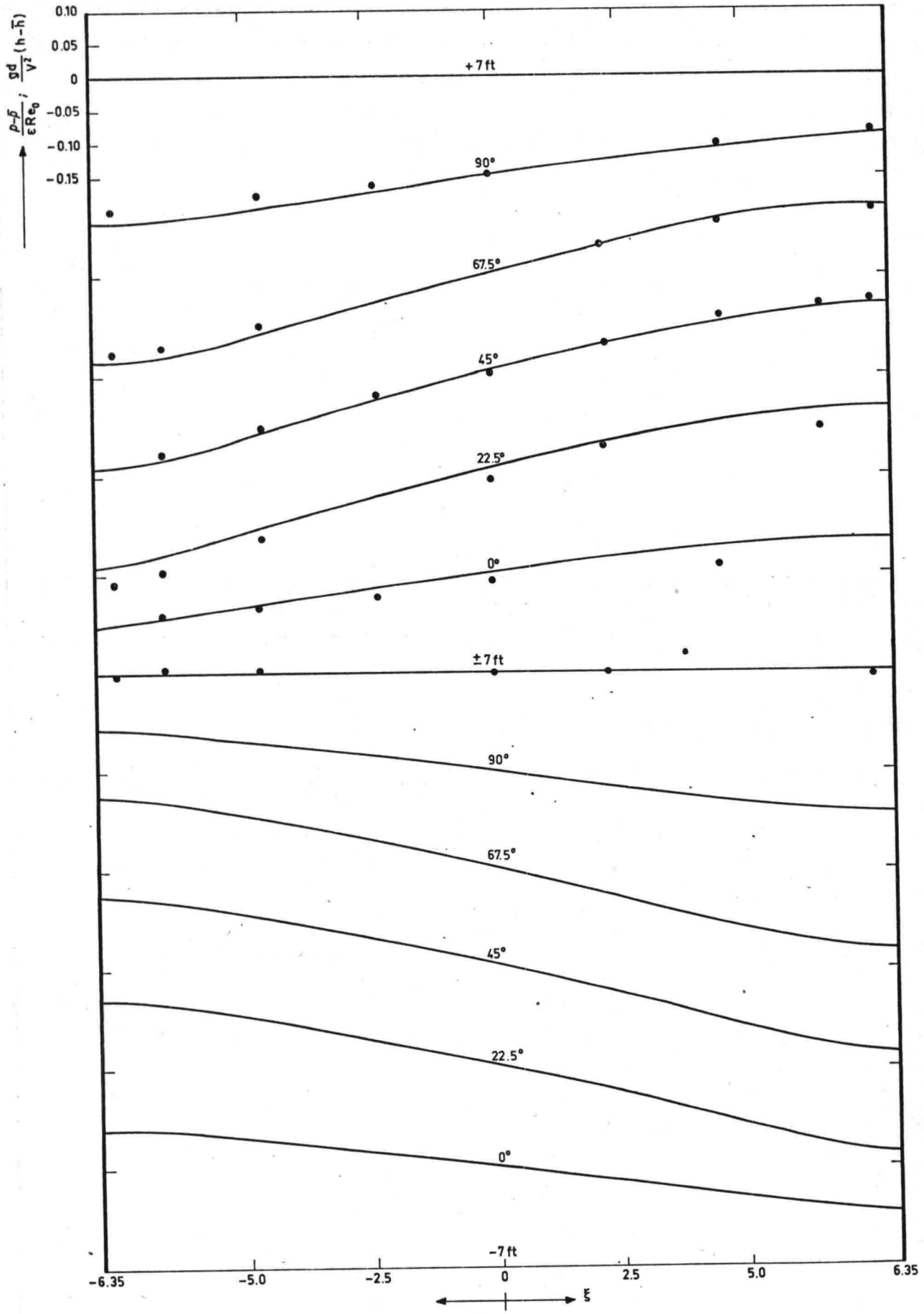

Figure 26. Results of the simulation of the IIHR-experiments

(g) Transverse pressure distribution and water surface configuration

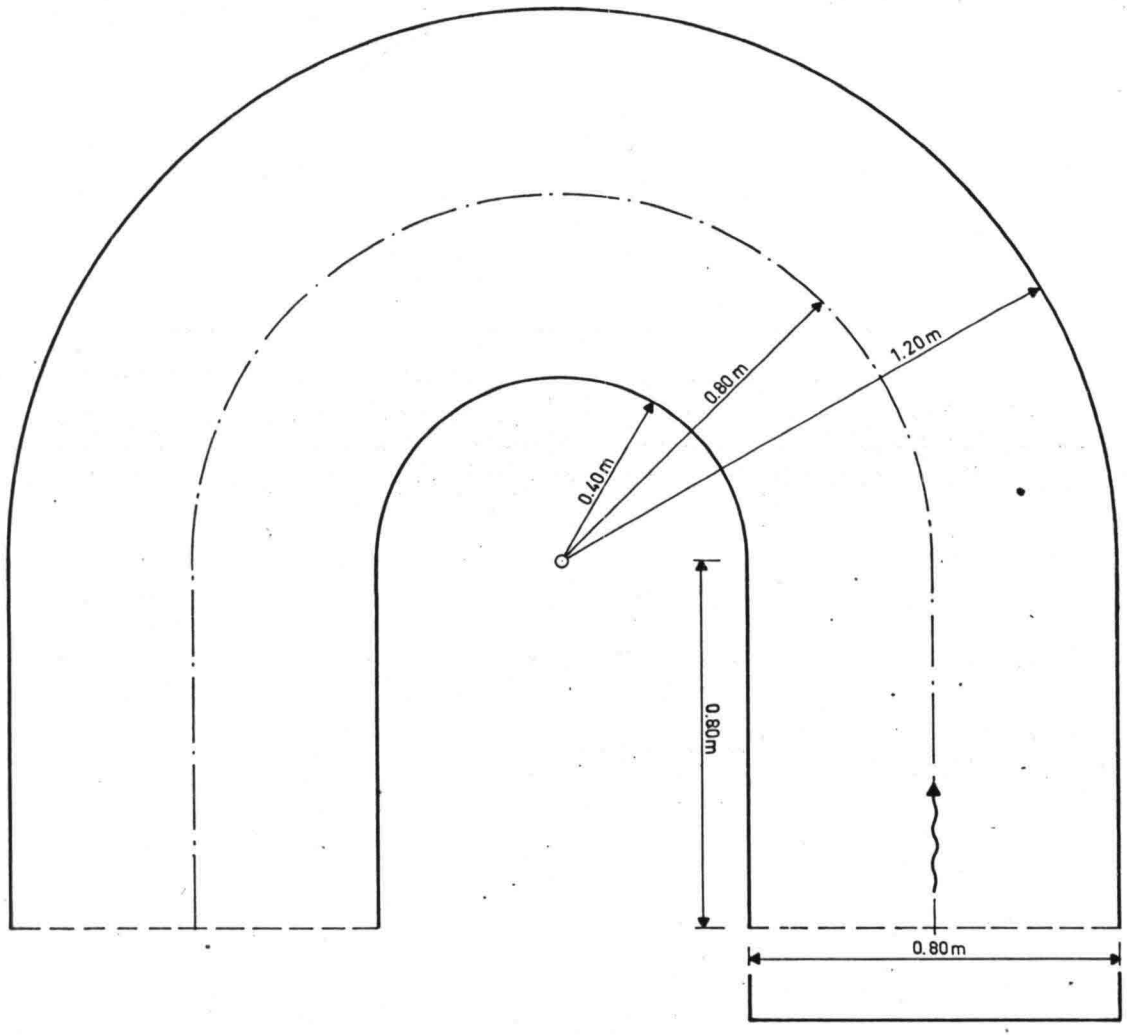

Figure 27. The IHHE-flume

APPENDIX A

Computation of the depth-averaged velocity in fully developed straight channel flow

Appendix A. Computation of the depth-averaged velocity in fully developed straight channel flow

If the vertical distribution of the velocity is given by a distribution function $f(\zeta)$, with $\overline{f} = 1$ by definition, the depth-averaged velocity distribution in fully developed turbulent flow in a straight shallow channel can be solved from the equation

$$0 = -\frac{\partial p}{\partial s} + a'\overline{f}\frac{\partial}{\partial \xi}\left(\bar{u}\frac{\partial \bar{u}}{\partial \xi}\right) - \left(a'\frac{\partial f}{\partial \zeta}\right)\Big|_{\zeta=-1}\bar{u}^2 \qquad (A.1)$$

where $a' = a/\bar{u}$. If f represent the logarithmic distribution

$$f = 1 + \frac{\sqrt{g}}{\kappa C} + \frac{\sqrt{g}}{\kappa C}\ln(1+\zeta) \qquad (A.2)$$

and a is given by (3.12), equation (A.1) reduces to equation (3.22). In addition to equation (A.1), the integral condition of continuity (2.20) and the boundary conditions

$$\bar{u} = k_l\left(1 + \frac{\sqrt{g}}{\kappa C} + \frac{\sqrt{g}}{\kappa C}\ln \delta_l\right) \qquad \text{at } \xi = -\frac{B}{2d} + \delta_l \qquad (A.3)$$

$$\bar{u} = k_r\left(1 + \frac{\sqrt{g}}{\kappa C} + \frac{\sqrt{g}}{\kappa C}\ln \delta_r\right) \qquad \text{at } \xi = \frac{B}{2d} - \delta_r \qquad (A.4)$$

have to be satisfied. The wall shear stress factors k_l and k_r can be determined from the additional conditions

$$\bar{u} = k_l\left\{1 + \frac{\sqrt{g}}{\kappa C} + \frac{\sqrt{g}}{\kappa C}\ln\left(\xi_l + \frac{B}{2d}\right)\right\} \qquad \text{at } \xi = \xi_l \qquad (A.5)$$

$$\bar{u} = k_r\left\{1 + \frac{\sqrt{g}}{\kappa C} + \frac{\sqrt{g}}{\kappa C}\ln\left(\frac{B}{2d} - \xi_2\right)\right\} \qquad \text{at } \xi = \xi_2 \qquad (A.6)$$

If δ_l and δ_r and also $-\xi_l$ and ξ_2 are taken equal, the solution of this mathematical system will be symmetric about the channel axis, i.e. conditions (A.3) through(A.6) can be simplified to

$$\bar{u} = k(1 + \frac{\sqrt{g}}{\kappa C} + \frac{\sqrt{g}}{\kappa C} \ln \delta) = kt_0 \text{ at } \xi = -\frac{B}{2d} + \delta \text{ and at } \xi = \frac{B}{2d} - \delta \qquad (A.7)$$

and

$$\bar{u} = k(1 + \frac{\sqrt{g}}{\kappa C} + \frac{\sqrt{g}}{\kappa C} \ln \Delta\xi) = kt_1 \text{ at } \xi = -\frac{B}{2d} + \Delta\xi \text{ and at } \xi = \frac{B}{2d} - \Delta\xi \qquad (A.8)$$

As the pressure gradient will be a constant, equation (A.1) is a non-linear ordinary differential equation of the second order for $\bar{u}$ as a function of ξ. It may be attempted to solve this equation iteratively, using the linearization

$$0 = -\frac{\partial p}{\partial s} + \overline{a'f}\,\frac{\partial f}{\partial \xi}\,(\tilde{\bar{u}}\,\frac{\partial \bar{u}}{\partial \xi}) - (a'\,\frac{\partial f}{\partial \zeta})\Big|_{\zeta=-1}\,\tilde{\bar{u}}\bar{u} \qquad (A.9)$$

in which $\tilde{\bar{u}}$ denotes the estimate of $\bar{u}$ found in the foregoing iteration step. The convergence of this iteration procedure, however, appears to be very poor, probably as a consequence of disturbances generated near the side-walls.

On the other hand, it is possible to write equation (A.1) in a closed form

$$0 = -\frac{\partial p}{\partial s} + \frac{1}{2}\,\overline{a'f}\,\frac{\partial^{2-2}u}{\partial \xi^{2}} - (a'\,\frac{\partial f}{\partial \zeta})\Big|_{\zeta=-1}\,\bar{u}^2 \qquad (A.10)$$

, from which the quantity $\bar{u}^2$ can be solved directly, thus avoiding all convergence problems.

In order to solve equation (A.10) with the relevant boundary conditions to be derived from (A.7) and (A.8), $\bar{u}^2$ is split up into two parts

$$\bar{u}^2 = k^{2-2}u_1 - \frac{\partial p}{\partial s}\,\bar{u}_2^2 \qquad (A.11)$$

in such a way that

$$\frac{1}{2}\,\overline{a'f}\,\frac{\partial^{2-2}u_1}{\partial \xi^{2}} - (a'\,\frac{\partial f}{\partial \zeta})\Big|_{\zeta=-1}\,\bar{u}_1^2 = 0 \quad \text{with} \quad \bar{u}_1^2 = t_0^2 \quad \text{at } \xi = \pm\,(\frac{B}{2d} - \delta) \qquad (A.12)$$

$$\frac{1}{2}\overline{a'f}\,\frac{\partial^2 \bar{u}_2^2}{\partial \xi^2} - \left(a'\,\frac{\partial f}{\partial \zeta}\right)\Big|_{\zeta=-1}\bar{u}_2^2 = -1 \qquad \text{with} \quad \bar{u}_2^2 = 0 \quad \text{at} \quad \xi = \pm\left(\frac{B}{2d} - \delta\right) \tag{A.13}$$

If $t = \{(a'\,\frac{\partial f}{\partial \zeta})\big|_{\zeta=-1} / (\frac{1}{2}\,\overline{a'f})\}^{1/2}$, the solutions of these systems read

$$\bar{u}_1^2 = t_0^2\,\frac{\cosh t\xi}{\cosh t(\frac{B}{2d} - \delta)} \tag{A.14}$$

and

$$\bar{u}_2^2 = \frac{1}{(a'\,\frac{\partial f}{\partial \zeta})\big|_{\zeta=-1}}\left\{1 - \frac{\cosh t\xi}{\cosh t(\frac{B}{2d} - \delta)}\right\} \tag{A.15}$$

The additional conditions (A.8) are satisfied if

$$k^2\,\bar{u}_1^2\big|_{\xi_1} - \frac{\partial p}{\partial s}\,\bar{u}_2^2\big|_{\xi_1} = k^2 t_1^2 \tag{A.16}$$

, whence

$$k^2 = \frac{\partial p}{\partial s}\,\frac{\bar{u}_2^2\big|_{\xi_1}}{\bar{u}_1^2\big|_{\xi} - t_1^2} = -\frac{\partial p}{\partial s}\,K^2 \tag{A.17}$$

and

$$\bar{u}^2 = \frac{\partial p}{\partial s}\left(-\bar{u}_2^2 - \frac{\bar{u}_2^2\big|_{\xi_1}}{\bar{u}_1^2\big|_{\xi} - t_1^2}\,\bar{u}_1^2\right) \tag{A.18}$$

Substituting this result into the integral condition of continuity (2.20) yields

$$\left(-\frac{\partial p}{\partial s}\right)^{\frac{1}{2}} = \frac{B/d}{2K\,\delta\left(1+\frac{\sqrt{g}}{\kappa C}\ln\delta\right) + \int_{-B/2d+\delta}^{B/2d-\delta} \left(K^2\bar{u}_1^2 + \bar{u}_2^2\right)^{\frac{1}{2}}\,d\xi} \tag{A.19}$$

, with which the depth-averaged velocity distribution and the shear stress factor at the sidewalls are known.

The friction velocity at the sidewalls follows from

$$|u_{\tau w}| = \frac{\sqrt{g}}{C}\,k \tag{A.20}$$

APPENDIX B

Computation of the vertical distribution of the main flow

Appendix B. Computation of the vertical distribution of the main flow

If the quantities $\bar{u}$, $\bar{v}$, $\bar{\psi}$, $\bar{f}(\zeta)$ and $g(\zeta)$ are known, equation (5.1) for the vertical distribution function f of the main flow is an ordinary differential equation of the form

$$a_1 \frac{\partial^2 f}{\partial \zeta^2} + a_2 \frac{\partial f}{\partial \zeta} + a_3 f = \frac{1}{r} \frac{\partial p}{\partial \phi} \tag{B.1}$$

, in which a_1, a_2 and a_3 are known function of ξ, ϕ and ζ. The boundary conditions to be satisfied are

$$f = k_m \{1 + \frac{\sqrt{g}}{\kappa C} + \frac{\sqrt{g}}{\kappa C} \ln \delta_0\} = k_m t_0 \qquad \text{at} \qquad \zeta = -1 + \delta_0 \tag{B.2}$$

and

$$\zeta(1+\zeta) \frac{\partial f}{\partial \zeta} = 0 \quad \text{at} \quad \zeta = 0 \tag{B.3}$$

In addition, the following condition must be satisfied

$$f = k_m \{1 + \frac{\sqrt{g}}{\kappa C} + \frac{\sqrt{g}}{\kappa C} \ln (1+\zeta_1)\} = k_m t_1 \quad \text{at} \quad \zeta = \zeta_1 \tag{B.4}$$

In accordance with one of the conclusions drawn from the investigation of fully developed curved laminar flow (DE VRIEND, 1978a), the pressure is assumed to be hydrostatic, at least in the main flow computation step. Hence the tangential gradient of the total pressure is independent of ζ and the function f can be split up as follows:

$$f = k_m f_1 - \frac{1}{r} \frac{\partial p}{\partial \phi} f_2 \tag{B.5}$$

Herein the functions f_1 and f_2 are chosen such, that

$$a_1 \frac{\partial^2 f_1}{\partial \zeta^2} + a_2 \frac{\partial f_1}{\partial \zeta} + a_3 f_1 = 0 \tag{B.6}$$

with the boundary conditions

$$f_1 = t_0 \quad \text{at} \quad = -1 + \delta_0 \text{ and } \quad \zeta(1+\zeta)\frac{\partial f_1}{\partial \zeta} = 0 \quad \text{at } \zeta = 0 \tag{B.7}$$

and

$$a_1 \frac{\partial^2 f_2}{\partial \zeta^2} + a_2 \frac{\partial f_2}{\partial \zeta} + a_3 f_2 = -1 \tag{B.8}$$

with the boundary conditions

$$f_2 = 0 \quad \text{at } \zeta = -1+\delta_0 \text{ and } \zeta(1+\zeta)\frac{\partial f_2}{\partial \zeta} = 0 \quad \text{at } \zeta = 0 \tag{B.9}$$

These two systems of differential equations and boundary conditions can be solved to yield f_1 and f_2.
Once the functions f_1 and f_2 are known, the constants k_m and $\frac{1}{r}\frac{\partial p}{\partial \phi}$ remain to be determined. Substituting (B.5) into the additional condition near the bottom (B.4) yields

$$k_m f_1\Big|_{\zeta_1} - \frac{1}{r}\frac{\partial p}{\partial \phi} f_2\Big|_{\zeta_1} = k\, t_1 \tag{B.10}$$

whence

$$k_m = \frac{1}{r}\frac{\partial p}{\partial \phi} f_2\Big|_{\zeta_1} / (f_1\Big|_{\zeta_1} - t_1) \tag{B.11}$$

and so

$$f = \frac{1}{r}\frac{\partial p}{\partial \phi}\left\{\frac{f_{2|\zeta_1}}{f_1\Big|_{\zeta_1} - t_1} f_1 - f_2\right\} \tag{B.12}$$

Finally, $\bar{f} = 1$ by definition, so

$$\frac{1}{r}\frac{\partial p}{\partial \phi} = \frac{f\Big|_{\zeta_1} - t_1}{f_2\Big|_{\zeta_1}\bar{f}_1 - (f_1\Big|_{\zeta_1} - t_1)\bar{f}_2} \tag{B.13}$$

, whence

$$k_m = \frac{f_2\big|_{\zeta_1}}{f_2\big|_{\zeta_1}\bar{f}_1 - (f_1\big|_{\zeta_1} - t_1)\,\bar{f}_2} \tag{B.14}$$

and

$$f = \frac{f_2\big|_{\zeta_1} f_1 - (f_1\big|_{\zeta_1} - t_1) f_2}{f_2\big|_{\zeta_1}\bar{f}_1 - (f_1\big|_{\zeta_1} - t_1)\bar{f}_2} \tag{B.15}$$

APPENDIX C

Solution of the longitudinal momentum equation

Appendix C. Solution of the longitudinal momentum equation

In each cross-section j the longitudinal momentum equation (5.9) can be rewritten as an ordinary differential equation in ξ that is linear in $\bar{u}_j$. This equation has the form

$$a_1 \frac{\partial^2 \bar{u}_j}{\partial \xi^2} + a_2 \frac{\partial \bar{u}_j}{\partial \xi} + a_3 \bar{u}_j = a_4 \frac{\partial \bar{p}}{\partial s} + a_5 \qquad (C.1)$$

, in which a_1 through a_5 are known functions of ξ and $\frac{\partial \bar{p}}{\partial s}$ is considered as an unknown constant.

The sidewall-boundary conditions can be formulated as

$$\bar{u}_j = k_1 (1 + \frac{\sqrt{g}}{\kappa C} + \frac{\sqrt{g}}{\kappa C} \ln \delta_1) = k_1 t_0 \qquad \text{at } \xi = -\frac{B}{2d} + \delta_1 \qquad (C.2)$$

$$\bar{u}_j = k_r t_0 \qquad \text{at } \xi = \frac{B}{2d} - \delta_1 \qquad (C.3)$$

with k_1 and k_r as unknown constants, to be determined from the additional conditions

$$\bar{u}_j = k_1 \{1 + \frac{\sqrt{g}}{\kappa C} + \frac{\sqrt{g}}{\kappa C} \ln(\delta_1 + \Delta\xi)\} = k_1 t_1 \quad \text{at } \xi = -\frac{B}{2d} + \delta_1 + \Delta\xi \qquad (C.4)$$

$$\bar{u}_j = k_r t_1 \qquad \text{at } \xi = \frac{B}{2d} - \delta_1 - \Delta\xi \qquad (C.5)$$

Now the velocity $\bar{u}_j$ is split up into four constituents

$$\bar{u}_j = k_1 \bar{u}_1 + k_r \bar{u}_2 + \frac{\partial \bar{p}}{\partial s} \bar{u}_3 + \bar{u}_4 \qquad (C.6)$$

in such a way that

$$a_1 \frac{\partial^2 \bar{u}_1}{\partial \xi^2} + a_2 \frac{\partial \bar{u}_1}{\partial \xi} + a_3 \bar{u}_1 = 0 \qquad \text{with } \bar{u}_1 = t_0 \text{ at } \xi = -\frac{B}{2d} + \delta_1 \qquad (C.7)$$

$$\text{and } \bar{u}_1 = 0 \qquad \text{at } \xi = \frac{B}{2d} - \delta_1$$

$$a_1 \frac{\partial^2 \bar{u}_2}{\partial \xi^2} + a_2 \frac{\partial \bar{u}_2}{\partial \xi} + a_3 \bar{u}_2 = 0 \qquad \text{with } \bar{u}_2 = 0 \text{ at } \xi = -\frac{B}{2d} + \delta_1 \qquad (C.8)$$

$$\text{and } \bar{u}_2 = t_0 \text{ at } \xi = \frac{B}{2d} - \delta_1$$

$$a_1 \frac{\partial^2 \bar{u}_3}{\partial \xi^2} + a_2 \frac{\partial \bar{u}_3}{\partial \xi} + a_3 \bar{u}_3 = a_4 \qquad \text{with } \bar{u}_3 = 0 \text{ at } \xi = -\frac{B}{2d} + \delta_1 \qquad (C.9)$$

$$\text{and } \bar{u}_3 = 0 \text{ at } \xi = \frac{B}{2d} - \delta_1$$

$$a_1 \frac{\partial^2 \bar{u}_4}{\partial \xi^2} + a_2 \frac{\partial \bar{u}_4}{\partial \xi} + a_3 \bar{u}_4 = a_5 \qquad \text{with } \bar{u}_4 = 0 \text{ at } \xi = -\frac{B}{2d} + \delta_1 \qquad (C.10)$$

$$\text{and } \bar{u}_4 = 0 \text{ at } \xi = \frac{B}{2d} - \delta_1$$

The solution of $\bar{u}_j$ must satisfy the additional conditions (C.4) and (C.5) and the integral condition of continuity (5.22), which can be reformulated as

$$\bar{\bar{u}}_j = 1 \qquad \text{with} \qquad \bar{\bar{u}}_j = \frac{d}{B} \int_{-B/2d}^{B/2d} \bar{u}_j \, d\xi \qquad (C.11)$$

Consequently, the unknown constants k_1, k_r and $\frac{\partial \bar{p}}{\partial s}$ can be solved from

$$k_1 \bar{u}_1\Big|_{\xi_1} + k_r \bar{u}_2\Big|_{\xi_1} + \frac{\partial \bar{p}}{\partial s} \bar{u}_3\Big|_{\xi_1} + \bar{u}_4\Big|_{\xi_1} = k_1 t_1 \qquad (C.12)$$

$$k_1 \bar{u}_1\Big|_{\xi_2} + k_r \bar{u}_2\Big|_{\xi_2} + \frac{\partial \bar{p}}{\partial s} \bar{u}_3\Big|_{\xi_2} + \bar{u}_4\Big|_{\xi_2} = k_r t_1 \qquad (C.13)$$

$$k_1 \bar{\bar{u}}_1 + k_r \bar{\bar{u}}_2 + \frac{\partial \bar{p}}{\partial s} \bar{\bar{u}}_3 + \bar{\bar{u}}_4 = 1 \qquad (C.14)$$

, where $\xi_1 = -\frac{B}{2d} + \delta_1 + \Delta\xi$ and $\xi_2 = \frac{B}{2d} - \delta_1 - \Delta\xi$.

The cross-sectional mean value of the pressure p_{j+1} is corrected by setting

$$\bar{p}_{j+1} = \bar{p}_j + \Delta s \frac{\partial \bar{p}}{\partial s} \tag{C.15}$$

and the sidewall friction velocities follow from

$$\bar{u}_{\tau 1} = \frac{\sqrt{g}}{C} k_1 \quad \text{and} \quad \bar{u}_{\tau r} = \frac{\sqrt{g}}{C} k_r \tag{C.16}$$

APPENDIX D

Stream function equation for the secondary flow

Appendix D. Stream function equation for the secondary flow

Making use of the similarity hypothesis (4.15) for the main flow and the expressions for the curvatures of the streamlines and the normal lines in terms of the depth-averaged velocity components (see DE VRIEND, 1978b)

$$\frac{1}{r_s} = \frac{1}{\bar{u}_t^3}\{\bar{u}(\varepsilon\frac{\bar{u}}{r}\frac{\partial\bar{v}}{\partial\phi} + \varepsilon\bar{v}\frac{\partial\bar{v}}{\partial\xi} - \frac{\bar{u}^2}{r}) - \varepsilon\bar{v}(\frac{\bar{u}}{r}\frac{\partial\bar{u}}{\partial\phi} + \bar{v}\frac{\partial\bar{u}}{\partial\xi} + \frac{\varepsilon}{r}\overline{\overline{uv}})\} \tag{D.1}$$

$$\frac{1}{r_n} = \frac{1}{\bar{u}_t^3}\{\varepsilon\bar{v}(\varepsilon\frac{\bar{u}}{r}\frac{\partial\bar{v}}{\partial\phi} + \varepsilon\bar{v}\frac{\partial\bar{v}}{\partial\xi} - \frac{\bar{u}^2}{r}) + \bar{u}(\frac{\bar{u}}{r}\frac{\partial\bar{u}}{\partial\phi} + \bar{v}\frac{\partial\bar{u}}{\partial\xi} + \frac{\varepsilon}{r}\overline{\overline{uv}})\} \tag{D.2}$$

, the transverse momentum equations (4.8) and (4.9) can be elaborated to

$$\varepsilon^2 Re_0 f^2(\bar{u}\frac{\bar{u}_t}{r_s} + \varepsilon\bar{v}\frac{\bar{u}_t}{r_n}) + \varepsilon^3 Re_0 f\,(\frac{\bar{u}}{r}\frac{\partial v_s}{\partial\phi} + \bar{v}\frac{\partial v_s}{\partial\xi}) +$$

$$+ \varepsilon^3 Re_0\,(w_s\bar{v}\frac{\partial f}{\partial\zeta} + v_s\frac{\partial\bar{v}}{\partial\xi}f) = -\frac{\partial p}{\partial\xi} + \varepsilon^2 a\nabla_1^2 v_s + \varepsilon^2 a\frac{f}{r}\frac{\partial\bar{\omega}}{\partial\phi} +$$

$$+ \varepsilon^2 a\bar{v}\frac{\partial^2 f}{\partial\zeta^2} + \frac{\varepsilon^2}{r}\frac{\partial a}{\partial\phi}f(-\bar{\omega} - 2\frac{\varepsilon}{r}\bar{u}) + \varepsilon^2\frac{\partial a}{\partial\xi}(2\frac{\partial v_s}{\partial\xi} + 2f\frac{\partial\bar{v}}{\partial\xi}) +$$

$$+ \varepsilon^2\frac{\partial a}{\partial\zeta}(\frac{\partial v_s}{\partial\zeta} + \frac{\partial w_s}{\partial\xi} + \bar{v}\frac{\partial f}{\partial\zeta}) \tag{D.3}$$

and

$$\varepsilon^3 Re_0 f\,(\frac{\bar{u}}{r}\frac{\partial w_s}{\partial\phi} + \bar{v}\frac{\partial w_s}{\partial\xi}) = -\frac{\partial p}{\partial\zeta} + \varepsilon^2 a\nabla_1^2 w_s + \frac{\varepsilon^2}{r}\frac{\partial a}{\partial\phi}\bar{u}\frac{\partial f}{\partial\zeta} +$$

$$+ \varepsilon^2\frac{\partial a}{\partial\xi}(\frac{\partial v_s}{\partial\zeta} + \frac{\partial w_s}{\partial\xi} + \bar{v}\frac{\partial f}{\partial\zeta}) + 2\varepsilon^2\frac{\partial a}{\partial\zeta}\frac{\partial w_s}{\partial\zeta} \tag{D.4}$$

Elimination of the pressure from these equations yields

$$- \varepsilon^2 Re_0 \frac{\partial(f^2)}{\partial\zeta} \left(\bar{u} \frac{\bar{u}_t}{r_s} + \varepsilon \bar{v} \frac{\bar{u}_t}{r_n}\right) + \varepsilon^3 Re_0 f\{\frac{\bar{u}}{r} \frac{\partial\omega_s}{\partial\phi} + \bar{v} \frac{\partial\omega_s}{\partial\xi} + \frac{\partial\bar{v}}{\partial\xi} \omega_s +$$

$$+ \frac{1}{r} \frac{\partial w_s}{\partial\phi} \left(\frac{\partial\bar{u}}{\partial\xi} - \frac{\varepsilon}{r} \bar{u}\right)\} - \varepsilon^3 Re_0 \frac{\partial f}{\partial\zeta} \left(\frac{\bar{u}}{r} \frac{\partial v_s}{\partial\phi} + v_s \frac{\partial\bar{v}}{\partial\xi} - \frac{\varepsilon}{r} v_s \bar{v}\right) - \varepsilon^3 Re w_s \bar{v} \frac{\partial^2 f}{\partial\zeta^2}$$

$$= \varepsilon^2 a \left(\frac{\partial^2\omega_s}{\partial\zeta^2} + \frac{\partial^2\omega_s}{\partial\xi^2} + \frac{\varepsilon}{r} \frac{\partial\omega_s}{\partial\xi}\right) + \varepsilon^2 \frac{\partial a}{\partial\xi} \left(\frac{\partial\omega_s}{\partial\xi} + \frac{\partial^2 w_s}{\partial\zeta^2} + \frac{\varepsilon}{r} \frac{\partial w_s}{\partial\xi} + \frac{\partial^2 w_s}{\partial\xi^2}\right) +$$

$$+ \varepsilon^2 \frac{\partial a}{\partial\zeta} \left(\frac{\partial\omega_s}{\partial\zeta} - \frac{\partial^2 v_s}{\partial\zeta^2} - \frac{\partial^2 v_s}{\partial\xi^2} - \frac{\varepsilon}{r} \frac{\partial v_s}{\partial\xi}\right) + \varepsilon^2 \left(\frac{\partial^2 a}{\partial\xi^2} - \frac{\partial^2 a}{\partial\zeta^2}\right) \left(\frac{\partial v_s}{\partial\zeta} + \frac{\partial w_s}{\partial\xi}\right) +$$

$$+ 2\varepsilon^2 \frac{\partial^2 a}{\partial\xi\partial\zeta} \left(\frac{\partial w_s}{\partial\zeta} - \frac{\partial v_s}{\partial\xi}\right) + \varepsilon^2 a \left(- \frac{1}{r} \frac{\partial\bar{\omega}}{\partial\phi} \frac{\partial f}{\partial\zeta} - \bar{v} \frac{\partial^3 f}{\partial\zeta^3}\right) - \varepsilon^2 \frac{\partial a}{\partial\xi} \frac{\partial\bar{v}}{\partial\zeta} \frac{\partial f}{\partial\zeta} +$$

$$- \varepsilon^2 \frac{\partial a}{\partial\zeta} \bar{v} \frac{\partial^2 f}{\partial\zeta^2} + \frac{\varepsilon^2}{r} \frac{\partial^2 a}{\partial\xi\partial\phi} \bar{u} \frac{\partial f}{\partial\zeta} + \frac{\varepsilon^2}{r} \frac{\partial^2 a}{\partial\zeta\partial\phi} f(\bar{\omega} + 2 \frac{\varepsilon}{r} \bar{u}) - 2\varepsilon^2 \frac{\partial^2 a}{\partial\xi\partial\zeta} \frac{\partial\bar{v}}{\partial\xi} f +$$

$$+ \varepsilon^2 \left(\frac{\partial^2 a}{\partial\xi^2} - \frac{\partial^2 a}{\partial\zeta^2}\right) \bar{v} \frac{\partial f}{\partial\zeta} \qquad (D.5)$$

, in which ω_s denotes the vorticity of the secondary flow, defined by

$$\omega_s = \frac{\partial w_s}{\partial\xi} - \frac{\partial v_s}{\partial\zeta} \qquad (D.6)$$

A relationship between this vorticity and the stream function ψ of the secondary flow can be derived by combining definitions (D.6) and (4.17), to yield

$$\omega_s = \frac{Re_0}{r} \left(\frac{\partial^2\psi}{\partial\zeta^2} + \frac{\partial^2\psi}{\partial\xi^2} - \frac{\varepsilon}{r} \frac{\partial\psi}{\partial\xi}\right) \qquad (D.7)$$

Now equation (D.5) can be elaborated to a differential equation for ψ by substituting (D.7) and (4.17). This stream function equation for the secondary flow reads

$$\frac{a}{r} \{\frac{\partial^4\psi}{\partial\xi^4} + 2 \frac{\partial^4\psi}{\partial\xi^2\partial\zeta^2} + \frac{\partial^4\psi}{\partial\zeta^4} - 2 \frac{\varepsilon}{r} \left(\frac{\partial^3\psi}{\partial\xi^3} + \frac{\partial^3\psi}{\partial\xi\partial\zeta^2}\right)\} +$$

$$+ \frac{1}{r} \frac{\partial a}{\partial\xi} \{2\left(\frac{\partial^3\psi}{\partial\xi^3} + \frac{\partial^3\psi}{\partial\xi\partial\zeta^2}\right) - \frac{\varepsilon}{r} \left(3 \frac{\partial^2\psi}{\partial\xi^2} + \frac{\partial^2\psi}{\partial\zeta^2}\right)\} +$$

$$+\frac{1}{r}\frac{\partial a}{\partial\zeta}\left(2\frac{\partial^3\psi}{\partial\zeta^3}+2\frac{\partial^3\psi}{\partial\xi^2\partial\zeta}-2\frac{\varepsilon}{r}\frac{\partial^2\psi}{\partial\xi\partial\zeta}\right)+\frac{2}{r}\frac{\partial^2 a}{\partial\xi\partial\zeta}\left(2\frac{\partial^2\psi}{\partial\xi\partial\zeta}-\frac{\varepsilon}{r}\frac{\partial\psi}{\partial\zeta}\right)+$$

$$+\frac{1}{r}\left(\frac{\partial^2 a}{\partial\xi^2}-\frac{\partial^2 a}{\partial\zeta^2}\right)\left(\frac{\partial^2\psi}{\partial\xi^2}-\frac{\partial^2\psi}{\partial\zeta^2}-\frac{\varepsilon}{r}\frac{\partial\psi}{\partial\xi}\right)-\varepsilon Re_0\frac{f}{r}\left[\left(\frac{\bar{u}}{r}\frac{\partial}{\partial\phi}+\bar{v}\frac{\partial}{\partial\xi}\right)\left(\frac{\partial^2\psi}{\partial\xi^2}+\frac{\partial^2\psi}{\partial\zeta^2}\right)+\right.$$

$$\left.+\frac{\partial\bar{v}}{\partial\xi}\left(\frac{\partial^2\psi}{\partial\xi^2}-\frac{\partial^2\psi}{\partial\zeta^2}\right)+\frac{\partial u}{\partial\xi}\frac{1}{r}\frac{\partial^2\psi}{\partial\xi\partial\phi}-\frac{\varepsilon}{r}\left\{2\frac{\bar{u}}{r}\frac{\partial^2\psi}{\partial\xi\partial\phi}+\bar{v}\left(2\frac{\partial^2\psi}{\partial\xi^2}+\frac{\partial^2\psi}{\partial\zeta^2}\right)+\frac{\partial\bar{v}}{\partial\xi}\frac{\partial\psi}{\partial\xi}\right\}\right]$$

$$-\varepsilon Re_0\frac{1}{r}\frac{\partial f}{\partial\zeta}\left\{\frac{\bar{u}}{r}\frac{\partial^2\psi}{\partial\zeta\partial\phi}+\left(\frac{\partial\bar{v}}{\partial\xi}-\frac{\varepsilon}{r}\bar{v}\right)\frac{\partial\psi}{\partial\zeta}\right\}+\varepsilon Re_0\frac{1}{r}\frac{\partial^2 f}{\partial\zeta^2}\bar{v}\frac{\partial\psi}{\partial\xi}=$$

$$\frac{a}{Re_0}\left(\frac{1}{r}\frac{\partial\bar{\omega}}{\partial\phi}\frac{\partial f}{\partial\zeta}+\bar{v}\frac{\partial^3 f}{\partial\zeta^3}\right)+\frac{1}{Re_0}\frac{\partial a}{\partial\xi}\frac{\partial\bar{v}}{\partial\xi}\frac{\partial f}{\partial\zeta}+\frac{1}{Re_0}\frac{\partial a}{\partial\zeta}\bar{v}\frac{\partial^2 f}{\partial\zeta^2}-\frac{1}{Re_0 r}\frac{\partial^2 a}{\partial\xi\partial\phi}\bar{u}\frac{\partial f}{\partial\zeta}+$$

$$-\frac{1}{Re_0 r}\frac{\partial^2 a}{\partial\zeta\partial\phi}f\left(\bar{\omega}+2\frac{\varepsilon}{r}\bar{u}\right)+\frac{2}{Re_0}\frac{\partial^2 a}{\partial\xi\partial\zeta}\frac{\partial\bar{v}}{\partial\xi}f-\left(\frac{\partial^2 a}{\partial\xi^2}-\frac{\partial^2 a}{\partial\zeta^2}\right)\frac{\bar{v}}{Re_0}\frac{\partial f}{\partial\zeta}+$$

$$-\frac{\partial(f^2)}{\partial\zeta}\left(\bar{u}\frac{\bar{u}_t}{r_s}+\varepsilon\bar{v}\frac{\bar{u}_t}{r_n}\right) \qquad (D.8)$$

If the secondary flow is assumed to be described with sufficient accuracy when retaining only the most important terms of this equation, viz. the main diffusion terms, the main streamwise inertia terms and the source term due to the main flow curvature, the equation reduces to

$$a\left\{\frac{\partial^4\psi}{\partial\xi^4}+2\frac{\partial^4\psi}{\partial\xi^2\partial\zeta^2}+\frac{\partial^4\psi}{\partial\zeta^4}\right\}+2\frac{\partial a}{\partial\xi}\left(\frac{\partial^3\psi}{\partial\xi^3}+\frac{\partial^3\psi}{\partial\xi\partial\zeta^2}\right)+2\frac{\partial a}{\partial\zeta}\left(\frac{\partial^3\psi}{\partial\xi^2\partial\zeta}+\frac{\partial^3\psi}{\partial\zeta^3}\right)+$$

$$+4\frac{\partial^2 a}{\partial\xi\partial\zeta}\frac{\partial^2\psi}{\partial\xi\partial\zeta}+\left(\frac{\partial^2 a}{\partial\xi^2}-\frac{\partial^2 a}{\partial\zeta^2}\right)\left(\frac{\partial^2\psi}{\partial\xi^2}-\frac{\partial^2\psi}{\partial\zeta^2}\right)-\varepsilon Re_0 f\left(\frac{\bar{u}}{r}\frac{\partial}{\partial\phi}+\bar{v}\frac{\partial}{\partial\xi}\right)\left(\frac{\partial^2\psi}{\partial\xi^2}+\frac{\partial^2\psi}{\partial\zeta^2}\right)+$$

$$-\varepsilon Re_0\left[f\left\{\frac{\partial\bar{u}}{\partial\xi}\frac{1}{r}\frac{\partial^2\psi}{\partial\xi\partial\phi}+\frac{\partial\bar{v}}{\partial\xi}\left(\frac{\partial^2\psi}{\partial\xi^2}+\frac{\partial^2\psi}{\partial\zeta^2}\right)\right\}+\frac{\partial f}{\partial\zeta}\left\{\frac{\bar{u}}{r}\frac{\partial^2\psi}{\partial\zeta\partial\phi}+\frac{\partial\bar{v}}{\partial\xi}\frac{\partial\psi}{\partial\zeta}\right\}+\right.$$

$$\left.-\frac{\partial^2 f}{\partial\zeta^2}\bar{v}\frac{\partial\psi}{\partial\xi}\right]=-\frac{\partial(f^2)}{\partial\zeta}\frac{r\bar{u}^2}{r_s} \qquad (D.9)$$

Substituting the similarity hypothesis (4.18) and $a = k_m \bar{u} a'$ into this equation and averaging the result over the depth of flow yields

$$\overline{a'g}\left(\bar{u}\frac{\partial^4\bar{\psi}}{\partial\xi^4}+2\frac{\partial\bar{u}}{\partial\xi}\frac{\partial^3\bar{\psi}}{\partial\xi^3}+\frac{\partial^2\bar{u}}{\partial\xi^2}\frac{\partial^2\bar{\psi}}{\partial\xi^2}\right)+\left(\overline{a'\frac{\partial^2 g}{\partial\zeta^2}}+\overline{\frac{\partial a'}{\partial\zeta}\frac{\partial g}{\partial\zeta}}\right)2\left(\bar{u}\frac{\partial^2\bar{\psi}}{\partial\xi^2}+\frac{\partial\bar{u}}{\partial\xi}\frac{\partial\bar{\psi}}{\partial\xi}\right)+$$

$$+ \overline{(a' \frac{\partial^4 g}{\partial \zeta^4} + 2 \frac{\partial a'}{\partial \zeta} \frac{\partial^3 g}{\partial \zeta^3} + \frac{\partial^2 a'}{\partial \zeta^2} \frac{\partial^2 g}{\partial \zeta^2})\ \bar{u}\ \bar{\psi}} - \overline{a' \frac{\partial^2 g}{\partial \zeta^2} \frac{\partial^2 \bar{u}}{\partial \xi^2}\ \bar{\psi}} + 2 \overline{\frac{\partial a'}{\partial \zeta} \frac{\partial g}{\partial \zeta} \frac{\partial \bar{u}}{\partial \xi} \frac{\partial \bar{\psi}}{\partial \xi}} +$$

$$- \overline{\frac{\partial^2 a'}{\partial \zeta^2}\ g\ \bar{u} \frac{\partial^2 \bar{\psi}}{\partial \xi^2}} - \frac{\varepsilon Re_0}{k_m} \{\overline{fg}\ (\frac{\bar{u}}{r} \frac{\partial^3 \bar{\psi}}{\partial \phi \partial \xi^2} + \bar{v} \frac{\partial^3 \bar{\psi}}{\partial \xi^3} + \frac{\partial \bar{u}}{\partial \xi} \frac{1}{r} \frac{\partial^2 \bar{\psi}}{\partial \phi \partial \xi} + \frac{\partial \bar{v}}{\partial \xi} \frac{\partial^2 \bar{\psi}}{\partial \xi^2}) +$$

$$+ (\overline{f \frac{\partial^2 g}{\partial \zeta^2}} + \overline{\frac{\partial f}{\partial \zeta} \frac{\partial g}{\partial \zeta}})(\frac{\bar{u}}{r} \frac{\partial \bar{\psi}}{\partial \phi} + \frac{\partial \bar{v}}{\partial \xi} \bar{\psi}) + (\overline{f \frac{\partial^2 g}{\partial \zeta^2}} - \overline{g \frac{\partial^2 f}{\partial \zeta^2}})\ \bar{v} \frac{\partial \bar{\psi}}{\partial \xi}\} = - \frac{\overline{\partial (f^2)}}{\partial \zeta} \frac{\bar{ru}^2}{k_m r_s}$$

(D.10)

For $a' = -6\ \zeta(1+\zeta)$, the vertical distribution products can further be elaborated as follows.

$$\overline{a' \frac{\partial^2 g}{\partial \zeta^2}} = a' \frac{\partial g}{\partial \zeta}\Big|_{-1}^{0} - g \frac{\partial a'}{\partial \zeta}\Big|_{-1}^{0} + \int_{-1}^{0} g \frac{\partial^2 a'}{\partial \zeta^2}\, d\zeta = \overline{g \frac{\partial^2 a'}{\partial \zeta^2}} = -\ 12\ \bar{g} = -12$$

(D.11)

$$\overline{a' \frac{\partial^4 g}{\partial \zeta^4} + 2 \frac{\partial a'}{\partial \zeta} \frac{\partial g}{\partial \zeta} + \frac{\partial^2 a'}{\partial \zeta^2} \frac{\partial^2 g}{\partial \zeta^2}} = cf^2\Big|_{\zeta=0} \quad \text{(for c: see Appendix E)} \qquad \text{(D.12)}$$

$$\overline{\frac{\partial a'}{\partial \zeta} \frac{\partial g}{\partial \zeta}} = \frac{\partial a'}{\partial \zeta}\ g\Big|_{-1}^{0} - \int_{-1}^{0} g \frac{\partial^2 a'}{\partial \zeta^2}\, d\zeta = +12 \qquad \text{(D.13)}$$

$$\overline{\frac{\partial f}{\partial \zeta} \frac{\partial g}{\partial \zeta}} = f \frac{\partial g}{\partial \zeta}\Big|_{-1}^{0} - \int_{-1}^{0} f \frac{\partial^2 g}{\partial \zeta^2}\, d\zeta = f \frac{\partial g}{\partial \zeta}\Big|_{\zeta=0} - \overline{f \frac{\partial^2 g}{\partial \zeta^2}} \qquad \text{(D.14)}$$

$$\overline{g \frac{\partial^2 f}{\partial \zeta^2}} = g \frac{\partial f}{\partial \zeta}\Big|_{-1}^{0} - \int_{-1}^{0} \frac{\partial g}{\partial \zeta} \frac{\partial f}{\partial \zeta}\, d\zeta = -f \frac{\partial g}{\partial \zeta}\Big|_{\zeta=0} + \overline{f \frac{\partial^2 g}{\partial \zeta^2}} \qquad \text{(D.15)}$$

$$\overline{\frac{\partial (f^2)}{\partial \zeta}} = f^2\Big|_{\zeta=0} \qquad \text{(D.16)}$$

Making use of (D.11) through (D.16), equation (D.10) can be elaborated to

$$\overline{a'g}\left(\bar{u}\frac{\partial^4\bar{\psi}}{\partial\xi^4}+2\frac{\partial\bar{u}}{\partial\xi}\frac{\partial^3\bar{\psi}}{\partial\xi^3}+\frac{\partial^2\bar{u}}{\partial\xi^2}\frac{\partial^2\bar{\psi}}{\partial\xi^2}\right)+12\left(\bar{u}\frac{\partial^2\bar{\psi}}{\partial\xi^2}+2\frac{\partial\bar{u}}{\partial\xi}\frac{\partial\bar{\psi}}{\partial\xi}+\frac{\partial^2\bar{u}}{\partial\xi^2}\bar{\psi}\right)+$$

$$+\left.cf^2\right|_{\zeta=0}\bar{u}\,\bar{\psi}-\frac{\varepsilon Re_0}{k_m}\left\{\overline{fg}\left(\frac{\bar{u}}{r}\frac{\partial^3\bar{\psi}}{\partial\phi\partial\xi^2}+\bar{v}\frac{\partial^3\bar{\psi}}{\partial\xi^3}+\frac{\partial\bar{u}}{\partial\xi}\frac{1}{r}\frac{\partial^2\bar{\psi}}{\partial\phi\partial\xi}+\frac{\partial\bar{v}}{\partial\xi}\frac{\partial^2\bar{\psi}}{\partial\xi^2}\right)+\right.$$

$$\left.+f\left.\frac{\partial g}{\partial\zeta}\right|_{\zeta=0}\left(\frac{\bar{u}}{r}\frac{\partial\bar{\psi}}{\partial\phi}+\bar{v}\frac{\partial\bar{\psi}}{\partial\xi}+\frac{\partial\bar{v}}{\partial\xi}\bar{\psi}\right)\right\}=-\left.\frac{r\bar{u}^2}{k_m r_s}f^2\right|_{\zeta=0}\qquad\text{(D.17)}$$

APPENDIX E

Computation of the vertical distribution of the secondary flow

Appendix E. Computation of the vertical distribution of the secondary flow

The vertical distribution function g of the stream function of the secondary flow is solved from equation (5.63), which can be rewritten as

$$\frac{\partial^2}{\partial\zeta^2}\left(\alpha' \frac{\partial^2 g}{\partial\zeta^2}\right) = c \frac{\partial(f^2)}{\partial\zeta} \tag{E.1}$$

in which c is considered as an unknown constant to be determined from the condition $\bar{g} = 1$, which follows from the definition of g by the similarity hypothesis (4.18). From the point of view of convergence, this approach is preferable to evaluating

$$c = -\frac{\bar{ru}}{k_m r_s} \frac{1}{\bar{\psi}} \tag{E.2}$$

on the basis of the most recent results of the depth-averaged flow computations, since g satisfies all conditions in each iteration step now.

The boundary conditions to be satisfied can be written as

$$g = 0 \quad \text{and} \quad \alpha' \frac{\partial^2 g}{\partial\zeta^2} = 0 \qquad \text{at} \quad \zeta = 0 \tag{E.3}$$

$$\left.\begin{aligned} g &= k_s\delta_0 \left(1 + \frac{\sqrt{g}}{\kappa C} \ln \delta_0\right) = k_s t_1 \\ \frac{\partial g}{\partial\zeta} &= k_s \left(1 + \frac{\sqrt{g}}{\kappa C} + \frac{\sqrt{g}}{\kappa C} \ln \delta_0\right) = k_s t_0 \end{aligned}\right\} \text{at } \zeta = -1 + \delta_0 \tag{E.4}$$

in which the constant k_s $\left(= -\frac{C}{\sqrt{g}} rv_{\tau s}/\bar{\psi}Re_0\right)$ is determined from

$$g = k_s (1 + \zeta_1)\left\{1 + \frac{\sqrt{g}}{\kappa C} \ln (1 + \zeta_1)\right\} = k_s t_2 \quad \text{at } \zeta = \zeta_1 \tag{E.5}$$

The procedure used to solve g from equation (E.1) with conditions (E.3) through (E.5) is based on repeated integration of (E.1) with respect to ζ (see also DE VRIEND, 1978a and 1978b). To that end g is split up into two parts

$$g = k_s g_1 + c g_2 \tag{E.6}$$

in such a way that

$$\frac{\partial^2}{\partial\zeta^2}\left(a' \frac{\partial^2 g_1}{\partial\zeta^2}\right) = 0 \quad \text{with } g_1 = 0 \text{ and } a' \frac{\partial^2 g_1}{\partial\zeta^2} = 0 \text{ at } \zeta = 0 \tag{E.7}$$

$$\text{and } g_1 = t_1 \text{ and } \frac{\partial g_1}{\partial\zeta} = t_0 \text{ at } \zeta = -1+\delta_0$$

$$\frac{\partial^2}{\partial\zeta^2}\left(a' \frac{\partial^2 g_2}{\partial\zeta^2}\right) = \frac{\partial(f^2)}{\partial\zeta} \text{ with } g_2 = 0 \text{ and } a' \frac{\partial^2 g_2}{\partial\zeta^2} = 0 \text{ at } \zeta = 0 \tag{E.8}$$

$$\text{and } g_2 = 0 \text{ and } \frac{\partial g_2}{\partial\zeta} = 0 \text{ at } \zeta = -1+\delta_0$$

The former system allows for an analytical solution, viz.

$$g_1 = \frac{1 + \frac{\sqrt{g}}{\kappa C}(1 + \ln\delta_0 - \delta_0)}{1 + \ln\delta_0 - \delta_0}\{(1+\zeta)\ln(1+\zeta) - \zeta(1+\ln\delta)\} + t_0\zeta \tag{E.9}$$

, the latter system must be solved numerically. The solution of this system can be written as

$$g_2 = \int_{-1+\delta_0}^{\zeta} d\zeta \int_{-1+\delta_0}^{\zeta} \frac{-d\zeta}{6\zeta(1+\zeta)} \int_0^{\zeta} f^2\, d\zeta +$$

$$+ \frac{\delta_0 + (1+\zeta)\{\ln(1+\zeta) - \ln\delta_0 - 1\}}{1 + \ln\delta_0 - \delta_0} \int_{-1+\delta_0}^{0} d\zeta \int_{-1+\delta_0}^{\zeta} \frac{-d\zeta}{6\zeta(1+\zeta)} \int_0^{\zeta} f^2\, d\zeta \tag{E.10}$$

The evaluation of the integrals near the surface requires some further attention, since the factor $\zeta(1+\zeta)$ goes to zero there, which

could raise numerical trouble. A Taylor series expansion about the point $\zeta = 0$, however, shows that

$$\frac{1}{\zeta(1+\zeta)} \int_0^{\zeta} f^2 d\zeta = \frac{1-\zeta}{\zeta} \{\zeta f^2\big|_{\zeta=0} + O(\zeta^2)\} = f^2\big|_{\zeta=0} + O(\zeta) \tag{E.11}$$

, so that all problems are avoided by using $f^2\big|_{\zeta=0}$ instead of

$$\{\frac{1}{\zeta(1+\zeta)} \int_0^{\zeta} f^2 d\zeta\}\Big|_{\zeta=0}$$

The functions g_1 and g_2 being known, the constants k_s and c must be determined from the condition $\bar{g} = 1$ and the additional condition (E.5). These two conditions are satisfied if

$$k_s \bar{g}_1 + c\bar{g}_2 = 1 \tag{E.12}$$

and

$$k_s g_1(\zeta_1) + c\, g_2(\zeta_1) = k_s t_2 \tag{E.13}$$

Hence

$$k_s = \frac{g_2(\zeta_1)}{\bar{g}_1 g_2(\zeta_1) - \bar{g}_2 \{g_1(\zeta_1) - t_2\}} \tag{E.14}$$

and

$$c = \frac{t_2 - g_1(\zeta_1)}{\bar{g}_1 g_2(\zeta_1) - \bar{g}_2 \{g_1(\zeta_1) - t_2\}} \tag{E.15}$$

Finally it should be noted that if the point $\zeta = \zeta_1$ and $\zeta = -1+\delta_0$ are so close to one another that between these points $g(\zeta)$ can be approximated by a straight line, the counters and the denominators

of (E.14) and (E.15) may become very small. In extreme cases it may be preferable from the point of view of accuracy to replace the additional condition (E.5) by

$$\frac{\partial g}{\partial \zeta} = k_s \left\{1 + \frac{\sqrt{g}}{\kappa C} + \frac{\sqrt{g}}{\kappa C} \ln(1+\zeta_1)\right\} \qquad \text{at} \qquad \zeta = \zeta_1 \tag{E.16}$$

APPENDIX F

Computation of the depth-averaged stream function of the secondary flow

Appendix F Computation of the depth-averaged stream function of the secondary flow

The depth-averaged stream function of the secondary flow $\bar{\psi}$ is solved from the partial differential equation (5.48), which is first order in ϕ and fourth order in ξ. This equation is solved using an implicit forward marching technique, i.e. starting from the upstream boundary $\bar{\psi}$ is solved implicitly in each subsequent cross-section.

The differential equation in ξ to be solved in a cross-section can be written in the form

$$a_1 \frac{\partial^4 \bar{\psi}}{\partial \xi^4} + a_2 \frac{\partial^3 \bar{\psi}}{\partial \xi^3} + a_3 \frac{\partial^2 \bar{\psi}}{\partial \xi^2} + a_4 \frac{\partial \bar{\psi}}{\partial \xi} + a_5 \bar{\psi} = a_6 \tag{F.1}$$

The relevant boundary conditions are

$$\left.\begin{aligned} \bar{\psi} &= \bar{k}_{1s}\, \delta_1 \left(1 + \frac{\sqrt{g}}{\kappa C} \ln \delta_1\right) = \bar{k}_{1s} t_2 \\ \frac{\partial \bar{\psi}}{\partial \xi} &= \bar{k}_{1s} \left(1 + \frac{\sqrt{g}}{\kappa C} + \frac{\sqrt{g}}{\kappa C} \ln \delta_1\right) = \bar{k}_{1s} t_0 \end{aligned}\right\} \text{at } \xi = -\frac{B}{2d} + \delta_1 \tag{F.2}$$

$$\left.\begin{aligned} \bar{\psi} &= -\bar{k}_{rs} t_2 \\ \frac{\partial \bar{\psi}}{\partial \xi} &= -\bar{k}_{rs} t_0 \end{aligned}\right\} \text{at } \xi = \frac{B}{2d} - \delta_1 \tag{F.3}$$

and the additional conditions from which $\bar{k}_{1s}$ and $\bar{k}_{rs}$ are determined read

$$\bar{\psi} = \bar{k}_{1s} \left(\frac{B}{2d} + \xi_1\right) \left\{1 + \frac{\sqrt{g}}{\kappa C} + \frac{\sqrt{g}}{\kappa C} \ln\left(\frac{B}{2d} + \xi_1\right)\right\} = \bar{k}_{1s} t_1 \quad \text{at} \quad \xi = \xi_1 \tag{F.4}$$

$$\bar{\psi} = -\bar{k}_{rs} t_1 \quad \text{at } \xi = \xi_2 \tag{F.5}$$

Now $\bar{\psi}$ is split up into three parts

$$\bar{\psi} = \bar{k}_{1s}\,\bar{\psi}_1 + \bar{k}_{rs}\bar{\psi}_2 + \bar{\psi}_3 \tag{F.6}$$

in such a way, that the components $\bar{\psi}_1$, $\bar{\psi}_2$ and $\bar{\psi}_3$ follow from

$$a_1 \frac{\partial^4\bar{\psi}_1}{\partial\xi^4} + a_2 \frac{\partial^3\bar{\psi}_1}{\partial\xi^3} + a_3 \frac{\partial^2\bar{\psi}_1}{\partial\xi^2} + a_4 \frac{\partial\bar{\psi}_1}{\partial\xi} + a_5\,\bar{\psi}_1 = 0 \tag{F.7}$$

with $\bar{\psi}_1 = t_2$ and $\frac{\partial\bar{\psi}1}{\partial\xi} = t_0$ at $\xi = -\frac{B}{2d} + \delta_1$

and $\bar{\psi}_1 = 0$ and $\frac{\partial\bar{\psi}_1}{\partial\xi} = 0$ at $\xi = \frac{B}{2d} - \delta_1$

$$a_1 \frac{\partial^4\bar{\psi}_2}{\partial\xi^4} + a_2 \frac{\partial^3\bar{\psi}_2}{\partial\xi^3} + a_3 \frac{\partial^2\bar{\psi}_2}{\partial\xi^2} + a_4 \frac{\partial\bar{\psi}_2}{\partial\xi} + a_5\bar{\psi}_2 = 0 \tag{F.8}$$

with $\bar{\psi}_2 = 0$ and $\frac{\partial\bar{\psi}_2}{\partial\xi} = 0$ at $\xi = -\frac{B}{2d} + \delta_1$

and $\bar{\psi}_2 = -t_2$ and $\frac{\partial\bar{\psi}_2}{\partial\xi} = -t_0$ at $\xi = \frac{B}{2d} - \delta_1$

$$a_1 \frac{\partial^4\bar{\psi}_3}{\partial\xi^4} + a_2 \frac{\partial^3\bar{\psi}_3}{\partial\xi^3} + a_3 \frac{\partial^2\bar{\psi}_3}{\partial\xi^2} + a_4 \frac{\partial\bar{\psi}_3}{\partial\xi} + a_5\bar{\psi}_3 = 0 \tag{F.9}$$

with $\bar{\psi}_3 = 0$ and $\frac{\partial\bar{\psi}_3}{\partial\xi} = 0$ at $\xi = \pm\,(\frac{B}{2d} - \delta_1)$

Once the functions $\bar{\psi}_1$, $\bar{\psi}_2$ and $\bar{\psi}_3$ are known, the wall shear stress constants $\bar{k}_{1s}$ and k_{rs} can be determined from conditions (F.4) and (F.5), which are satisfied if

$$\bar{k}_{1s}\,\bar{\psi}_1\big|_{\xi_1} + \bar{k}_{rs}\,\bar{\psi}_2\big|_{\xi_1} + \bar{\psi}_3\big|_{\xi_1} = \bar{k}_{1s}\,t_1 \tag{F.10}$$

and

$$\bar{k}_{1s}\,\bar{\psi}_1\big|_{\xi_2} + \bar{k}_{rs}\,\bar{\psi}_2\big|_{\xi_2} + \bar{\psi}_3\big|_{\xi_2} = -\,\bar{k}_{rs}t_1 \tag{F.11}$$

Hence

$$\bar{k}_{1s} = \frac{-\bar{\psi}_3\big|_{\xi_1}(\bar{\psi}_2\big|_{\xi_2} + t_1) + \bar{\psi}_3\big|_{\xi_2}\,\bar{\psi}_2\big|_{\xi_1}}{(\bar{\psi}_1\big|_{\xi_1} - t_1)(\bar{\psi}_2\big|_{\xi_2} + t_1) - \bar{\psi}_1\big|_{\xi_2}\,\bar{\psi}_2\big|_{\xi_1}} \qquad \text{(F.12)}$$

and

$$\bar{k}_{rs} = \frac{-\bar{\psi}_3\big|_{\xi_1}(\bar{\psi}_1\big|_{\xi_1} - t_1) + \bar{\psi}_3\big|_{\xi_1}\,\bar{\psi}_1\big|_{\xi_2}}{(\bar{\psi}_1\big|_{\xi_1} - t_1)(\bar{\psi}_2\big|_{\xi_2} + t_1) - \bar{\psi}_1\big|_{\xi_2}\,\bar{\psi}_2\big|_{\xi_1}} \qquad \text{(F.13)}$$

Then the depth-averaged sidewall friction velocities follow from

$$w_{\tau 1} = \frac{\sqrt{g}}{C}\frac{\bar{k}_{1s}}{r}\,Re_0 \quad \text{and} \quad w_{\tau r} = \frac{\sqrt{g}}{C}\frac{\bar{k}_{rs}}{r}\,Re_0 \qquad \text{(F.14)}$$